HEAT TRANSFER AND FLOW FRICTION CHARACTERISTICS OF FIBROUS METALS

Richard Harrison Funke

NAVAL POSTGRADUATE SCHOOL
Monterey, California

THESIS

HEAT TRANSFER AND FLOW FRICTION
CHARACTERISTICS OF
FIBROUS METALS

by

Richard Harrison Funke

Thesis Advisor: P. F. Pucci

June 1972

Heat Transfer and Flow Friction Characteristics of Fibrous Metals

by

Richard Harrison Funke
Ensign, United States Navy
B.S., Cornell University, 1971

Submitted in partial fulfillment of the
requirements for the degree of

MASTER OF SCIENCE IN MECHANICAL ENGINEERING

from the

NAVAL POSTGRADUATE SCHOOL
June 1972

ABSTRACT

The single-blow transient testing facility of the Naval Postgraduate School was reconstructed. With this apparatus the flow friction and heat transfer characteristics of four grades of steel wool, considered to be representative of fibrous metals, were determined. The flow friction characteristics were determined on the basis of the isothermal pressure drop across the medium, while the heat transfer results were determined by means of the single-blow transient testing technique.

The heat transfer results are presented as the Colburn j-factor. The flow friction results are presented in two forms: as the Fanning friction factor, f; and as the correlating friction factor, C_f. All results are presented as a function of Reynolds number based on the product of the experimentally determined permeability and tortuosity parameter of each sample.

TABLE OF CONTENTS

LIST OF TABLES

LIST OF FIGURES

NOMENCLATURE

English Letter Symbols		Typical Units
a	Linear coefficient of Reynold's equation, reciprocal of the permeability (1/K)	ft^{-2}
A	Matrix total heat transfer area	ft^2
A_c	Matrix minimum free flow area	ft^2
A_{fr}	Matrix total frontal area	ft^2
A_s	Matrix solid cross-sectional area available for longitudinal conduction	ft^2
b	Quadratic coefficient of Reynold's equation, interpreted as a tortuosity parameter	ft^{-1}
c	Cubic coefficient of the empirical equation for the pressure gradient	dimensionless
C_f	Correlating friction factor	dimensionless
c_p	Fluid specific heat at constant pressure	BTU/(lbm-°F)
c_s	Matrix material specific heat	BTU/(lbm-°F)
C_s	Matrix thermal capacity ($W_s c_s$)	BTU/°F
d	Rod diameter in stacked screen model	ft
d_H	Fiber hydraulic diameter	ft
D_H	Flow passage hydraulic diameter	ft
E	Friction power per unit area	hp/ft^2
G	Mass flux ($\dot{m}/A_c$) or ($\dot{m}/A_{fr}$)	$lbm/(hr\text{-}ft^2)$
g	Gravitational acceleration	ft/sec^2
g_c	Proportionality factor in Newton's Second Law	32.2 lbm-ft/(lbf-sec^2)
h	Surface heat transfer coefficient for convection; heat transfer power per unit area per degree temperature difference	$BTU/(hr\text{-}ft^2\text{-}°F)$

k	Fluid thermal conductivity	BTU/(hr-ft-°F)
K	Matrix permeability	ft^2
K_c	Contraction coefficient	dimensionless
K_e	Expansion coefficient	dimensionless
k_s	Matrix thermal conductivity	BTU/(hr-ft-°F)
l	Length parameter in N_{Re}	ft
L	Total matrix flow length	ft
$\dot{m}$	Mass flow rate	lbm/hr
p	Pressure	lbf/ft^2
φ	Matrix porosity $(1-W_s/(\rho_s A_{fr} L))$	dimensionless
q	Heat transfer rate	BTU/hr
R	Specific gas constant (53.35 for air)	ft-lbf/(lbm-°R)
r_H	Flow passage hydraulic radius $(D_H/4)$	ft
t	Temperature	°F
T	Absolute temperature	°R
t^*	Normalized temperature	dimensionless
u	Flow velocity	ft/sec
U	Bulk velocity (G/ρ)	ft/sec
v	Specific volume $(1/\rho)$	ft^3/lbm
V_m	Matrix volume	ft^3
w	Average fiber width	in
W_f	Fluid mass in matrix	lbm
W_s	Matrix mass	lbm
w_y	Uncertainty interval for quantity y	units of y
x	Distance along flow passage from the matrix inlet	ft
x_t	Pitch of rods in stacked screens model	dimensionless
Z	Reduced length $(N_{tu}(x/L))$	dimensionless

Greek Letter Symbols

β	Specific surface (compactness), $(A/A_{fr}/L)$	ft^{-1}
$\bar{\beta}$	Ratio of orifice diameter to pipe diameter	dimensionless
Δ	Difference or change (of time, temperature, etc.)	
θ	Time	sec, hr
μ	Fluid viscosity	lbm/(hr-ft) $lbf\text{-}hr/ft^2$
μ^*	Free time	dimensionless
ρ	Density	lbm/ft^3
ν	Kinematic viscosity	ft^2/hr

Subscripts

atm	Local atmosphere
ave	Average
f	Fluid (gas, air)
i	Initial; inlet
m	Matrix; mean
o	At orifice
s	Solid (matrix material)
STD	Standard (temperature and pressure)
x	Local conditions
1	Inlet conditions (upstream of matrix and heaters)
2	Inlet conditions at matrix entrance
3	Exit conditions at matrix outlet

Dimensionless Groupings

C_f	Correlating friction factor; ratio of dissipative effects to inertial effects

f Fanning friction factor; ratio of wall shear stress to fluid dynamic head

j Colburn j factor ($N_{St}N_{Pr}^{2/3}$). This factor plotted versus Reynolds number defines the surface heat transfer characteristics

λ Longitudinal heat conduction parameter for solid material ($k_s A_s / \dot{m} L c_{fluid}$)

τ Time parameter ($hA\theta / W_s c_s$)

N_{Pr} Prandtl number; ratio of viscous dissipation to thermal dissipation (i.e., kinematic viscosity/thermal diffusivity)

N_{Re} Reynolds number; ratio of inertial effects to viscous effects ($\rho U l / \mu$)

N_{St} Stanton number; ratio of heat transfer power per unit surface area to fluid thermal capacity per unit flow area (h/Gc_p)

N_{tu} Number of transfer units; ratio of total heat transfer power to total fluid thermal capacity ($hA/\dot{m}c_p$).

ACKNOWLEDGEMENT

The author would like to express his appreciation to Dr. Paul F. Pucci, Professor of Mechanical Engineering, for his guidance, assistance, and patience during the course of this study.

Without the skilled craftsmanship of Messers. K. Mothersell, G. Baxter, J. Beck, G. Bixler, and J. McKay there would have been no apparatus with which to conduct this experimental investigation. In addition the author would like to particularly thank Mr. Thomas Christian, whose electronic expertise, willingness to come to the rescue, and sense of humor have made the results presented herein possible.

I. INTRODUCTION

Regenerators add on the order of ten percent to the thermal efficiency of the basic gas turbine power cycle. Due to the current emphasis on the use of gas turbines, as well as the reawakening interest in the Stirling and Ericsson cycles, where a regenerator is an integral part of the cycle, much attention has been paid to the design of these heat exchangers. Frequently the applications of such cycles are weight or volume-limited, and therefore regenerators must possess a high heat transfer surface density.

However, as noted by Kays and London in their monograph on compact heat exchangers [13][1], increasing the heat transfer area necessarily increases the pressure drop (hence the pump work required) across the heat exchanger, particularly when the working fluid is a gas. Thus, the consideration of the heat transfer characteristics of a surface for compact heat exchanger applications cannot be divorced from a consideration of the friction characteristics of the surface.

Between 1965 and 1968 several compact heat exchanger surfaces were extensively studied at the Naval Postgraduate School. These included perforated nickel plate matrices and offset rectangular fin matrices of the AiResearch Manufacturing Company studied by Piersall [23]; six different plate-and-fin cores by the Solar Division of International Harvester studied by Ball [2], Traister [29], and Trost [30]; and the ceramic cores by Corning Glass, studied by Bruno [5]. All of these

---

[1] Numbers in brackets refer to items in the bibliography.

surfaces were fundamentally porous to flow in one direction only and were intended for use in gas turbine plants.

Fibrous metals (such as steel wool) possess the high surface density requisite for a compact heat exchanger. Moreover, the apparent small hydraulic diameter of the effective flow channels of such materials should lead to large values of the convective heat transfer coefficient h, since h always varies with a negative power of the channel hydraulic diameter [13]. Also the tortuous nature of the three-dimensional flow through fibrous media hinders the development of the momentum and thermal boundary layers, which should further increase the value of h. Although the high surface area to volume ratio of the individual fibers excludes fibrous metals from high temperature environments (e.g., the open cycle gas turbine regenerator), such materials do have application in low-temperature closed power cycles and in refrigeration cycles such as the reversed Brayton, reversed Stirling, Gifford-McMahon, or Pulse Tube cycles.

This thesis was directed at four objectives:

1. Reconstruct the transient test apparatus (dismantled since 1968), including new instrumentation.

2. Test a previously studied compact heat exchanger surface to insure reliability of the reconstructed apparatus.

3. Determine the heat transfer and flow friction characteristics of various grades of fibrous metals, specifically steel wool. (The "grade" of a fibrous metal refers to the size of the fiber, and not necessarily to the porosity of the fibrous metal matrix. Porosity was not an independent test variable).

4. Ascertain the appropriate length parameter to be used in the definition of a Reynolds number upon which a unified correlation of the heat transfer and flow friction characteristics may be based.

II. SUMMARY OF THEORY

A. REYNOLDS NUMBERS FOR POROUS MEDIA FLOWS

Flow friction and heat transfer data are usually correlated with the flow Reynolds number for the surface geometry under consideration:

$$N_{Re} = \rho U l / \mu$$

where l is a characteristic length parameter for the surface geometry. The results thus correlated are independent of any particular geometrically similar surface. For flow in fibrous media the dilemma is the selection of the characteristic length parameter. If the fibers were packed so tightly that the flow could be unambiguously considered internal in nature, the obvious choice would be some sort of effective hydraulic diameter of a representative flow channel. This was the procedure in the previously tested cores (e.g., the Solar series, Cercor, etc.), which were porous to flow in one dimension only and possessed a well-defined channel hydraulic diameter. At the other extreme, if only one fiber of the medium were under consideration (i.e., purely external flow), the characteristic length parameter would be the hydraulic diameter of the fiber. However, neither such simple case exists.

Three approaches were made to the selection of the characteristic length parameter. In the first, fibrous metals were assumed to be porous to flow in only one dimension and the equations applied to the previously tested cores were used. The second approach is based on the in-line stacking of crossed-rod matrices. Both of these idealized models produce a physically conceivable characteristic length. The third approach was based on the fundamentals of flow in porous media, but produces no such conceivable dimension.

1. Uni-dimensional Porosity Model

Consider a heat exchanger with n uniform channels of length L. If A_c is the free flow area of the entire cross-section, and A is the heat transfer area of the entire exchanger, then:

Free flow area/channel = A_c/n

Nominal volume/channel = $(A_c/n)L$

Interior surface/channel = A/n

But the interior surface of a channel equals the cross-sectional perimeter times the length of the channel. Therefore

Perimeter/channel = $A/(nL)$

The hydraulic diameter of the channel is defined as four times the cross-sectional area of the channel divided by the wetted perimeter, or:

$$D_H = 4\frac{(A_c/n)}{(A/[nL])} = 4\frac{A_c L}{A} \qquad (1)$$

For such a model which is porous to flow in only one dimension, the porosity (i.e., volume of voids over nominal volume) is:

$$\phi = A_c / A_{fr} \qquad (2)$$

where A_{fr} equals the total frontal area of the medium. Since the nominal volume of the exchanger is the product of A_{fr} and L, the specific surface (i.e., heat transfer area per unit of volume) is, with substitution from (1) and (2):

$$\beta = \frac{A}{A_{fr} L} = 4\frac{A_c}{A_{fr} D_H} = 4\frac{\phi}{D_H} \qquad (3)$$

As explained in Appendix B, the porosity and heat transfer area (hence also the specific surface) may be determined independently of these relations for fibrous metals. Thus the equivalent channel hydraulic diameter for this model may be computed from (3). This is the characteristic length used in the Reynolds number under this idealization.

2. In-line Crossed Rod Matrices Model

This model consists of square-mesh cross-rod screens which are stacked so that there is no separation between layers and so that the mesh in one layer coincides with the meshes in adjacent layers (see inset). The rods are assumed to be of diameter d and separated by uniform distance $x_t d$.

On the basis of a repeatable unit cell (similar to the procedure in the preceding section) the following relations are easily derived [13]:

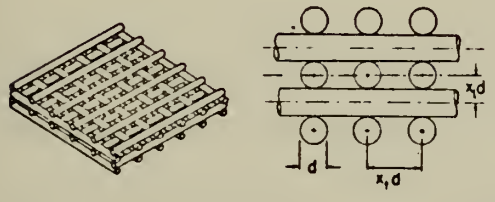

$$\varphi = 1 - \pi/(4x_t) \qquad (4)$$

$$A_c/A_{fr} = [(x_t - 1)/x_t]^2 \qquad (4a)$$

$$\beta = \pi/(x_t d) \qquad (5)$$

$$D_H = 4x_t/\pi - 1 \qquad (6)$$

The pitch, x_t, is calculated from the known porosity, φ, with the use of (4). Again this equivalent channel hydraulic diameter is used as the length parameter for this model. Note that this model differs from the previous in that it is porous to flow in three dimensions, rather than one. For the cases where the fiber is not of circular cross-section, the rod diameter d is replaced by the fiber hydraulic diameter in the equation for the specific surface (5).

3. Flow in Porous Media

Analysis of the fundamentals of flow in porous media provides a length parameter which is more justifiable, in the sense that no geometrical approximations are made.

In 1856 Darcy, after a study of the flow of water through the sand filters of the water purification plant at Dijon, France, made the empirical observation that the bulk (i.e., nominal) flow rate of fluid through the filters is proportional to the difference between the fluid inlet and outlet heads, and inversely proportional to the thickness of the filter. Since this observation was valid only macroscopically, and therefore over finite distances, it was later formulated on a differential basis as what is now known as Darcy's Law of fluid flow in porous media:

$$U = -\frac{K}{\mu}(\nabla p - \rho_f g) \tag{7}$$

Here U is the bulk velocity of the fluid flow (i.e., based on the total frontal area of the medium and not the internal free flow area), p is the fluid pressure in the medium, and g is the gravitational acceleration. The constant K is known as the permeability of the medium.

Darcy's Law is the fundamental relation describing the flow of fluids in porous media. The significance of this law is that it relates the internal pressure field to the bulk velocity U, a quantity which is measured external to the medium. Together with the continuity equation for fluid flow in a porous medium:

$$\phi \frac{\partial}{\partial t}(\rho_f) = \nabla \cdot (\rho_f U) \tag{8}$$

(ϕ = total porosity of the medium).

Darcy's Law completely specifies the flow field. Under steady state conditions these two equations then reduce to Laplace's equation, and a solution is possible. It must be emphasized that Darcy's Law is an empirical relation; it has no analytical basis. Theoretically, if a satisfactory model can be formulated for the porous medium, and sufficient boundary conditions stated, the same result could be achieved by a solution (closed form or numerical) of the Navier-Stokes equations (which would involve the internal velocities rather than the external, bulk velocity). In practice this analytical approach has rarely been successful, largely because of difficulties with the boundary conditions.

It is convenient at this point to define some terms of importance in the study of Darcy's Law:

a) Porosity, ϕ, is the volume of voids divided by the total (i.e., nominal) volume.

b) Permeability, K is, a measure of the ease with which a fluid may transverse a medium under the influence of a given pressure gradient. It is important to note that the permeability has units of length squared and is independent of the fluid. Permeability is defined by Darcy's Law (7).

c) Tortuosity is the relative average length of the flow path of a fluid particle from one side of the porous medium to the other.

Clearly the permeability is the important parameter of the medium for predicting the pressure drop across it. Unfortunately, it is the porosity of the medium, and not the permeability, which is generally known. For a given porous medium, the permeability is a unique, but unknown function of the porosity [22, 27]. Several theories have been advanced which purport to theoretically relate porosity and permeability. The oldest is that due to Kozeny (1927) but his own experimental data shows discrepancies from the theory of -68.7 to +85.7

per cent [22]. The most recent theory is based on statistical mechanics, but regretably attaches the randomness to the fluid flow, and not the medium, where it properly belongs [27]. Thus it may be seen that the most accurate determination of the permeability is by experiment.

If Darcy's Law (7) is written for one-dimensional flow in the absence of significant changes in gravitational potential, it becomes (after rearrangement):

$$-\frac{dP}{dx} = \frac{\mu U}{K} \tag{9}$$

Obviously the permeability, K, can be determined by measuring the isothermal pressure drop across a thin slice of medium at different bulk velocities, U. (Constant temperature is required so that μ remains constant).

Mother Nature has not been so kind, however, for Darcy's Law is strictly valid only for low flow rates. At higher velocities the magnitude of the pressure gradient increases with velocity more rapidly than the linear rate indicated by Darcy's Law. Based on experimental data gathered in the non-Darcy regime, Reynolds (1900) suggested the relation:

$$-\frac{dP}{dx} = a\mu U + \frac{b\rho U^2}{g_c} \tag{10}$$

Forchheimer (1901) added a cubic term to better fit the data. However, the coefficient of the cubic term was found to be of such small magnitude that the term is generally neglected. Missbach (1937) proposed that the pressure gradient in non-Darcy flow be proportional to U to some exponent between one and two. As this relation could not even be partially justified theoretically, it has generally been ignored in favor of Reynold's

equation. The most refined formulation is that of Polubarinova-Kochina, which includes momentum changes due to compressibility effects:

$$-\frac{dp}{dx} = a\mu U + \frac{b\rho U^2}{g_c} + \frac{\rho}{g_c}\frac{dU}{d\theta} \tag{11}$$

This additional term is the acceleration across the medium due to the decrease in the density of the fluid. Since both a stationary frame of reference and a frame moving at the bulk velocity are inertial frames, this time-dependent acceleration may be rewritten as a convective acceleration [8]:

$$-\frac{dp}{dx} = a\mu U + \frac{b\rho U^2}{g_c} + \frac{\rho}{g_c}\frac{dU}{dx}\frac{dx}{d\theta} \tag{11a}$$

$$-\frac{dp}{dx} = a\mu U + \frac{b\rho U^2}{g_c} + \frac{\rho}{g_c} U\frac{dU}{dx} \tag{11b}$$

Although (10) is of experimental origin, it was initially justified on quasi-theoretical grounds by analogy to the pressure drop in pipe flow. In laminar pipe flow the pressure gradient is proportional to the velocity (the Hagen-Poiseuille equation), while in turbulent pipe flow the gradient is proportional to the square of the velocity. Since transition between laminar and turbulent flow in fibrous media would not be as sharply defined as in pipe flow, the reasoning went, the pressure loss must be the sum of the two analagous losses [22].

It will be recalled that the non-linear (viz., inertial) terms in the Navier-Stokes equations do not become significant until the Reynolds number exceeds some critical value [28]. This critical value marks the end of the "slow flow" regime. Separation of the boundary layer in external flow over bluff bodies and similar effects in curved

channel flow occur in this new regime. For both internal and external flows, there is a dramatic increase in the pressure drop long before the flow becomes turbulent itself. It is now thought that non-Darcy flow is due to the emerging influence of these inertial terms [9, 26]. Hubbert [12] proposed such a completely laminar theory wherein the increasingly important inertial forces (which increase with velocity more rapidly than do the viscous forces) distort the streamlines of flow. This leads to increased velocity gradients and therefore, increased negative pressure gradients (by Bernoulli's Law). These increased velocities also lead to increased viscous forces. The effects are lumped as inertial resistance, hence a greater pressure drop than that predicted by Darcy's Law.

Dimensional analysis of Reynolds equation

$$-\frac{dp}{dx} = a\mu U + \frac{b\rho U^2}{g_c} \tag{10}$$

shows that a must have dimensions of one over length squared ($1/L^2$), while b has dimensions of one over length ($1/L$). In fact, for small bulk velocity, U, the quadratic (i.e., inertial) term in Reynolds equation becomes negligible, and (10) reduces to the one-dimensional Darcy's Law (9). Therefore the constant a must be one over the permeability ($1/K$). Thus (10) becomes:

$$-\frac{dp}{dx} = \frac{\mu U}{K} + \frac{b\rho U^2}{g_c} \tag{12}$$

The coefficient b of the inertial term is an inertial resistance coefficient thought to be ude to the successive contractions and expansions of the flow in porous media. Green and Duwez [9] assert that b is

actually a measure of the tortuosity of the medium. However, there is no purely theoretical reason for assuming that b is independent of the fluid [3].

If (10) is arranged in the following form:

$$\frac{1}{\mu U}\left[-\frac{dp}{dx}\right] = \frac{1}{K} + b\left[\frac{\rho U}{\mu g_c}\right] \tag{13}$$

it is seen that a plot of $\frac{1}{\mu U}\left(-\frac{dp}{dx}\right)$ versus $\left(\frac{\rho U}{\mu g_c}\right)$ should be linear with slope equal to the tortuosity parameter, b, and intercept equal to one over the permeability, 1/K. Beavers and Sparrow [3] have examined the flow of water through a fibrous metal product known as FOAMETAL, which is structurally similar but not identical to steel wool. Their investigation covered a velocity range of 20:1 for 5 samples and showed no deviation in excess of 2.5% from the linear plot predicted by (13). This is considered to be a strong indication of the validity of Reynolds equation and suggests a simple means of determining the permeability and tortuosity parameter for a porous medium.

However, the use of this technique requires the approximation of $\frac{dp}{dx}$ by $\Delta P/L$. (in other words, a uniform gradient between pressure taps is assumed). This approximation may be eliminated by the integration of Reynolds equation (10) or the Polubarinova-Kochina equation (11b) under the assumption of isothermal flow of a perfect gas. Since (11b) is the more general of the two, it is used for the illustration of the integration procedure.

$$-\frac{dp}{dx} = a\mu U + \frac{b\rho U^2}{g_c} + \frac{\rho U}{g_c}\frac{dU}{dx} \tag{11b}$$

The viscosity is the absolute viscosity in units of force-time/length squared. Multiply (11b) through by the density

$$-\rho\frac{dp}{dx} = a\rho\mu U + \frac{b\rho U)^2}{g_c} + \rho\frac{(\rho U)}{g_c}\frac{dU}{dx} \qquad (14)$$

But $\rho = P/RT$ for a perfect gas, and $\rho U = G$, the mass flux. Substitution of these identities in (14) yields:

$$-\frac{P}{RT}\frac{dp}{dx} = a\mu G + \frac{b}{g_c}G^2 + \frac{1}{g_c}\left(\frac{P}{RT}\right)G\frac{d}{dx}\left(\frac{G}{\rho}\right) \qquad (15)$$

The mass flux, G, is constant across the medium since it is based on the frontal area, A_{fr} (i.e., $G = \dot{m}/A_{fr}$). Therefore

$$-\frac{P}{RT}\frac{dp}{dx} = a\mu G + \frac{b}{g_c}G^2 + \frac{G^2}{g_c}\left(\frac{P}{RT}\right)\frac{d}{dx}\left(\frac{RT}{P}\right) \qquad (16)$$

$$-\frac{P}{RT}\frac{dp}{dx} = a\mu G + \frac{b}{g_c}G^2 + \frac{G^2}{g_c}P\frac{d}{dp}(1/P)\frac{dp}{dx} \qquad (17)$$

$$-\frac{P}{RT}\frac{dp}{dx} = a\mu G + \frac{b}{g_c}G^2 + \frac{G^2}{g_c}P(-1/P^2)\frac{dp}{dx} \qquad (18)$$

$$-\frac{P}{RT}\frac{dp}{dx} = a\mu G + \frac{b}{g_c}G^2 - \frac{G^2}{g_c}\left(\frac{1}{P}\frac{dp}{dx}\right) \qquad (19)$$

$$-\frac{P}{RT}dP = a\mu G dx + \frac{b}{g_c}G^2 dx - \frac{G^2}{g_c}\left(\frac{dp}{P}\right) \qquad (20)$$

Equation (20) can be integrated from entry to exit of the medium (a length L):

$$-\frac{P^2}{2RT}\Bigg|_1^2 = a\mu GL + \frac{b}{g_c}G^2L - \frac{G^2}{g_c}\ln(P)\Bigg|_1^2 \qquad (21)$$

$$\frac{(P_1^2 - P_2^2)}{2RT} - \frac{G^2}{g_c}\ln\left(\frac{P_1}{P_2}\right) = a\mu GL + \frac{b}{g_c}G^2L \qquad (22)$$

This equation may also be arranged so that the slope is again equal to the tortuosity parameter b while the intercept is one over the permeability (a = 1/K):

$$\frac{1}{\mu GL}\left[\frac{P_1^2 - P_2^2}{2RT} - \frac{G^2}{g_c}\ln\left(\frac{P_1}{P_2}\right)\right] = \frac{1}{K} + \frac{bG}{\mu g_c} \qquad (23)$$

The choice between (13) or (23) to determine the permeability depends on the conditions of the experiment. The former is restricted to isothermal flow with a constant pressure gradient between pressure measurement stations. The latter is restricted to isothermal flow of a perfect gas, but places no further restriction on the nature of the pressure gradient.

Once the permeability has been determined for a medium, a Reynolds number can be defined. Since N_{Re} is the ratio of inertial effects to viscous effects, and since all the viscous effects are embodied in the linear term in (10) or (11), while all the inertial effects are in the quadratic term:

$$N_{Re} = \frac{b\rho U^2/g_c}{\mu U/K} = \frac{\rho U}{\mu g_c}(Kb) \qquad (24)$$

Since μ was previously identified as the absolute viscosity in force units, μg_c is the absolute viscosity in mass units. To avoid ambiguity, substitute the kinematic viscosity ν for $\mu g_c/\rho$. Therefore,

$$N_{Re} = \frac{U}{\nu}(Kb) \qquad (25)$$

It is seen that the characteristic length parameter based on this approach is the product of the permeability and the tortuosity parameter of the medium.

There are obvious disadvantages to this whole procedure in defining a Reynolds number. First, a length parameter involving the product of the permeability and some vague tortuosity parameter cannot be conceived as a physically identifiable length. Second, the medium must undergo a series of experiments before this pseudo-length parameter, Kb, can be determined. Third, even the most subtle difference between the internal geometries of two cores can make a unified correlation between them based on a Reynolds number defined by (25) impossible. For example, Beavers and Sparrow found that the presence of loose fiber ends within a medium made impossible any correlation with a medium that did not have loose fiber ends.

Nevertheless, the proper length parameter is the one which correlates friction and heat transfer data into single curves, and this is the ultimate test.

B. FRICTION FACTOR

The friction factor is the dimensionless variable which correlates the pressure loss behavior of similar surfaces. It is loosely defined as the ratio of dissipative forces to inertial forces. Any force (and not exclusively viscous forces) which causes a pressure drop across a medium is a dissipative force.

Again there is more than one approach. The first is the solution for the familiar Fanning friction factor, f, based on a channel analysis. The second is a friction factor which is an outgrowth of the definition of the Reynolds number in terms of the permeability, C_f.

1. Fanning Friction Factor, f:

Consider the following idealized situation [13]:

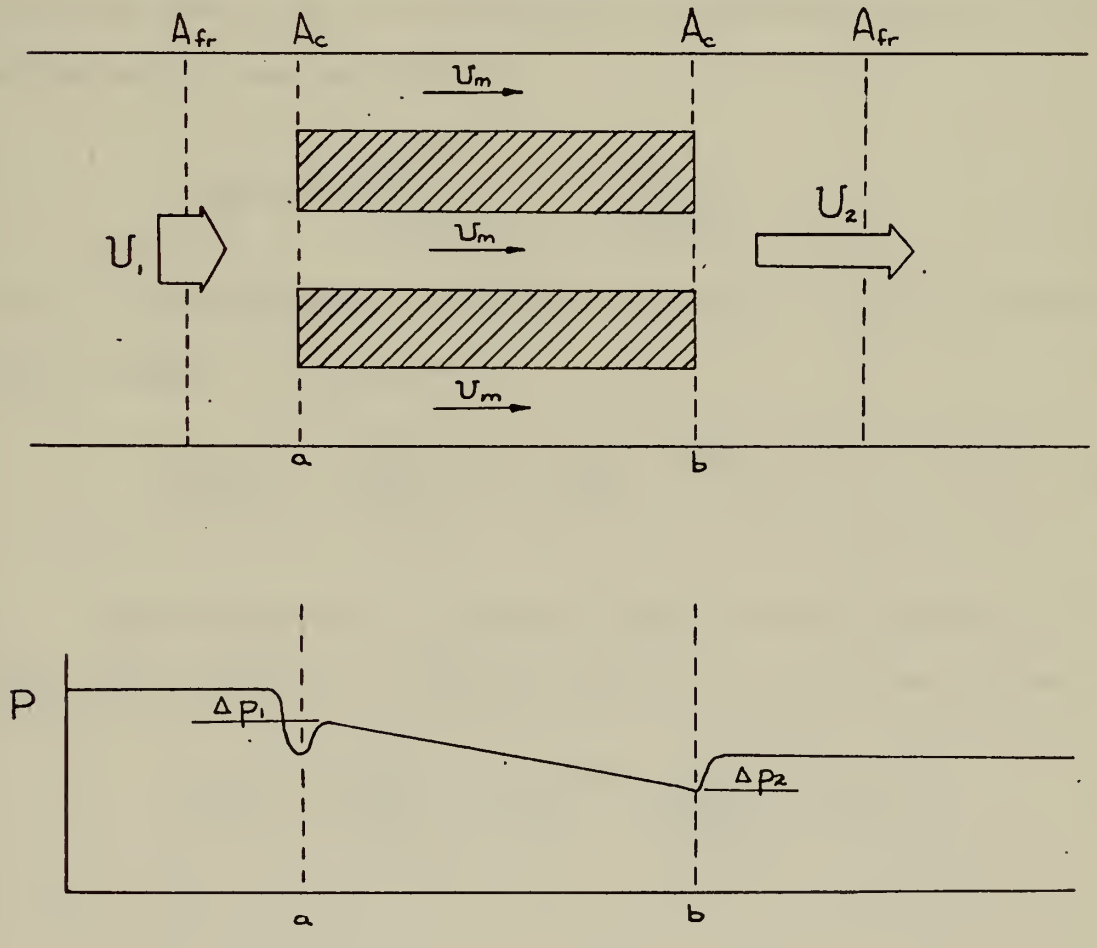

The pressure drop at entrance consists of two parts. First there is a pressure drop due to the decrease in the flow area, which from continuity results in a flow acceleration.

$$\Delta p = \frac{\rho}{2g_c}\left[U_1^2\right]\left[1-\left(\frac{A_c}{A_{fr}}\right)^2\right] = \frac{\rho U_1^2}{2g_c}\left[1-\beta^2\right] \tag{26}$$

Note that the identity (A_c/A_{fr}) equals the porosity (2) is strictly true only for the model which is porous to flow in only one direction. For the other two approaches this identity slightly overestimates A_c, since for these approaches the medium is porous to flow in three dimensions.

Second, there is a pressure loss caused by boundary layer separation, due to the irreversibilities of an abrupt contraction, and manifested by a vena contracta.

$$\Delta p = K_c \frac{\rho U_1^2}{2g_c} = K_c \frac{G^2}{2\rho_1 g_c} \tag{27}$$

where K_c is the empirical contraction coefficient. The total pressure loss at entrance is therefore:

$$(\Delta p)_1 = \frac{G^2}{2\rho_1 g_c}\left(1-\beta^2+K_c\right) \tag{28}$$

Similarly there is a pressure change at exit consisting of two parts. First, there is a pressure rise due to the increase in area:

$$-\Delta p = \frac{\rho U_2^2}{2g_c}\left(1-\beta^2\right) = \frac{G^2}{2\rho_2 g_c}\left(1-\beta^2\right) \tag{29}$$

Second there is a pressure loss due to the irreversibilities of a sudden expansion

$$\Delta p = K_e \frac{\rho U_2^2}{2g_c} = K_e \frac{G^2}{2\rho_2 g_c} \tag{30}$$

where K_e is the empirical expansion coefficient. The total pressure change at exit is the sum of (29) and (30):

$$(\Delta p)_2 = \frac{\rho U_2^2}{2g_c}(K_e - 1 + \beta^2) \tag{31}$$

$$= \frac{G^2}{2\rho_2 g_c}(K_e - 1 + \beta^2)$$

The remainder of the pressure drop across the heat exchanger is due to the overall fluid acceleration and the core friction. The pressure loss due to overall fluid acceleration is given by:

$$-\frac{dp}{dx} = \rho(x) u(x) \frac{du}{dx} \tag{32}$$

$$G = \rho(x) u(x) = \text{CONST.}$$

$$-\frac{dp}{dx} = [G] G \frac{d}{dx}(1/\rho) \tag{33}$$

$$(\Delta p)_{acc} = G^2 (1/\rho_1 - 1/\rho_2) \tag{34}$$

The pressure loss due to core friction defines the friction factor:

$$(\Delta p)_{CORE} = \frac{\rho U^2}{2g_c} f\left(\frac{A}{A_c}\right) \tag{35}$$

$$(\Delta p)_{CORE} \simeq \frac{G^2}{2\rho_m g_c} f\left(\frac{A}{A_c}\right) \tag{36}$$

After replacement of density by specific volume, the total pressure drop across the heat exchanger is:

$$(\Delta p)_{tot} = \frac{G^2}{2g_c} v_1 \left[(K_c + 1 - \sigma^2) - 2\left(\frac{v_2}{v_1} - 1\right) + f \frac{A}{A_c} \frac{v_m}{v_1} - (1 - \sigma^2 - K_e) \frac{v_2}{v_1} \right] \quad (37)$$

For the isothermal flow of a perfect gas, the pressure is inversely proportional to the specific volume and (37) may be solved for f in terms of pressures:

$$f = \left[2g_c \rho_m \left(\frac{\Delta P}{G^2}\right) - \frac{P_1 + P_2}{2} \left(\frac{K_c}{P_1} + \frac{K_e}{P_2}\right) - \left(\frac{P_1 + P_2}{2}\right)\left(\frac{1}{P_2} - \frac{1}{P_1}\right)(1 + \sigma^2) \right] \frac{A_c}{A} \quad (38)$$

For heat exchangers where there are successive contractions and expansions (such as fibrous materials) the entrance and exit coefficients are effectively lumped into the core friction factor [13]. Therefore in this study:

$$f = \left[2g_c \rho_m \left(\frac{\Delta P}{G^2}\right) - \left(\frac{P_1 + P_2}{2}\right)\left(\frac{1}{P_2} - \frac{1}{P_1}\right)(1 + \sigma^2) \right] \frac{A_c}{A} \quad (39)$$

For small pressure differentials, the first term in (39) is by far the greatest contributor to the friction factor. A further approximation then is:

$$\frac{P_1 + P_2}{2} = P_m \cong P_1 \cong P_2$$

$$f \cong \left[2g_c \rho_m \left(\frac{\Delta P}{G^2}\right) + \frac{\Delta P}{P_m}(1 + \sigma^2) \right] \frac{A_c}{A} \quad (40)$$

Equation (40) defines the Fanning friction factor for fluid flow in porous fibrous media.

2. Correlating Friction Factor, C_f:

Since the friction factor is the ratio of dissipative to inertial forces, the common practice in porous media studies is to divide the pressure gradient as given by Reynolds equation by one-half of the inertial term and define the quotient as a correlating friction factor [3, 9]:

$$C_f = \frac{\left(-\frac{dp}{dx}\right)}{\frac{1}{2}\frac{b\rho U^2}{g_c}} \tag{41}$$

Recall that the Reynolds number in terms of the permeability and tortuosity parameter is:

$$N_{Re} = \frac{U}{\nu}(Kb) \tag{25}$$

Substitution of Reynolds equation

$$-\frac{dp}{dx} = \frac{\mu U}{K} + \frac{b\rho U^2}{g_c} \tag{12}$$

into (41) yields

$$C_f = \frac{2g_c}{b\rho U^2}\left[\frac{\mu U}{K} + \frac{b\rho U^2}{g_c}\right] \tag{42}$$

$$C_f = 2\left[\frac{\mu g_c}{\rho U K b} + 1\right] \tag{43}$$

The kinematic viscosity is $\nu = \frac{\mu g_c}{\rho}$. Thus

$$C_f = 2\left[\frac{\nu}{UKb} + 1\right]$$

$$C_f = \frac{2}{N_{Re}} + 2 \tag{44}$$

It should be noted that $\rho U^2 = G^2/\rho$ and that therefore equation (41) for C_f might be written (with $\frac{dP}{dx}$ replaced by $\Delta P/L$)

$$C_f = \left\{2 g_c \rho_m \left(\frac{\Delta P}{G^2}\right)\right\}\left(\frac{1}{Lb}\right) \tag{45}$$

The term in braces is the first term in brackets in the expression for the Fanning friction factor, f, equation (40). Therefore the correlating friction factor is related to the Fanning factor by:

$$f = \left[Lb C_f + \frac{\Delta P}{P_m}(1+\rho^2)\right]\frac{A_c}{A} \tag{46}$$

C. HEAT TRANSFER

The parameters which characterize the ability of a surface to transfer heat include the heat transfer power per unit heat transfer area (h), and two non-dimensional forms of h: the number of transfer units (N_{tu}) and the Colburn j-factor. The heat transfer power per unit heat transfer area, h, is actually the experimental constant in Newton's Law of Cooling:

$$q = hA(\Delta T) \tag{47}$$

and is more commonly termed the "convective heat transfer coefficient." The number of transfer units, N_{tu}, is the ratio of heat transferred by the surface per unit of time to the thermal capacity rate of the fluid:

$$N_{tu} = hA/(\dot{m} c_p) \tag{48}$$

The Colburn j-factor is a heat transfer parameter based on Reynolds analogy and empirical observation which is found to behave in a nearly identical manner as the friction factor for most fully-developed internal flows [6]:

$$j = N_{St} N_{Pr}^{2/3} = N_{tu} \frac{A_c}{A} N_{Pr}^{2/3} \tag{49}$$

Due to instrumentation difficulties inherent with complex geometries, the usual steady state method of determining these characteristic parameters are generally unsatisfactory for compact heat exchanger surfaces, and it is necessary to resort to transient techniques. In this "first-cut" analysis of heat transfer from fibrous metals, the simplest such technique, the "single blow transient test" or "maximum slope" technique was used. This method has been amply described in references [2, 5, 11, 15, 16, 17, 19, 23, 24, 25, 29, 30, and 31].

The problem of analytically determining the fluid and solid temperatures as a function of position and time for a porous solid with constant initial temperature and step change in the fluid entering temperature was studied independently by Anzelius, Nusselt, Hausen, and Schumann between 1926 and 1929. The Anzelius solution is overly simplified, while Schumann's solution is valid only for liquids.

The approach of Hausen, however, appears to be valid for the problem at hand. If the fluid is flowing under the influence of a pressure gradient in one direction only, the problem may be lumped in the other two coordinate directions, and a one-dimensional energy balance may be made on a differential element of the solid.

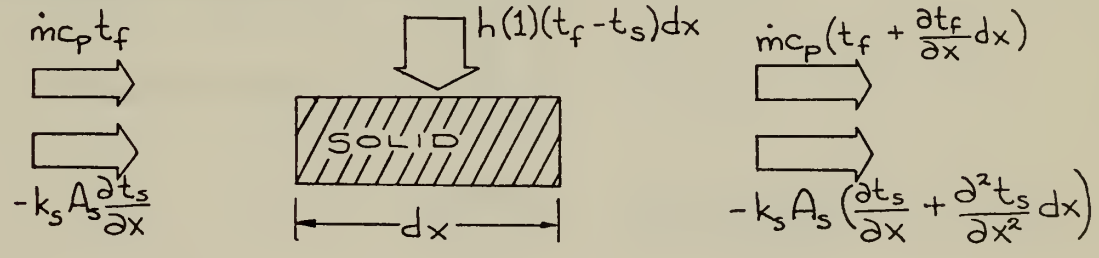

Assumptions made are:

a) Properties of the fluid are temperature-independent.

b) Fluid flow is steady.

c) Porous solid is homogeneous.

d) Thermal conductivities of both fluid and solid are infinite perpendicular to the fluid flow direction.

e) Thermal conductivity of fluid is zero in the flow direction.

The boundary conditions are:

a) The matrix is initially at uniform temperature.

b) At time equals zero there is a step change in the entering fluid temperature.

c) Matrix boundaries are adiabatic.

The energy terms (on a per unit time basis) are then:

a) Heat absorbed by solid $= \rho_s A_s c_s \left(\frac{\partial t_s}{\partial \theta}\right) dx$

b) Heat transferred to solid by convection $= h(1)(t_f - t_s)dx$

c) Heat transferred from the fluid by convection $= \dot{m} c_p \left(\frac{\partial t_f}{\partial x}\right) dx$

d) Heat transferred from solid by conduction $= -k_s A_s \left(\frac{\partial^2 t_s}{\partial x^2}\right) dx$

Therefore energy balances on the solid and fluid are:

$$\rho_s A_s c_s \frac{\partial t_s}{\partial \theta} dx = k_s A_s \frac{\partial^2 t_s}{\partial x^2} dx + h(1)(t_f - t_s)dx \tag{50}$$

$$\dot{m} c_p \frac{\partial t_f}{\partial x} dx + h(1)(t_f - t_s)dx = 0 \tag{51}$$

The following non-dimensional variables are now introduced:

a) Reduced length, $Z = \frac{hA}{\dot{m} c_p}\left(\frac{x}{L}\right) = N_{tu}\left(\frac{x}{L}\right)$

b) Generalized time, $T = \frac{hA}{W_s c_s}\left[\theta - \frac{W_f x}{\dot{m} L}\right]$

$$= \frac{hA}{W_s c_s}\theta - \frac{hA W_f c_p x}{\dot{m} W_s c_s c_p L}$$

c) Longitudinal conduction parameter, $\lambda = \frac{k_s A_s}{\dot{m} c_p L}$

Since the thermal capacity of the fluid ($W_f c_p$) within the solid matrix at any instant of time is much less than the thermal capacity of the solid, the second term in the definition of is negligible compared to the first. Therefore,

$$T \cong \frac{hA}{W_s c_s} \theta \tag{52}$$

In terms of λ, Z, and T equations (50) and (51) become:

$$\frac{\partial t_s}{\partial T} = \lambda N_{tu} \frac{\partial^2 t_s}{\partial Z^2} + (t_f - t_s) \tag{53}$$

$$\frac{\partial t_f}{\partial Z} = t_s - t_f \tag{54}$$

For the case of zero longitudinal conduction (i.e., $\lambda = 0$), the above equations become simply:

$$\frac{\partial t_s}{\partial T} = t_f - t_s \tag{55}$$

$$\frac{\partial t_f}{\partial Z} = t_s - t_f \tag{56}$$

This system of differential equations, subject to the initial and boundary conditions previously specified may be solved analytically using Bessel functions. Theoretical fluid temperature - time curves at constant Z (in particular at the matrix exit, where $Z = N_{tu} \frac{L}{L} = N_{tu}$) may be plotted. To determine the N_{tu} of a heat exchanger surface, the experimental temperature-time history at the matrix exit is matched to one of the family of theoretical curves. This procedure is not only tedious, but also depends on the assumption of zero longitudinal conduction.

In 1950 Locke [19] eliminated the necessity of matching experimental and theoretical curves. A new time variable is defined:

$$\mu^* = \tau / N_{tu} \tag{57}$$

He differentiated the analytical solution to Hausen's equations (retaining the assumption $\lambda = 0$) and evaluated the derivative at the matrix exit ($Z = N_{tu}$):

$$\frac{d}{d\mu^*}\left\{\frac{t_{f_2} - t_i}{t_{f_1} - t_i}\right\} = \frac{N_{tu}}{\sqrt{\mu^*}}\left\{-J_1\left(2iN_{tu}\sqrt{\mu^*}\right)\right\} e^{-N_{tu}(1+\mu^*)} \tag{58}$$

where t_{f_2} = fluid exit temperature for $\mu^* > 0$, t_{f_1} = fluid exit temperature for $\mu^* < 0$, and t_i = steady state temperature. Locke showed that as long as the change in the fluid entry temperature is a step change (and longitudinal conduction is zero), the N_{tu} of a heat exchanger surface is uniquely related to the maximum slope of the temperature-time curve (i.e., the maximum value of (58)) at the matrix exit, hence the name "maximum slope technique."

Although the assumption of zero longitudinal conduction is essentially valid at large flow rates (i.e., high Reynolds numbers), it is quite invalid at low Reynolds numbers for most surfaces. If these longitudinal conduction effects are included in the analysis, the maximum slope is a function of λ as well as N_{tu}. With finite difference techniques, Howard [11] has included these effects and has tabulated (Table II) and plotted (Figs. 1,2) maximum slope as a function of N_{tu},λ). However, for fibrous metals such as steel wool, it is felt that any possible longitudinal conduction path would be too lengthy for there to be any pronounced effect. Thus in this study Howard's results are used only for the special case of $\lambda = 0$.

Kohlmayr [15, 17] showed that the maximum slope technique may be inaccurate for $3.0 > N_{tu} > 2.0$, unstable for $N_{tu} < 2.0$, and is singular at $N_{tu} = 2.0$ (Fig. 3). He proposed an indirect curve matching technique based on the first moments of the areas under the experimental and theoretical temperature-time curves to circumvent this difficulty [16]. Moreover, this "centroid technique" is not restricted to step changes in the fluid entry temperature. As will be mentioned in the Experimental Techniques section, in this study the step change is approximated by securing the electrical power to the heaters in the flow stream. The actual response of the air is exponential rather than stepped and therefore Kohlmayr's centroid technique could be used to correct this deviation from Locke's idealizations. However, Bruno [5] has studied the various transient testing techniques and reports that there is no measurable improvement in the results by using the centroid techniques for $N_{tu} > 3.5$. Due to the expected large surface area and restricted flow rate through fibrous metals, it was felt that all N_{tu} values would exceed 3.5, thereby eliminating the need to correct for deviation from step.

Thus the heat transfer parameters N_{tu}, j, h for fibrous metals were determined in this study by Locke's maximum slope technique, subject to the assumptions of exact step change in the fluid temperature, and zero longitudinal conduction.

III. DESCRIPTION OF SURFACES

Steel wool was selected as a representative fibrous metal. Steel wool is low carbon bessemer wire with high tensile strength. It may be a continuous piece up to 100,000 feet long. It usually has three edges, but may have five [4]. The federal government has set specifications on the fiber size and type of steel for seven grades between 0000 and 3. The restrictions on fiber size are listed in Table I [7].

TABLE I. *Thickness requirements for individual fibers*

Class	Not more than 5 percent under	Mean width of fiber	Not more than 5 percent over	No fiber to exceed
	Inch	*Inch*	*Inch*	*Inch*
0000	—	0.0006—0.0010	0.003	0.006
000	—	.0008— .0013	.004	.008
00	—	.0012— .0022	.005	.010
0	0.0003	.0016— .0024	.007	.012
1	0.0005	.0018— .0026	.010	.015
2	0.001	.0040— .0060	.014	.025
3	.002	.0070— .0095	.018	.040

Grades 0000 through 0 must be low carbon steel. Grades 1 through 3 may be low carbon steel or AIST 430 stainless steel.

Grades 00, 0, 1, and 3 were selected for testing. In the case of Grades 1 and 3 the type of steel was determined by a simple test. The plain carbon steel will take the copper out of a $CuSO_4$ solution, while AlSl 430 stainless steel will not. All grades tested were plain carbon steel. Sample fibers of the four grades were examined under a microscope with a movable platform. With the cross-hairs in the eyepiece and the platform movement control dial (graduated in hundredths of a millimeter) the fibers were checked against the federal specifications. Cross-sections of each fiber were examined to determine if the samples were three or five sided. All samples indeed were three sided. In particular, the samples of Grades 00 and 1 (which were

manufactured by the Brillo Corporation) appeared to have a very nearly equilateral cross-section.

Such an equilateral cross-section was assumed for all grades tested, with side length equal to the average of the range of mean widths of the fiber quoted in the federal specifications. (Table I). The volume of the material in each sample is equal to the weight of the sample divided by the density of the steel. The assumed cross-section and volume of steel specify the heat transfer area, A. (See Appendix B).

The steel wool was tested at essentially the same porosity as that with which it is packaged. The porosity may be crudely estimated from article 5.1.1 of [7] which states that one pound of steel wool shall be packaged in a sleeve approximately four inches in diameter and fourteen to sixteen inches long. Based on a density for plain carbon steel of 490 lbm/ft^3 [18], the porosity should be between 0.979 and 0.983. The porosity may be more precisely determined from the weight of the sample tested and the volume of the test cell in which it was packed. The free flow area is approximately determined from the porosity.

Complete geometrical descriptions of each sample, based on the assumptions stated, are found in Figs. 13, 15, 17, & 19.

A core known as Solar No. 4 tested by Bruno [5] was also tested to insure the reliability of the reconstructed apparatus.

IV. EXPERIMENTAL TECHNIQUES

The single blow transient test apparatus (Figs. 4,5) was designed to conform to the assumptions made for the analytical solution of the heat transfer problem (equations (50) and (51)). These idealizations are:

1. The velocity and temperature profiles of the fluid flow at any cross-section in the matrix are both steady and uniform.

2. The thermal conductivity of the matrix is finite (or zero) in the direction of the fluid flow and infinite in the direction normal to the flow.

3. The thermal capacity of the matrix is much greater than that of the fluid contained within it.

4. The thermal properties of the fluid and matrix are both constant and uniform.

5. The convective heat transfer coefficient is some suitable average and remains constant.

6. A step change in the inlet fluid temperature occurs at real time equals zero.

A specially designed nozzle, flow-straightening screens, and an even distribution of heater wires across the channel insure that the first assumption (i.e., uniform velocity and temperature profiles) is satisfied. Piersall [23] made velocity and temperature traverses at the matrix inlet section over the entire flow range and concluded that the velocity profiles were indeed uniform and that the temperature profile varied by no more than $\pm$ 0.5°F. Wheeler [31] has demonstrated the importance of the uniformity of these profiles.

For fibrous metals it is assumed that there is no effective solid area, A_s, available for longitudinal conduction. This has the same

effect as assuming zero matrix conductivity in the flow direction and therefore satisfies the second assumption.

As long as the fluid is restricted to gases, the assumption of negligible fluid thermal capacity compared to matrix thermal capacity is justified. It must be noted that the testing procedures and results of this study are not applicable to liquids.

By limiting the temperature rise to 20°F the assumption of constant properties is met. The worst offender is the viscosity, which may vary by as much as $\pm$ 1.5 percent from its value at the mean temperature. The limited temperature rise also insures that the convective coefficient, h, is effectively constant.

As has been discussed in Section II, the assumption of a step change in the fluid inlet temperature cannot be precisely satisfied. In the current testing method the step change is simulated by turning off the heaters. This actually leads to an exponential decay in the air temperature. Techniques are available to compensate for this deviation from step change, but Bruno [5] has indicated that these corrections are not required for $N_{tu} > 3.5$. Since it was expected that the N_{tu} range experienced would exceed this value, no effort was made to so compensate.

The data required for the computation of the various heat transfer and flow friction parameters is as follows:

P_{atm} - atmospheric pressure (inches Hg)

P_o - orifice static pressure (inches H_2O)

ΔP_o - pressure drop across orifice (inches H_2O)

ΔP_m - pressure drop across matrix (inches H_2O)

P_m - static pressure at matrix inlet (inches H_2O)

t_o - fluid temperature at orifice (millivolts)

d_o - orifice diameter (inches)

$\bar{\beta}$ - ratio of orifice diameter to pipe diameter

CS - chart speed (millimeters/second)

t_3-t_1 - downstream temperature response (mm)

Pressures were measured with water manometers and checked with inclined gages where the flow rates and orifice plates permitted. An exception was the atmospheric pressure, which was measured with a mercury barometer.

Only the matrix downstream temperature response, (t_3-t_1), was measured, although the upstream temperature (t_2-t_1) was monitored to check for the 20°F temperature rise from the heaters. A more complete description of the equipment and instrumentation is furnished in Appendix A. A sample output is shown in Fig. 6.

Because the turbocompressor which induces the draft through the apparatus, would not function for much more than seven minutes without overheating and tripping the circuit breaker, and because of the importance of isothermal flow to the permeability studies, the friction factor data runs were made separately from the heat transfer data runs. This was in contrast to previous studies where the friction factor data was collected immediately after the heat transfer data.

For a heat transfer data run the pressure drop across the ASME standard orifice plate corresponding to the desired mass flow rate was predetermined. The number of heaters required to achieve a 20°F temperature rise at that flow rate was also predetermined. When the desired pressure drop had been obtained, the recorder pens were zeroed, and the heaters were energized. The (t_2-t_1) channel indicated immediately whether the 20°F rise has occurred. When the core had reached

a steady state temperature (as indicated by the (t_3-t_1) trace) all pressure measurements and the orifice temperature were recorded. The heaters were then de-energized and the transient temperature response downstream of the matrix (t_3-t_1) was recorded. After the completion of the run the maximum slope was visually determined with a straight edge from the recorder output and entered in the data sheet. The data sheet conformed to the input format for a digital computer program written by Trost [30] and modified for fibrous media, which reduced the data. (See Appendix B).

A friction factor data run has made in the same manner as a heat transfer data run except that no heaters and therefore no recorder were required.

V. PRESENTATION OF RESULTS

For each of the four grades of steel wool tested, the heat transfer and flow friction characteristics have been computed and appear in Tables III to X. Although Fanning friction factors were computed for the heat transfer data runs (Tables VII to X), the flow state at the time of measurement cannot be guaranteed to have been isothermal (particularly at low flow rates). For this reason the friction factor results in Tables III to VI are preferred, since these runs were made without the heaters and are the basis for the permeability analysis. The Colburn j factor is plotted as a function of N_{Re} for each sample. The values of N_{tu} and h as a function of N_{Re} appear in Tables VII to X.

Figure 7 is a plot of the friction data in the form of (23). Figure 8 is the same plot in the form of (13). From these plots the sample permeabilities and tortuosity parameters are determined. This information is prerequisite for the selection of a length parameter for the Reynolds number and therefore appears first in the results. Figures 9, 10, and 11 plot the Fanning friction factor, f, as a function of N_{Re} based on the three different approaches attempted. The correlating friction factor, C_f, is plotted against N_{Re} based on Kb in Figure 12.

Figures 13, 15, 17, and 19 contain the geometric and physical characteristics of the four samples. Figures 14, 16, 18, and 20 graphically present the heat transfer and flow friction characteristics (i.e., j and f versus N_{Re} based on Kb) for each grade of steel wool. Figure 21 compares the j values of the various cores as a function of N_{Re} based on Kb. Figure 22 compares the heat transfer power per unit of area of each core as a function of the friction power per unit of area.

VI. DISCUSSION OF RESULTS

A. RELIABILITY OF APPARATUS

The Solar No. 4 core previously tested by Bruno was tested in the reconstructed apparatus to insure its reliability. An unsatisfactory amount of electrical noise was present in the thermocouple signals, apparently due to a combination of the unshielded 0.001 inch thermocouples (Appendix A), ultra-sensitive Brush amplifier, Variac power supply, and Physics Department linear accelerator, located immediately below the apparatus. With this system, N_{tu} values were found to deviate by as much as 23 percent and generally 12 percent from Bruno's plot. The installation of a more sensitive reference junction (see Appendix A) may be part of the explanation. Friction factor results deviated by as much as 12 percent and were consistently 7 to 8 percent higher than Bruno's plot.

Since the uncertainties were $\pm$ 7 to 9 percent in N_{tu} values, $\pm$ 2 percent in N_{Re} values, and $\pm$ 3 percent in f values for Bruno [2, 5] and somewhat higher in the reconstructed system due to the previously mentioned difficulties (see section on experimental uncertainties), it was felt that these results constituted satisfactory agreement. In other words, the problem was not felt to be with the thermocouples, and the research proceeded.

Subsequently a less sensitive amplifier-recorder system was installed, the Variac was replaced by a motor-generator DC source, and testing was performed when the linear accelerator was not in operation. Also a more elaborate manometer system was installed (Appendix A).

B. PERMEABILITY ANALYSIS

The permeabilities and tortuosity parameters for the four samples were determined by means of a first order polynomial least squares curve through the data plotted in the forms suggested by both (13) and (23). The former equation assumes isothermal, incompressible flow with a constant pressure gradient. This technique was used by Beavers and Sparrow in their study of water flow through porous, fibrous media [3]. The latter equation assumes isothermal flow of a perfect gas, but is not restricted to incompressible flow or constant pressure gradients. The permeabilities computed by the second method are on the order of one percent higher than those computed by the first method for the four samples examined. Therefore, compressibility effects are considered to be negligible in the computation of permeabilities and tortuosity parameters. This is not unexpected, since the maximum change in the pressure across the cores tested did not exceed 50 inches of water.

In Fig. 7 the results of the second type of analysis (i.e., compressibility effects included) are plotted. With the possible exception of grade 1, a straight line plot is a reasonable curve through the data points. Outside of the data points corresponding to very small flow rates (where the relative error in the pressure measurements is large) and those corresponding to very large flow rates (where the absolute error is large, due to fluctuations in the flow), the maximum deviation of the data points from the linear least squares plot is 11 percent. This is not nearly as good as the 2.5 percent maximum deviation reported by Beavers and Sparrow in [3]. However, their study was for the flow of an incompressible fluid (water) over a velocity span of 20:1, with 14 pressure taps, cathetometer, calming reservoirs, and direct flow

measurement. In this study the fluid was compressible, the velocity span was nearly 200:1, with indirect flow measurement (orifice plates), 2 taps, water manometers read by eye, and no calming reservoirs. With all this taken into consideration, Fig. 7 might be considered to be in adequate agreement with the empirical Reynolds equation (10).

Conversely, the data points show a marked concavity rather than random deviation from the linear least squares plot. This would indicate the presence of higher order terms than those in (10). Recall that Forchheimer proposed the addition of a cubic term to Reynolds equation, but that the coefficient was usually so small that the term was negligible except at very large velocities. In light of this and the extensive velocity range encountered in this study, a second order polynomial least squares curve was passed through the data points plotted according to the manner suggested by equation (13). (Hereafter compressibility effects are ignored.) The results appear in Fig. 8 along with the linear least squares curve. In general the data points deviate from the second order least squares curve by less than half the amount of deviation from the linear curve. This is considered to be strong justification for the replacement of Reynolds equation (10) by Forchheimer's equation:

$$-\frac{dp}{dx} = \frac{\mu U}{K} + \frac{b\rho U^2}{g_c} + c^* U^3 \tag{59}$$

The second order polynomial least squares curves plotted in Fig. 8 are representations of (59) recast in the following form:

$$-\rho\frac{dp}{dx} = \frac{\mu(\rho U)}{K} + \frac{b}{g_c}(\rho U)^2 + c^*\rho U^3 \tag{60}$$

$$-\rho\frac{dp}{dx} = \mu\frac{(\rho U)}{K} + \frac{b}{g_c}(\rho U)^2 + \left(\frac{c\rho^2}{g_c^2\mu}\right)(\rho U^3) \tag{61}$$

$$-\rho\frac{dp}{dx} = \mu\frac{G}{K} + \frac{b}{g_c}G^2 + \frac{c}{g_c^2\mu}G^3 \tag{62}$$

$$-\frac{\rho}{G\mu}\frac{dp}{dx} = \frac{1}{K} + b\left(\frac{G}{\mu g_c}\right) + c\left(\frac{G}{\mu g_c}\right)^2 \tag{63}$$

where compressibility effects have been neglected and

$$c^* = c\rho^2/(g_c^2\mu) \tag{64}$$

$$c^* = c\rho/(g_c\gamma) \tag{65}$$

It is not clear what physical significance this additional term has, but it evidently involves a coupling of inertial and viscous effects and is probably dependent on the fluid. Dimensional analysis shows that c* has units of (force-time^3/length^6) and that c is dimensionless.

The particular results from Fig. 8 are:

Grade Steel Wool	Permeability K (ft^2)	Tortuosity Parameter, b (1/ft)	c
00	0.479×10^{-7}	416.8	-9.57×10^{-4}
0	0.718×10^{-7}	243.1	-3.02×10^{-4}
1	1.50×10^{-7}	201.4	-3.98×10^{-4}
3	6.51×10^{-7}	61.51	-0.512×10^{-4}

From these results the characteristic length parameters (Kb) are 0.0000199 ft., 0.0000167 ft., 0.0000302 ft., and 0.0000346 ft. for Grades 00, 0, 1, and 3 respectively.

The presence of this cubic term raises questions regarding the derivation of the Reynolds number based on the product of the permeability and a tortuosity parameter (25) where one term was said to embody all the viscous effects while the other embodied all the inertial effects. It is now evident that there is a third term which may involve both effects. Nevertheless, the whole procedure was an approximate one, and if the resulting Reynolds number correlates the data there is no point in questioning the validity of the derivation.

C. CORRELATING LENGTH PARAMETER AND FRICTION FACTOR

The Fanning friction factor, f, was chosen as the test for the proper length parameter to be used in Reynolds number. Once the hydrodynamic correlation was obtained, it was thought that the heat transfer correlation would involve the same length parameter. In Fig. 9 a correlation of f and N_{Re} is attempted based on a flow passage hydraulic diameter from the model porous to flow in one direction. In Fig. 10 the same correlation is attempted based on the crossed-rod matrices model. Figure 11 is the same correlation based on the product Kb.

It is evident that the second model is better than the first in that the curves are somewhat closer together. However the plot of the curves f versus N_{Re} based on Kb represents the tightest grouping. In particular note that the curves for Grades 00 and 0 practically coincide. These two grades had practically the same characteristic length (1.99×10^{-5} ft. and 1.67×10^{-5} ft. respectively). The same is true of the curves for Grades 1 and 3 which also have comparable characteristic lengths (3.02×10^{-5} ft. and 3.46×10^{-5} ft. respectively). This is considered to be a clear indication of the superior correlation to be had by using a characteristic length equal to the product of the medium permeability, K, and the medium tortuosity parameter, b.

The fact that a perfect correlation was not obtained in Fig. 11 may be partly explained by the inverse proportionality between f and the heat transfer area, A. This area has the largest uncertainty of any variable in the study (see section on experimental uncertainties).

The correlating friction factor, C_f, is plotted against N_{Re} in Fig. 12. As was demonstrated in the section on theory, if Reynolds equation (10) is valid then C_f is automatically determined by the Reynolds number based on Kb:

$$C_f = 2/N_{Re} + 2 \tag{44}$$

The data points show adequate agreement with (44) for Reynolds numbers less than one. However, for Reynolds numbers greater than unity, equation (44) is seen to over-estimate C_f as defined by equation (41). This is no surprise, since there appears to be a cubic term in the empirical equation for the pressure gradient. This cubic term is insignificant except at large velocities, which explains the deviation of the data points from the theoretical curve in Fig. 12 at high Reynolds numbers.

D. HEAT TRANSFER AND FLOW FRICTION CHARACTERISTICS

The heat transfer (j) and flow friction (f) characteristics of Grades 00, 0, 1, and 3 are presented in Figs. 14, 16, 18, and 20 respectively and in Tables III to X. Table VII shows that for Grade 00 when $j < 0.00675$, the corresponding value of N_{tu} is less than 3.0, where the maximum slope method is highly unreliable. Similarly for Grade 0 when $j < 0.0118$ and Grade 3 when $j < 0.0579$. All heat transfer results which fall in these ranges must be disregarded, due to the high uncertainty in the N_{tu} values.

Also the (t_3-t_1) traces for all but the last five sets of Grade 00 data had an excessive amount of noise, and the determination of the maximum slope was at best a crude process. Inasmuch as the "noise" died off as the flow rate increased, it is thought that it is actually the random fluctuations in the temperature, similar to the fluctuations observed when the test section was removed and only the quiescent ambient air temperature was recorded. This is perhaps indicative of some flow disorder downstream of the Grade 00 sample, but there is insufficient information to draw any firm conclusion. Thus all but the data points taken at the five largest flow rates for Grade 00 must be regarded as qualitative only.

The Colburn j-factor is the result of an empirical correction to the Reynolds analogy for non-unit Prandtl numbers [6]. The Reynolds analogy assumes that for fully developed flow (particularly turbulent internal flows), the hydrodynamic and thermal boundary layers are similar. Therefore the heat flux at a surface is proportional to the shear stress at that same surface for a given fluid [8]. Thus the Stanton number is proportional to the friction factor and the curves of f and j as functions of Reynolds number are parallel.

In previous studies of compact heat exchanger surfaces, the flow passages were well defined channels, and the parallel behavior of the f and j factors predicted by Reynolds analogy (with Colburn's correction) was clearly observed [29]. This was not found to be the case for any of the four samples tested (Figs. 14, 16, 18, & 20). Whereas the friction factor was found to decrease with increasing Reynolds number, the j factor was found to rise to a maximum and then taper off. Figure 21 indicates that this peak in the j factor occurs between Reynolds numbers (based on Kb) of 0.5 and 1.5

There are three possible explanations for this anomalous behavior:

1. Experimental error
2. Longitudinal conduction effects
3. Thermal boundary layer does not behave in the same fashion as the hydrodynamic boundary layer.

If the cause were experimental error, then it would have to be a systematic error, as all the cores behave in a similar manner. Trost [30] observed the same sort of behavior for Solar No. 1, Solar No. 6, Stainless Steel Plate-Fin reference matrix, and the entire series of brass cores (with varying L/r_H ratio). He could offer no explanation, and none can be offered here from a systematic error viewpoint. It might also be noted that no such behavior (i.e., a peaking of the j curve) was observed during the testing of the Solar No. 4 core. This would seem to rule out systematic error as a cause.

The inclusion of non-zero longitudinal conduction would tend to shift the low flow rate portion of the j curve up to where it would be more nearly parallel to the f curve, as demonstrated by Ball [2]. It has already been established that an improper assumption of $\lambda = 0$ will cause substantial error in the heat transfer results at low flow rates. However, the small cross-section to surface area ratio and the sinuous path of the fibers make it difficult to conceive of such a mechanism at work in fibrous materials. A simple experiment to test this conclusion is discussed in the section on suggestions for further investigation.

The third explanation is the most plausible. When the thermal boundary layer no longer behaves analagously to the hydrodynamic boundary layer, the Reynolds analogy is clearly invalid. This frequently happens in external flows, where the turbulence induced by

the body contributes to the drag on the body, but only the skin friction is important for the transfer of heat. Significantly, Colburn [6] noted that "the use of a friction line for predicting heat transfer would be very unsafe for flow across tubes." In particular, when separation occurs, it is well known that the j and f factors no longer behave in the same manner [18]. Inasmuch as effects similar to separation have been postulated as the cause of non-Darcy flow [3, 9, 12, 26, & 27] and inasmuch as virtually all the data runs were in the non-Darcy regime, the occurrence of separation or similar phenomenom would seem to be the most probable explanation for the failure of the f and j curves to behave in a parallel fashion.

Figure 21 was an attempt to see how well the j factor for the four samples was correlated with a Reynolds number based on Kb. There is really too much scatter in the data to draw any firm conclusions. The j factor, like the friction factor, is inversely proportional to the heat transfer area, A. By the same reasoning as before, if A were more precisely known, the curves might be more closely grouped. It is of interest to note that Trost [30] experienced the same inability to correlate j with N_{Re} (based on a well-defined channel hydraulic radius) for six different brass cores.

Figure 21 also shows that the optimum Reynolds number for steel wool as a heat exchanger (neglecting friction considerations) is in the vicinity of $N_{Re} = 1$, since the j factor is a maximum. Therefore more heat is transferred per pound of air flow in that range of Reynolds numbers, hence the term optimum N_{Re} for heat exchange.

A figure of merit in evaluating heat exchanger surfaces is the heat transfer power at a given friction power level (all evaluated at standard

conditions of 500°F and 1 atmosphere), as in Fig. 22. The higher a curve is on such a plot, the better the surface it represents is as a heat exchanger. Under the conditions of an assumed average equilateral cross-section for each fiber (from which the total heat transfer area is computed), and the assumption of operation at standard conditions, Fig. 20 indicates that Grade 3 steel wool is the best surface of those tested. It appears that the higher the grade, the better it is as a heat exchanger. All grades of steel wool tested were evidently better heat exchangers (on a per unit area basis) than was Solar No. 4, which was also plotted.

VII. EXPERIMENTAL UNCERTAINTIES

No attempt was made to evaluate errors arising from failure to satisfy the idealizations discussed in Section IV.

The remaining sources of error are uncertainty in physical constants, inaccuracy in geometrical measurements, instrumentation error, and error in the permeability analysis. The method of Kline and McClintock [14] was used to determine the uncertainty in the final results.

A. UNCERTAINTY IN PHYSICAL CONSTANTS

Values for the physical constants of plain carbon steel were obtained from [18], while those for air were from [10]. The uncertainties (as defined by [14] and different from percentage error) in these values appear to be [23]:

$$\rho_s : \pm 0.5\%$$

$$c_s : \pm 0.5\%$$

$$c_p : \pm 0.5\%$$

$$N_{Pr} : \pm 2.0\%$$

$$k_s : \pm 0.5\%$$

$$\mu : \pm 1.5\%$$

The thermal conductivity, k_s, appears only in the longitudinal conduction parameter, λ, which in this study is assumed equal to zero. Since the material of construction is specified only as plain carbon steel, there is a fairly wide latitude in the value of ρ_s and in particular, c_s. The latter may be a major cause of inaccuracy [19].

B. GEOMETRICAL MEASUREMENT INACCURACIES

Contrary to previous studies, this area is a major source of error due to the deformable nature of fibrous media and the randomness of the internal geometry. The porosity of the sample seems to have the least uncertainty, since it was determined by two independent (though approximate) methods (see Section III) which agree to within one percent. There is variation in the length of the matrix (L) across its cross-section. This length also varies with flow rate because a certain amount of deformation occurs as the vacuum downstream grows larger. The free flow area, A_c, depends on the approach taken to the Reynolds number and the uncertainty in it is therefore a function of the accuracy of the approach. The crossed-rod matrices model yields a value of A_c approximately 3% less than that computed by the other two methods. The heat transfer area, A, has the largest uncertainty due to its extreme sensitivity to the assumed fiber cross-section. There is an uncertainty of 25% just in the selection of a mean fiber width. The assumption of 30% uncertainty in A may even be optimistic. However, as noted by London [20] errors in such geometrical measurements do not affect the numerical accuracy of the N_{tu} results. The Colburn j factor and convective heat transfer coefficient, h, are affected, but the same results may be obtained if future work on geometrically similar surfaces is based on the same geometrical assumptions.

The uncertainties assumed for the various geometrical measurements are:

$$\rho : \pm 1.0\%$$

$$L : \pm 3.0\%$$

$$A_{fr} : \pm 1.0\%$$

A_c : $\pm$ 5.0%

A : $\pm$ 30.0%

W_s : negligible

(W_s is the weight of the matrix).

C. INSTRUMENTATION ERROR

Instrumentation errors were primarily due to the pressure measurements. The uncertainties suggested by Piersall [23] for the various pressure measurements were not justified based on experience in this study of fibrous media. The following uncertainties are suggested in lieu of Piersall's values:

P_o: $\pm$ 2.0%

ΔP_o: $\pm$ 2.0%

ΔP_m: $\pm$ 2.5%

P_m: $\pm$ 2.5%

P_{atm} negligible.

The orifice temperature was measured with a sheathed copper-constantan thermocouple and read by a Leeds and Northrup potentiometer. Based on the manufacturer's calibration of the thermocouple, the estimated error is $\pm$ one-half of the smallest potentiometer gradation, or about $\pm$ 0.0025 millivolt (approximately $\pm$ 0.1°F). The transient temperature response (t_3-t_1) was measured directly from the recorder output in millimeters. The assumed uncertainty in the maximum slope thus measured is $\pm$ 3.0%.

Since the N_{tu} determined is a function solely of the maximum slope (for $\lambda = 0$), it is appropriate to evaluate the uncertainty at this point. The bulk of the N_{tu} values were in the range $22 > N_{tu} > 5$. From Fig. 3

for $\lambda = 0$ and an uncertainty in the maximum slope of 3%, the uncertainty in the N_{tu} is between 3.3% ($N_{tu} = 22$) and 3.75% ($N_{tu} = 5$). A few values of N_{tu} were in the vicinity of 2.0, where the uncertainty in the N_{tu} is indeterminate. These results must therefore be regarded with skepticism.

D. PERMEABILITY ANALYSIS ERROR

Although primary data was used in the determination of the permeability, K, tortuosity parameter, b, and cubic coefficient, c, of each grade, the uncertainty limits cannot be found by the method of Kline and McClintock, since these quantities are not the result of single or multiple sample experiments, but rather a least squares curve fitting. The uncertainties in K, b, and c are a function of the spread (i.e., uniform distribution over the mass flow range) and number of data points, as well as the accuracy of the individual points. For these reasons the relative uncertainties in K, b, and c at 20:1 odds must be estimated:

K: $\pm$ 10%

b: $\pm$ 10%

c: $\pm$ 25%.

E. RESULTS

The basic formula for the uncertainty w_R in result $R(V_1, V_2, \ldots V_n)$ at specified odds is:

$$w_R = \left[\left(\frac{\partial R}{\partial V_1} w_1\right)^2 + \left(\frac{\partial R}{\partial V_2} w_2\right)^2 + \ldots + \left(\frac{\partial R}{\partial V_n} w_n\right)^2\right]^{1/2} \quad (66)$$

where $w_1, w_2, \ldots, w_n$ are the uncertainty intervals at the same specified odds for the n variables of which R is a function. Note that w_R has the units of R. If the n variables appear in some form in the formula for

R as factors, rather than addends, simplification in (66) results from dividing through by R.

Consider, as an example, the evaluation of the uncertainty in the mass flow rate, $\dot{m}$. (See Appendix B for the origin of the following equation):

$$\dot{m} = (\text{constant}) \cdot \left[\Delta P_o \left(\frac{P_{atm} - P_o}{T_o} \right) \right]^{1/2} \tag{67}$$

Let $P_3 = P_{atm} - P_o$. With (66):

$$w_{\dot{m}} = (\text{CONST}) \cdot \left[\frac{P_3}{T_o} \left(\frac{1}{2} \frac{w_{\Delta P_o}}{\sqrt{\Delta P_o}} \right)^2 + \frac{\Delta P_o}{T_o} \left(\frac{1}{2} \frac{w_{P_3}}{\sqrt{P_3}} \right)^2 + \Delta P_o P_3 \left(-\frac{1}{2} \frac{w_{T_o}}{T_o^{3/2}} \right)^2 \right]^{1/2} \tag{68}$$

Divide through (68) by (67):

$$\frac{w_{\dot{m}}}{\dot{m}} = \left[\frac{1}{4} \left(\frac{w_{\Delta P_o}}{\Delta P_o} \right)^2 + \frac{1}{4} \left(\frac{w_{P_3}}{P_3} \right)^2 + \frac{1}{4} \left(\frac{w_{T_o}}{T_o} \right)^2 \right]^{1/2}$$

The following relative uncertainties (i.e., $\frac{w_i}{v_i}$) have already been postulated (based on 20:1 odds):

$$\left(\frac{w_{P_3}}{P_3} \right) = \left(\frac{w_{P_o}}{P_o} \right) = 0.02$$

$$\left(\frac{w_{\Delta P_o}}{\Delta P_o} \right) = 0.02$$

$$\left(\frac{w_{T_o}}{T_o} \right) < 0.0015 \qquad \text{(negligible)}$$

Therefore the relative uncertainty in the mass flow rate is:

$$\left(\frac{w_{\dot{m}}}{\dot{m}} \right) = \pm 1.4\%$$

In a similar manner, the relative error in the mass flux G is found to be 1.7%.

There is no reason to compute the uncertainty in the Reynolds number based on either the uni-dimensional porosity or crossed-rod matrices models, as these are completely artificial concepts. Conversely, the Reynolds number based on the product Kb does have physical significance (i.e., there is a correct value). The uncertainty for this Reynolds number is:

$$N_{Re}: \pm 14.3\%.$$

The uncertainties in the other results are as follows:

$$C_f: \pm 11.4\%$$

$$f: \pm 30.4\%$$

$$j: \pm 30.6\%.$$

It should be noted once again that these uncertainties are based on 20:1 odds and are not maximum percentages of error. No attempt has been made to include the effect of such theoretical assumptions as zero longitudinal conduction, step change in temperature, etc., in the uncertainty analysis.

VIII. CONCLUSIONS

Based on the experimental results of this study, the following conclusions may be made:

1. The pressure gradient in fibrous media may be represented by a cubic equation with the bulk velocity as the independent variable:

$$-\frac{dp}{dx} = \frac{\mu U}{K} + \frac{b\rho U^2}{g_c} + \frac{c\rho U^3}{b g_c}$$

   K is the permeability of the medium, b is a tortuosity parameter, and c is a small, negative, dimensionless number whose physical significance is unknown. The above equation assumes negligible compressibility effects, as found in this study.

2. The product of the permeability and the tortuosity parameter is superior to the artificial hydraulic diameter determined from either the uni-dimensional porosity or crossed-rod matrices models for use as the characteristic length in the Reynolds number for flow in fibrous media. The product of the permeability and tortuosity parameter is a function only of the medium, but is not a conceivable dimension as is a hydraulic diameter. Moreover, this quasi-length parameter must be determined experimentally, and is very sensitive to the subleties in the structure of the fibrous medium. In light of the above conclusion that there is a cubic term in the equation for the pressure gradient, it is possible that the precise characteristic length may involve the dimensionless number c as well.

3. A friction factor correlation, as a function of N_{Re} based on Kb, which is valid for steel wools at N_{Re} less than unity is:

$$C_f = 2/N_{Re} + 2$$

   For N_{Re} in excess of unity, this relation over-estimates C_f.

4. The Colburn j factor shows a peak value in the vicinity of Reynolds numbers of one for all grades of steel wool. This is the optimum operating point in terms of heat transferred per pound of air flow.

5. The thermal and hydrodynamic boundary layers in fibrous media do not behave in analagous manners. Separation, which causes deviation from the Darcy flow regime is the probable explanation for this dissimilar behavior.

6. Grade 3 steel wool (by far the largest fiber size) is the best overall heat exchanger, based on evaluation at standard conditions and an assumed equilateral cross-section. In general, the larger the fiber size, the better the performance as a heat exchanger.

IX. RECOMMENDATIONS FOR FURTHER STUDY

This first-cut analysis of heat transfer and flow friction characteristics of fibrous media has raised questions which merit further investigation.

1. Since the surface area, A, was the largest source of uncertainty in the experimental results, the use of gas diffusion and other more sophisticated techniques for determining specific surface [27] should be pursued.

2. The possibility of longitudinal conduction should be investigated. Since Grades 1, 2, 3 may be either stainless steel or plain carbon steel, and since these two metals differ greatly only in thermal conductivities, a simple experiment to determine if any longitudinal conduction exists is easily performed.

3. Inasmuch as values of N_{tu} less than 3.0 were experienced, the use of the cyclic testing technique for future studies is recommended.

4. In addition to sampling various grades of steel wool, it is suggested that the same grade of steel wool be tested at various compactnesses. Thus porosity, as well as fiber size becomes an independent variable.

5. Some further thought must be given to packaging a steel wool sample before testing, so that better control over homogeneity, dimensions, and boundary conditions may be had.

Prior to any further use of the single-blow transient testing apparatus, some improvements in the instrumentation should be made.

1. Radiation shielding should be applied to all thermocouple and heater leads to eliminate noise problems.

2. Water manometers should be replaced with pressure transducers. In this way a graphical output is obtained, eliminating the need to make a value judgement under the press of time (i.e., during the course of a test).

3. Additional pressure transducers should be installed downstream of both the matrix and the orifice. These would serve as a check, since the inlet pressure plus the pressure drop should equal the outlet pressure.

4. If all of the above instrumentation improvements are made, six pressures would be measured. Since an eight channel recorder is available, the orifice temperature could be placed on the seventh channel. Thus a complete graphical display for each data run would be available.

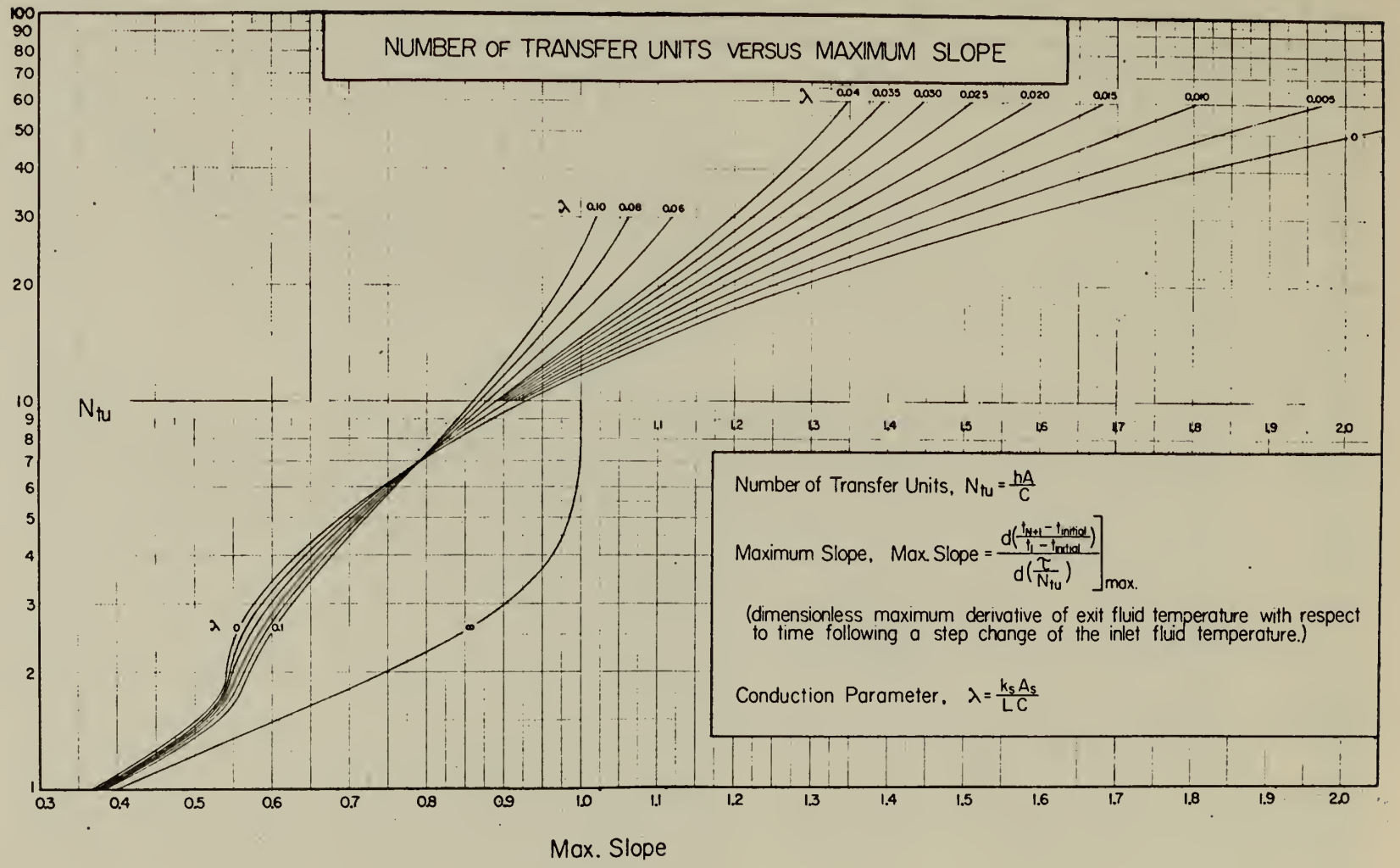

Figure 1. N_{tu} Versus Maximum Slope with Conduction Parameter (Max. Slope, 0.3-2.05).

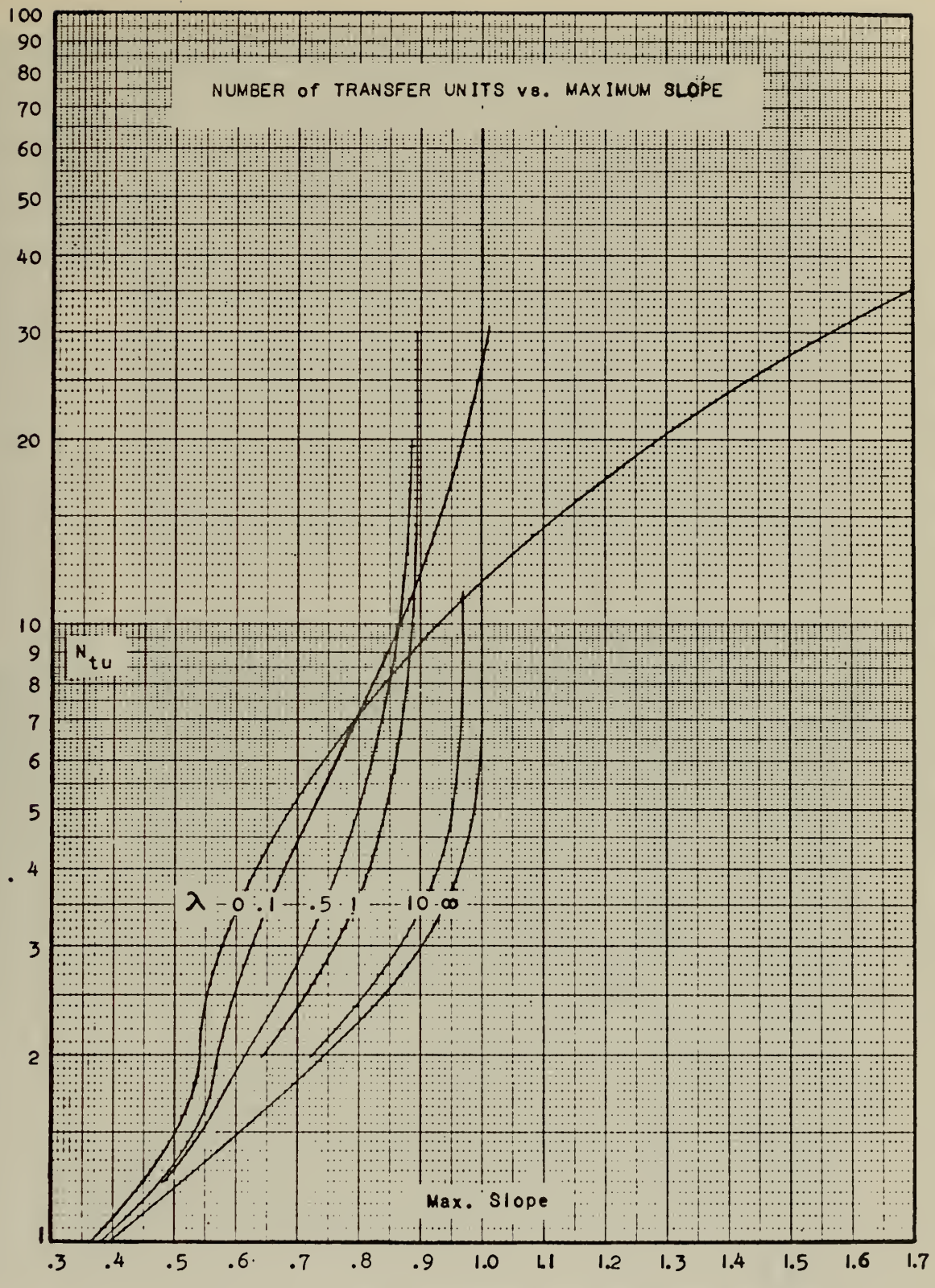

Figure 2. N_{tu} Versus Maximum Slope with Conduction Parameter (Max. Slope, 0.3-1.7).

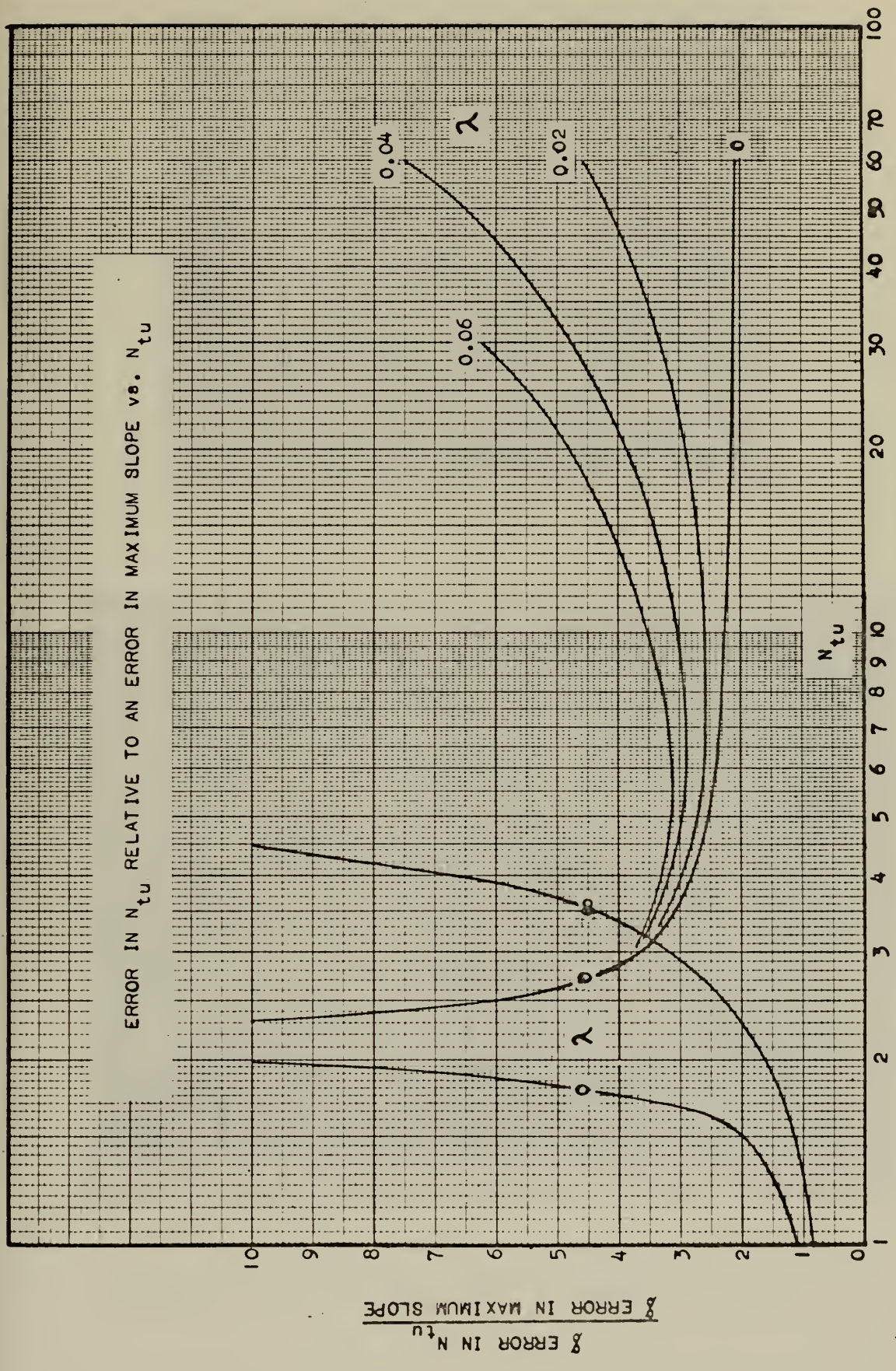

Figure 3. Error in N_{tu} Relative to an Error in Maximum Slope vs. N_{tu}.

Figure 4A. Experimental Setup

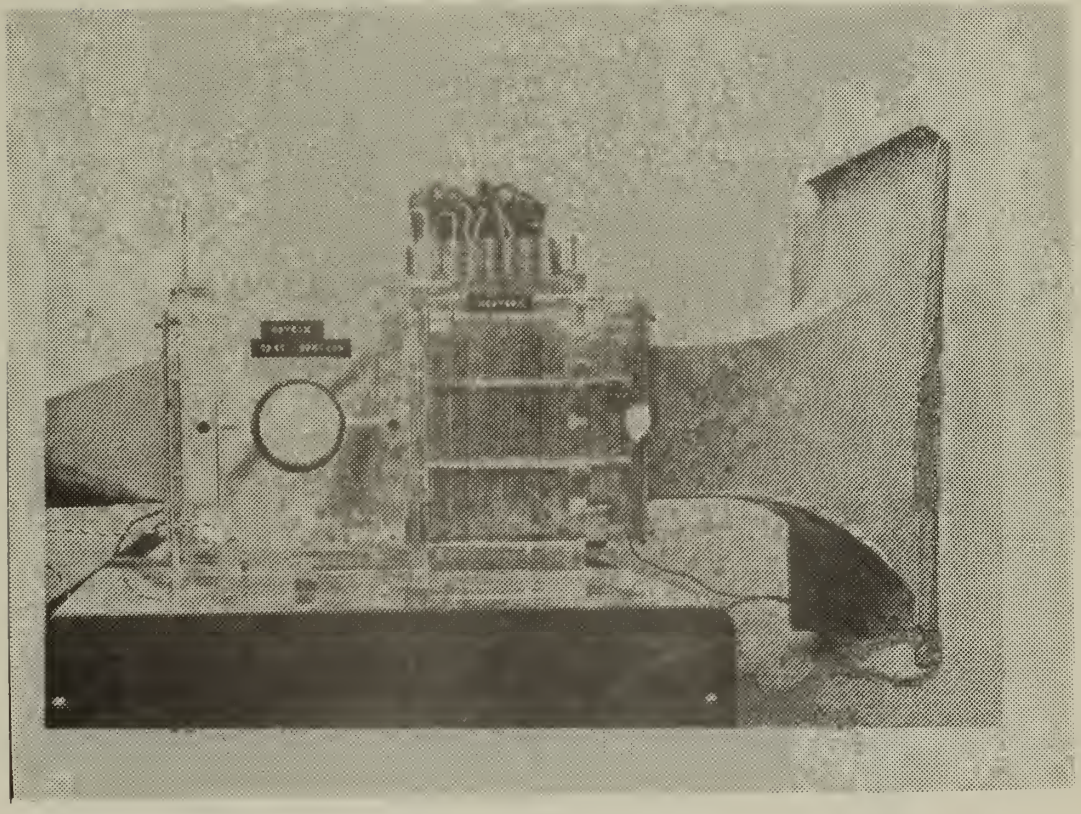

Figure 4B. Detail of Inlet Cone, Heaters, Test Section

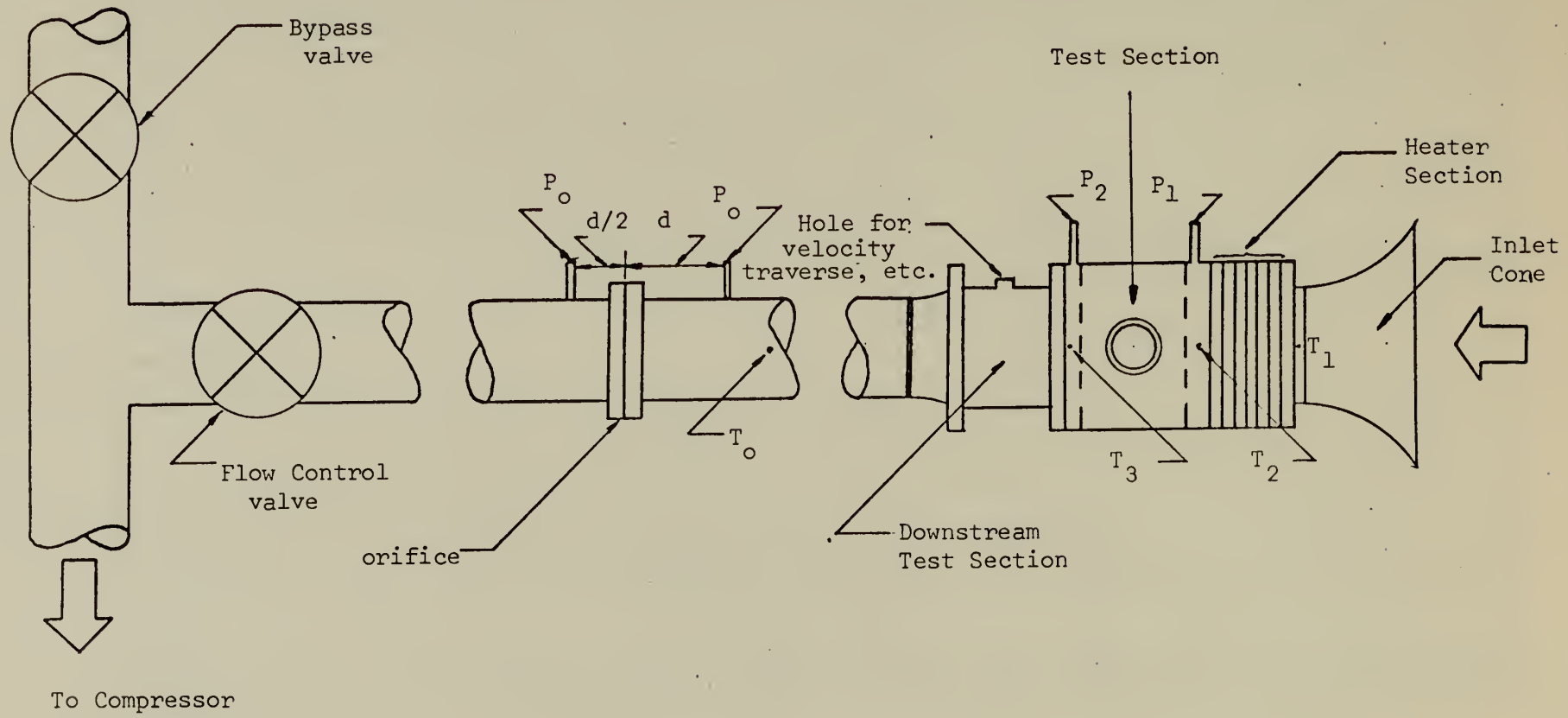

Figure 5. Schematic Diagram of Test Apparatus

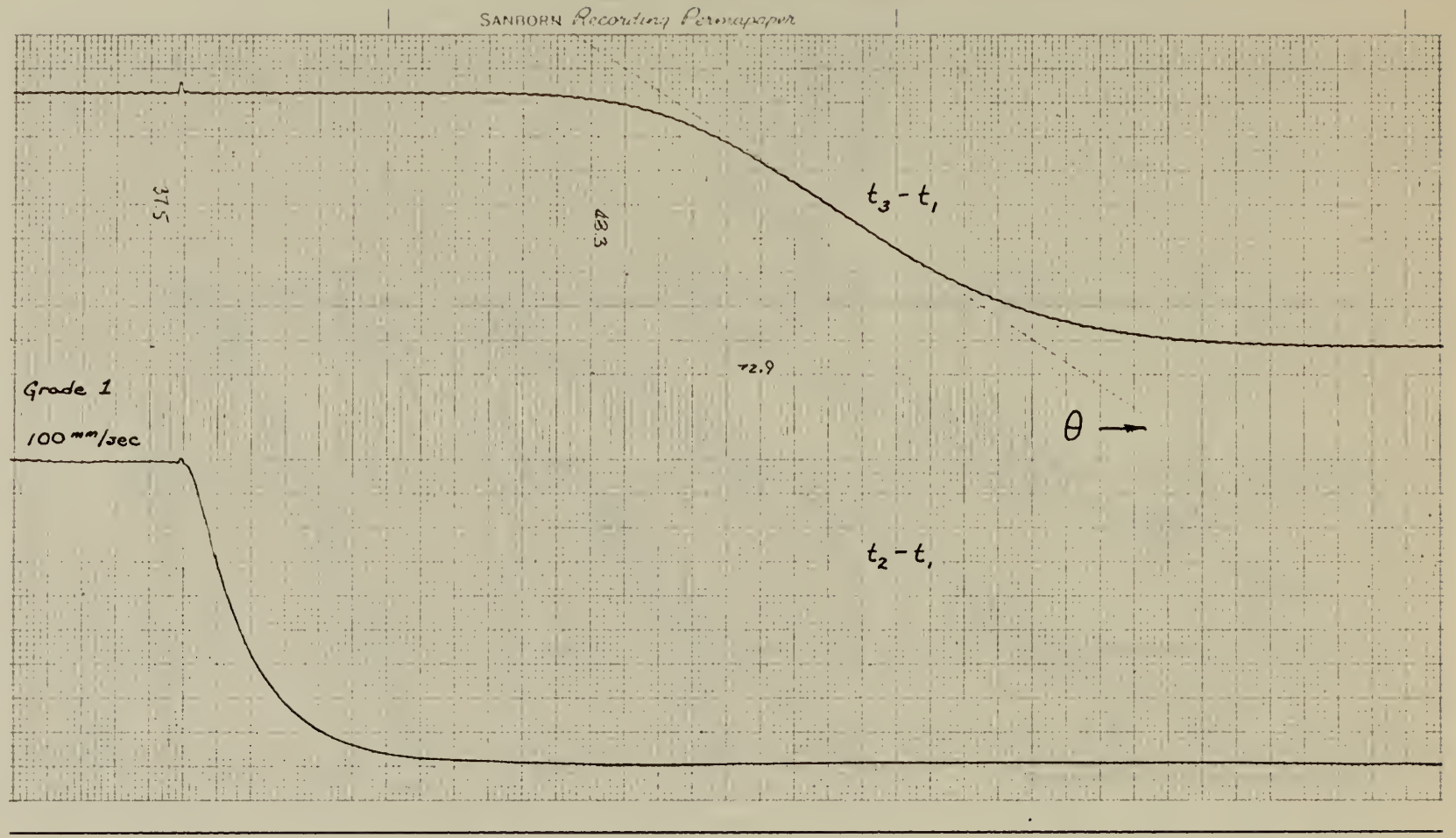

Figure 6. Sample of Temperature Responses

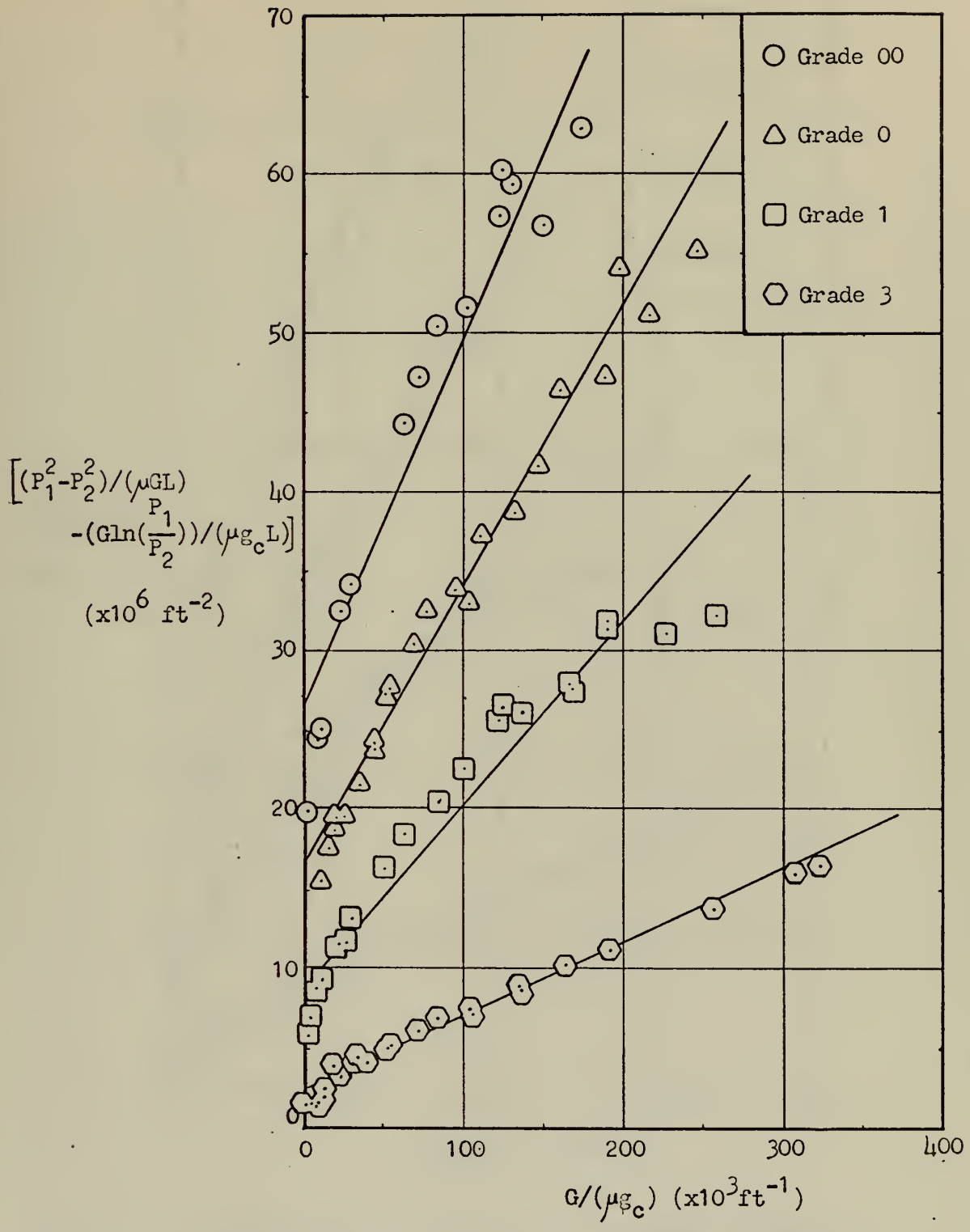

Figure 7. Determination of Permeability and Tortuosity Parameter from the Integrated Form of the Polubarinova-Kochina Equation.

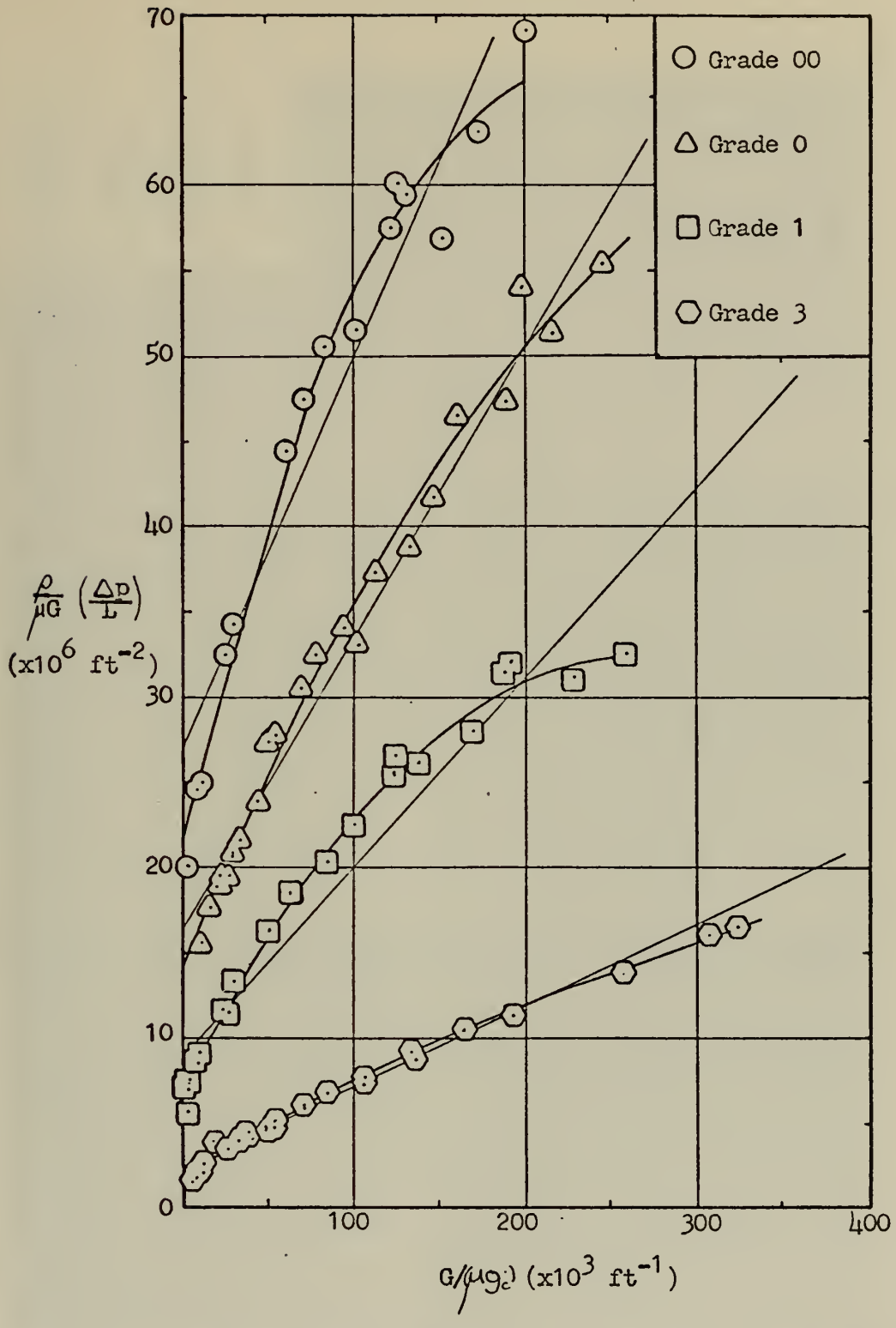

Figure 8. Determination of Permeability, Tortuosity Parameter, and Cubic Coefficient from the Differential Form of Reynolds Equation

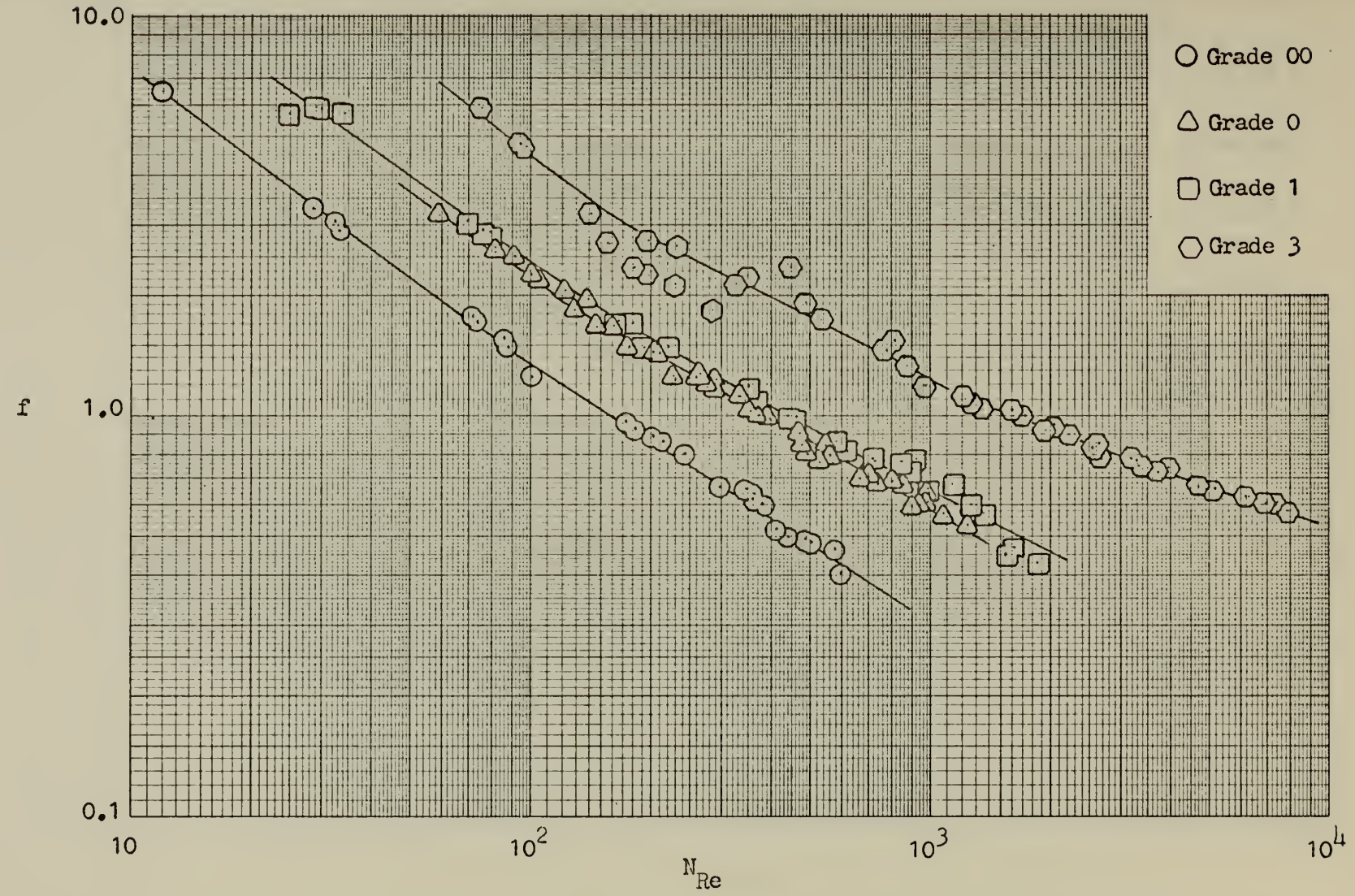

Figure 9. Fanning Friction Factor as a Function of Reynolds Number Based on a Model which is Porous to Flow in One Dimension Only.

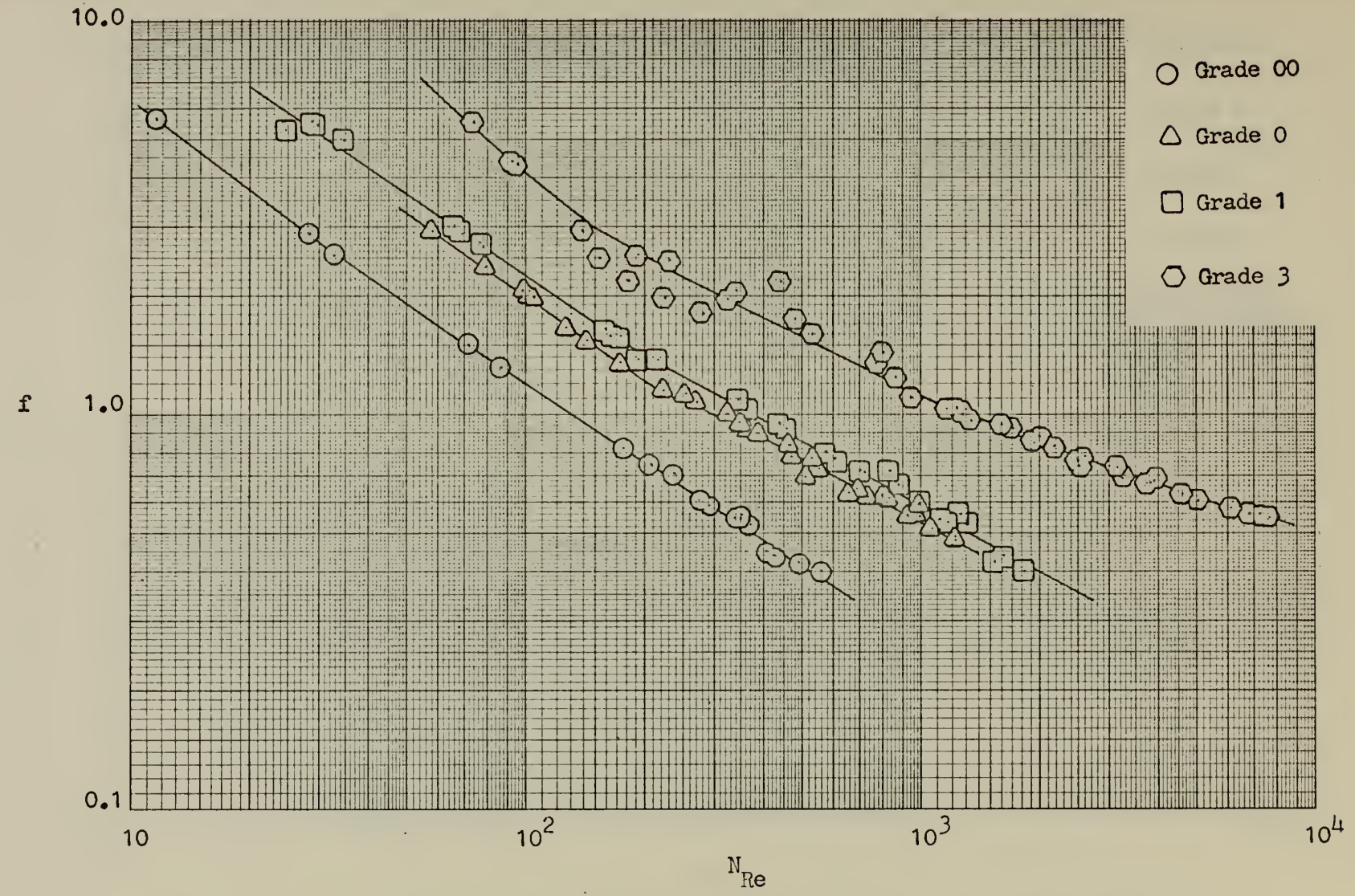

Figure 10. Fanning Friction Factor as a Function of Reynolds Number Based on the Crossed-Rod Matrices Model.

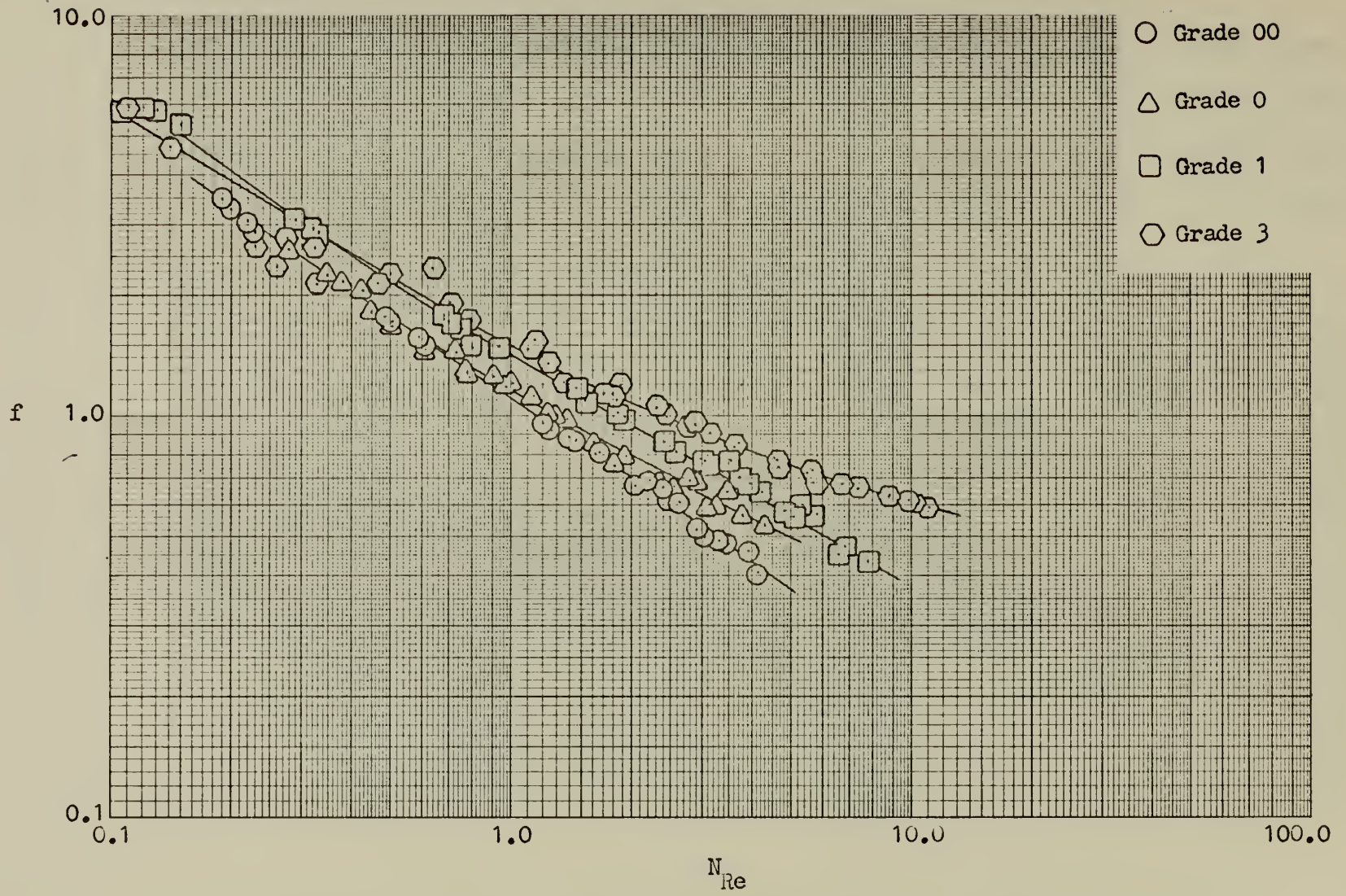

Figure 11. Fanning Friction Factor as a Function of Reynolds Number Based on the Product of the Medium Permeability and Tortuosity Parameter (Kb).

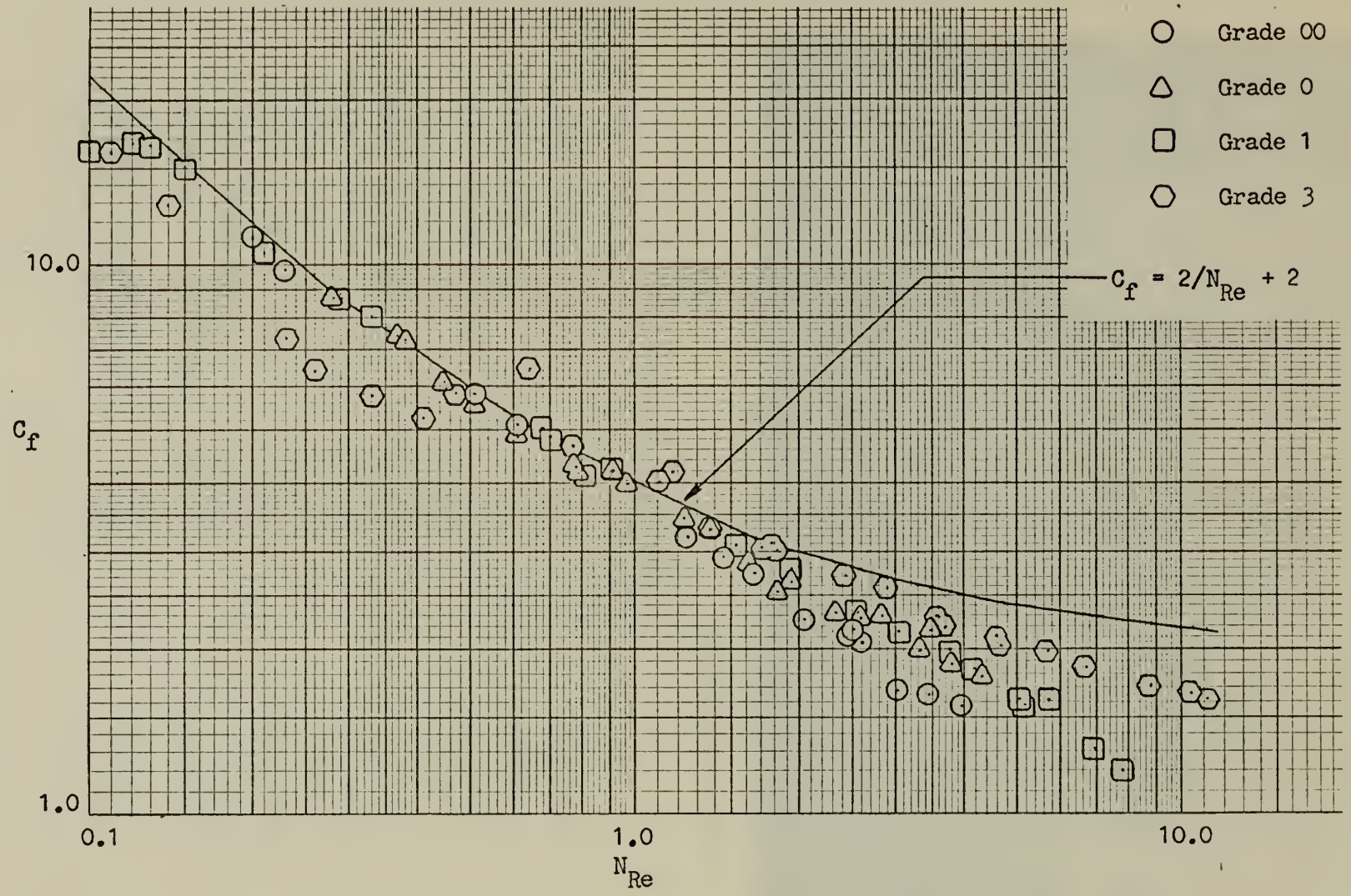

Figure 12. Correlating Friction Factor as a Function of Reynolds Number Based on Kb.

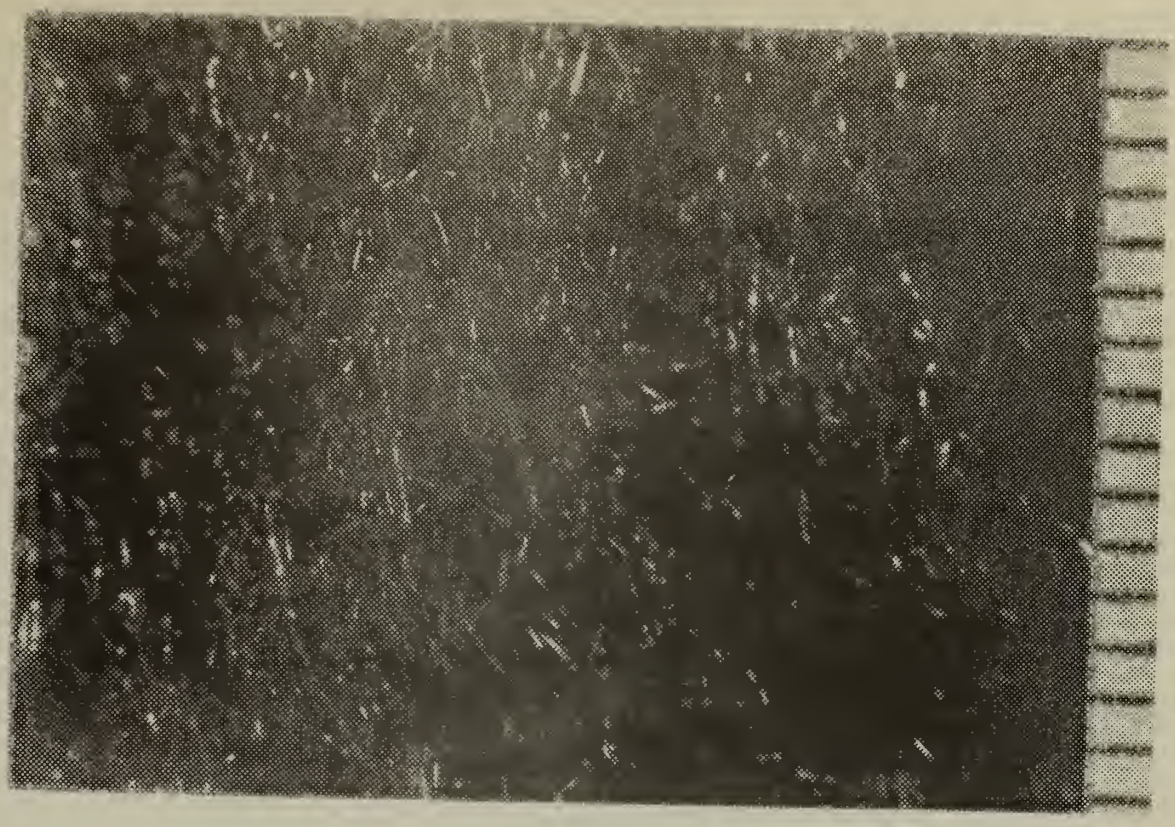

(Divisions in mm.)

Grade 00 Steel Wool

FRONTAL AREA	FT2	0.07056
FREE FLOW AREA	FT2	0.06858
HEAT TRANSFER AREA	FT2	24.20344
MATRIX DENSITY	LB/FT3	13.74215
SPECIFIC SURFACE	1/FT	1372.14233
FLOW LENGTH	FT	0.25000
POROSITY		0.97190
PERMEABILITY	FT2	0.0000000479
LENGTH PARAMETER	FT	0.00001996
TORTUOSITY PARAMETER	1/FT	416.80000
THERMAL CONDUCTIVITY	KS	26.40
MATRIX HEAT CAPACITY	CS	0.0267

Figure 13. Geometrical and Physical Properties of Grade 00 Steel Wool

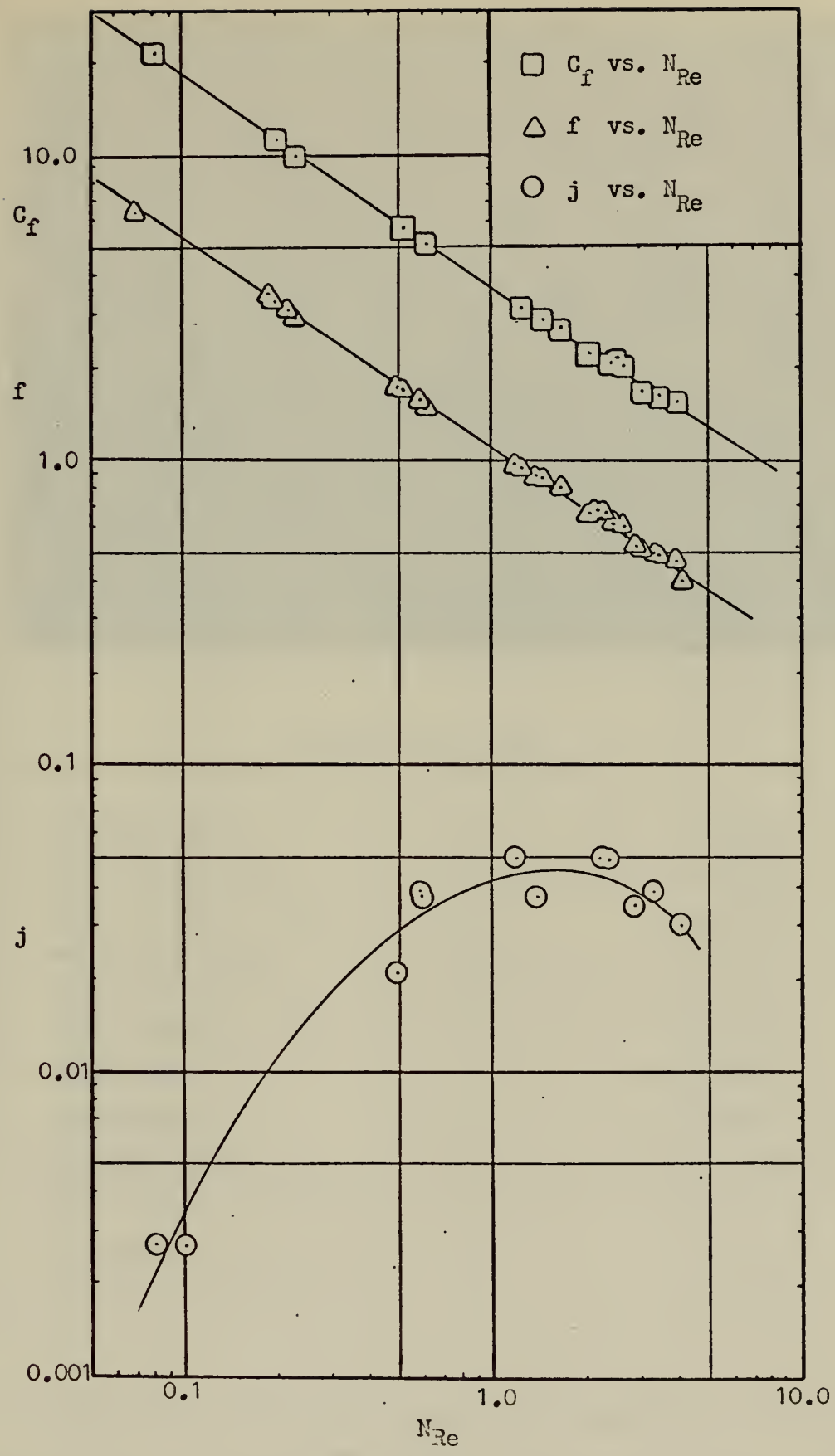

Figure 14. Heat Transfer and Flow Friction Characteristics of Grade 00 Steel Wool

(Divisions in mm.)

Grade 0 Steel Wool

FRONTAL AREA	FT2	0.07056
FREE FLOW AREA	FT2	0.06920
HEAT TRANSFER AREA	FT2	13.97000
MATRIX DENSITY	LB/FT3	9.31450
SPECIFIC SURFACE	1/FT	791.98782
FLOW LENGTH	FT	0.25000
POROSITY		0.98100
PERMEABILITY	FT2	0.0000000719
LENGTH PARAMETER	FT	0.00001748
TORTUOSITY PARAMETER	1/FT	243.10000
THERMAL CONDUCTIVITY	KS	26.40
MATRIX HEAT CAPACITY	CS	0.0181

Figure 15. Geometrical and Physical Properties of Grade 0 Steel Wool

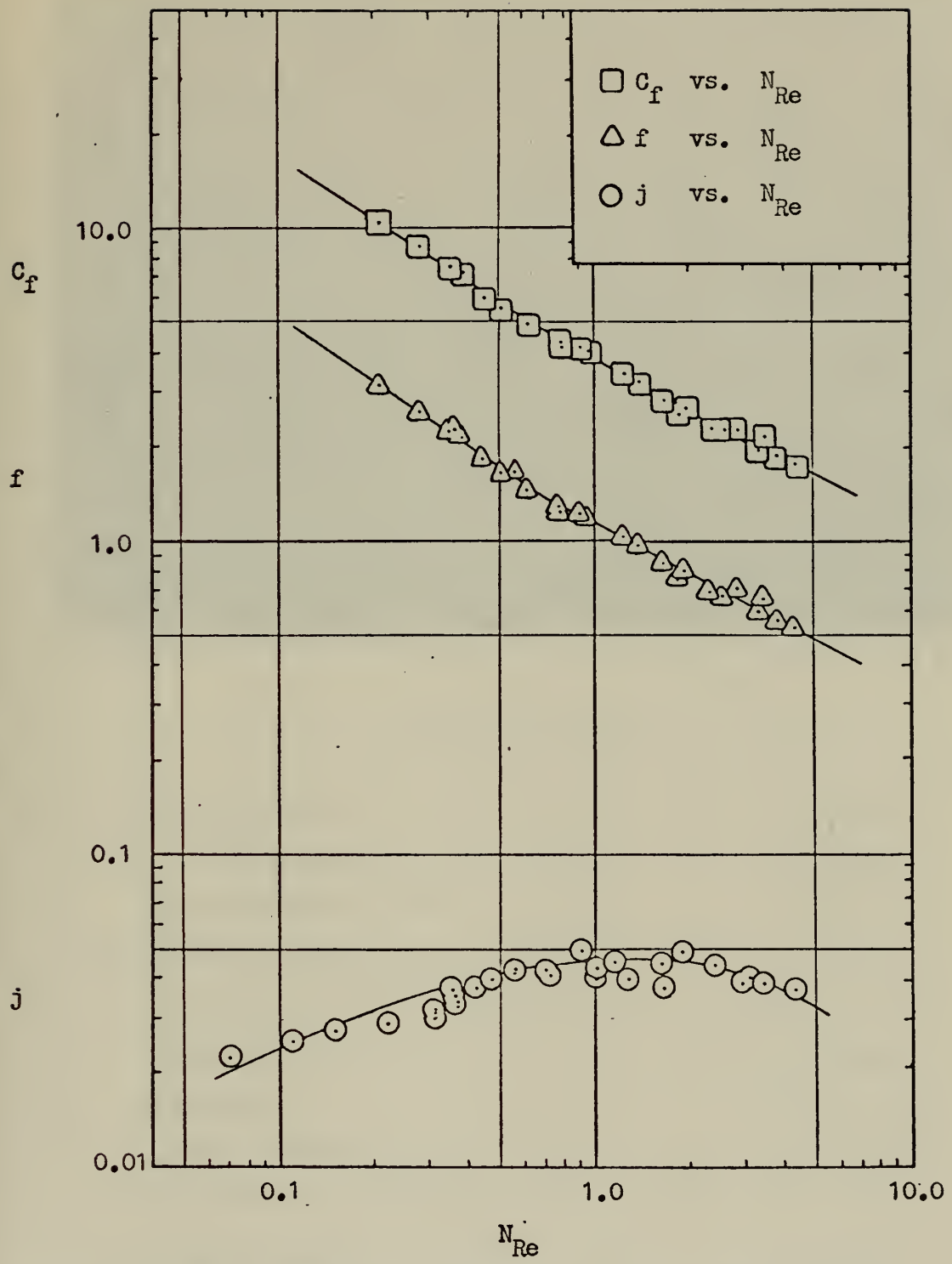

Figure 16. Heat Transfer and Flow Friction Characteristics of Grade 0 Steel Wool

(Divisions in mm.)

Grade 1 Steel Wool

FRONTAL AREA	FT2	0.07056
FREE FLOW AREA	FT2	0.06952
HEAT TRANSFER AREA	FT2	9.79700
MATRIX DENSITY	LB/FT3	7.19989
SPECIFIC SURFACE	1/FT	555.41193
FLOW LENGTH	FT	0.25000
POROSITY		0.98500
PERMEABILITY	FT2	0.0000001500
LENGTH PARAMETER	FT	0.00003021
TORTUOSITY PARAMETER	1/FT	201.40000
THERMAL CONDUCTIVITY	KS	26.40
MATRIX HEAT CAPACITY	CS	0.0140

Figure 17. Geometrical and Physical Properties of Grade 1 Steel Wool

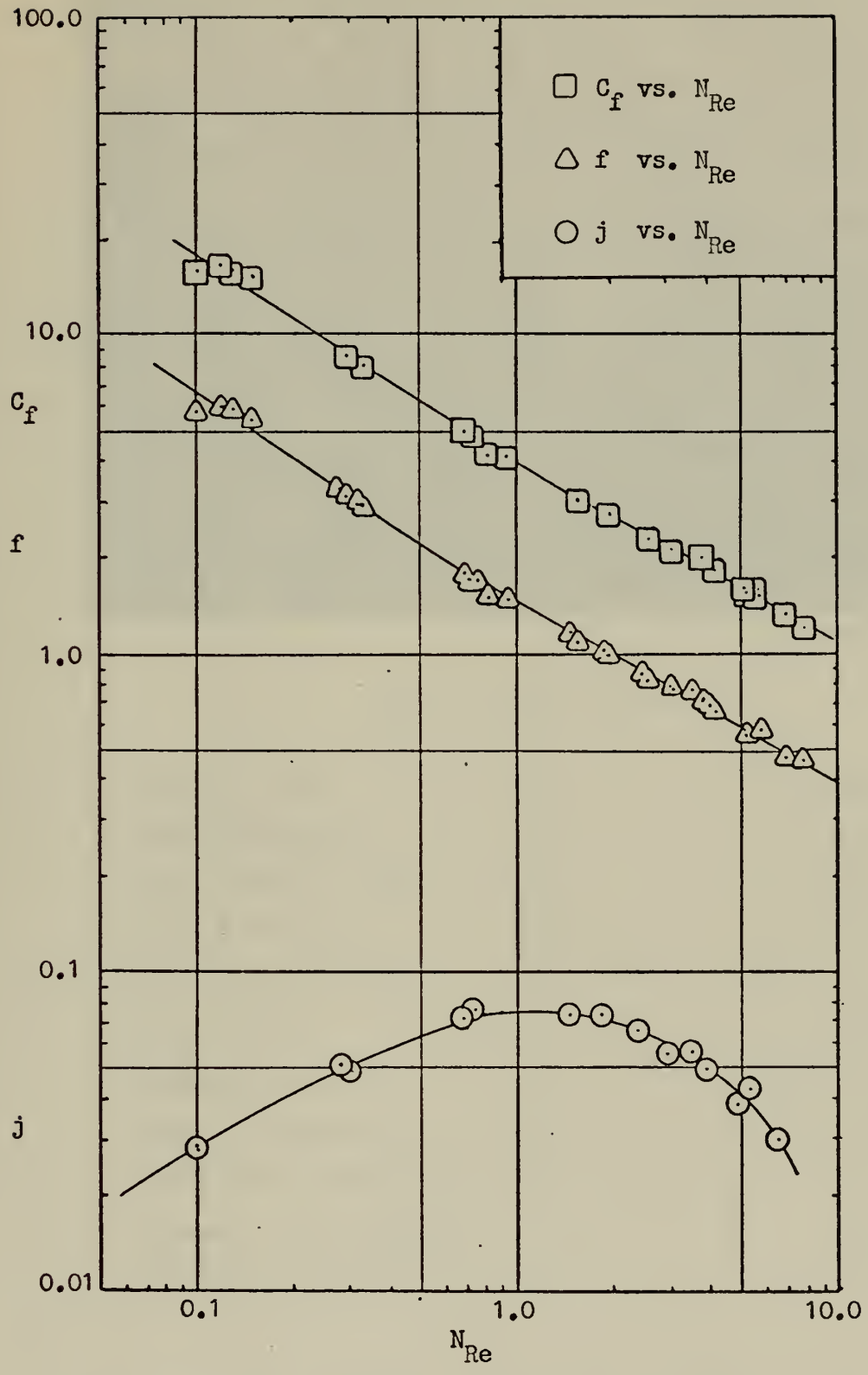

Figure 18. Heat Transfer and Flow Friction Characteristics of Grade 1 Steel Wool

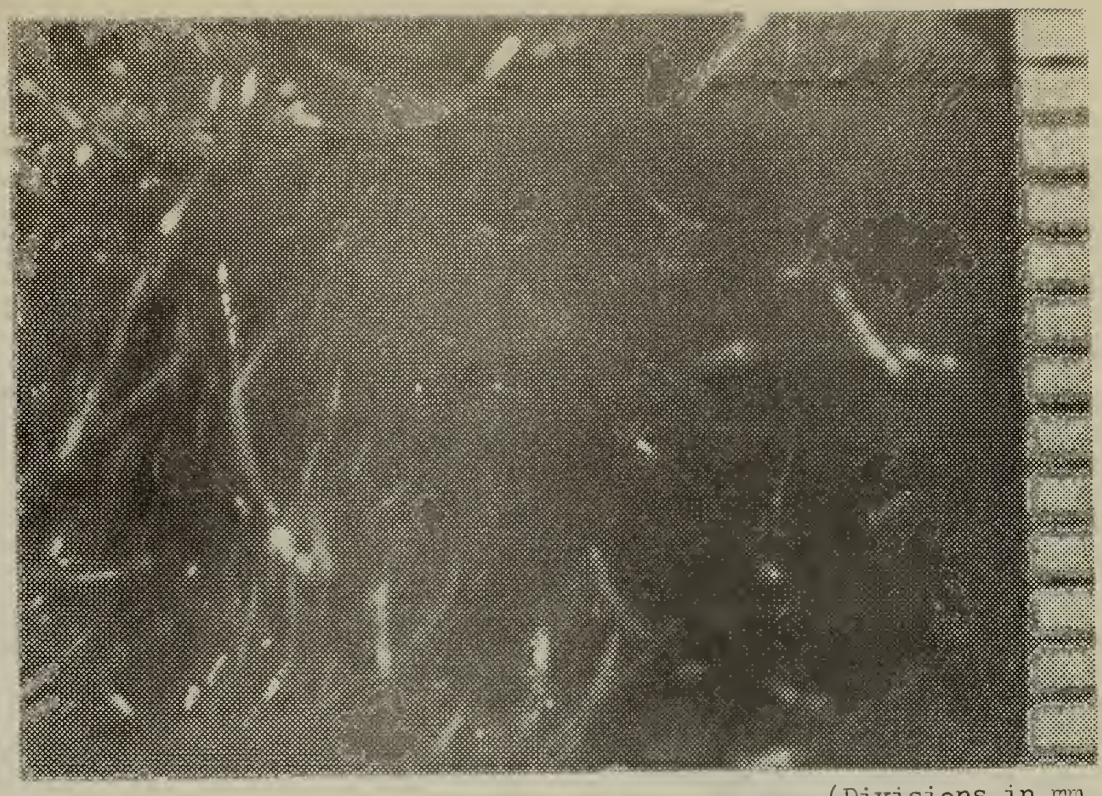

(Divisions in mm.)

Grade 3 Steel Wool

FRONTAL AREA	FT2	0.07056
FREE FLOW AREA	FT2	0.06940
HEAT TRANSFER AREA	FT2	2.90680
MATRIX DENSITY	LB/FT3	8.01059
SPECIFIC SURFACE	1/FT	164.79243
FLOW LENGTH	FT	0.25000
POROSITY		0.98360
PERMEABILITY	FT2	0.0000005610
LENGTH PARAMETER	FT	0.00003450
TORTUOSITY PARAMETER	1/FT	61.50000
THERMAL CONDUCTIVITY	KS	26.40
MATRIX HEAT CAPACITY	CS	0.0155

Figure 19: Geometrical and Physical Properties of Grade 3 Steel Wool

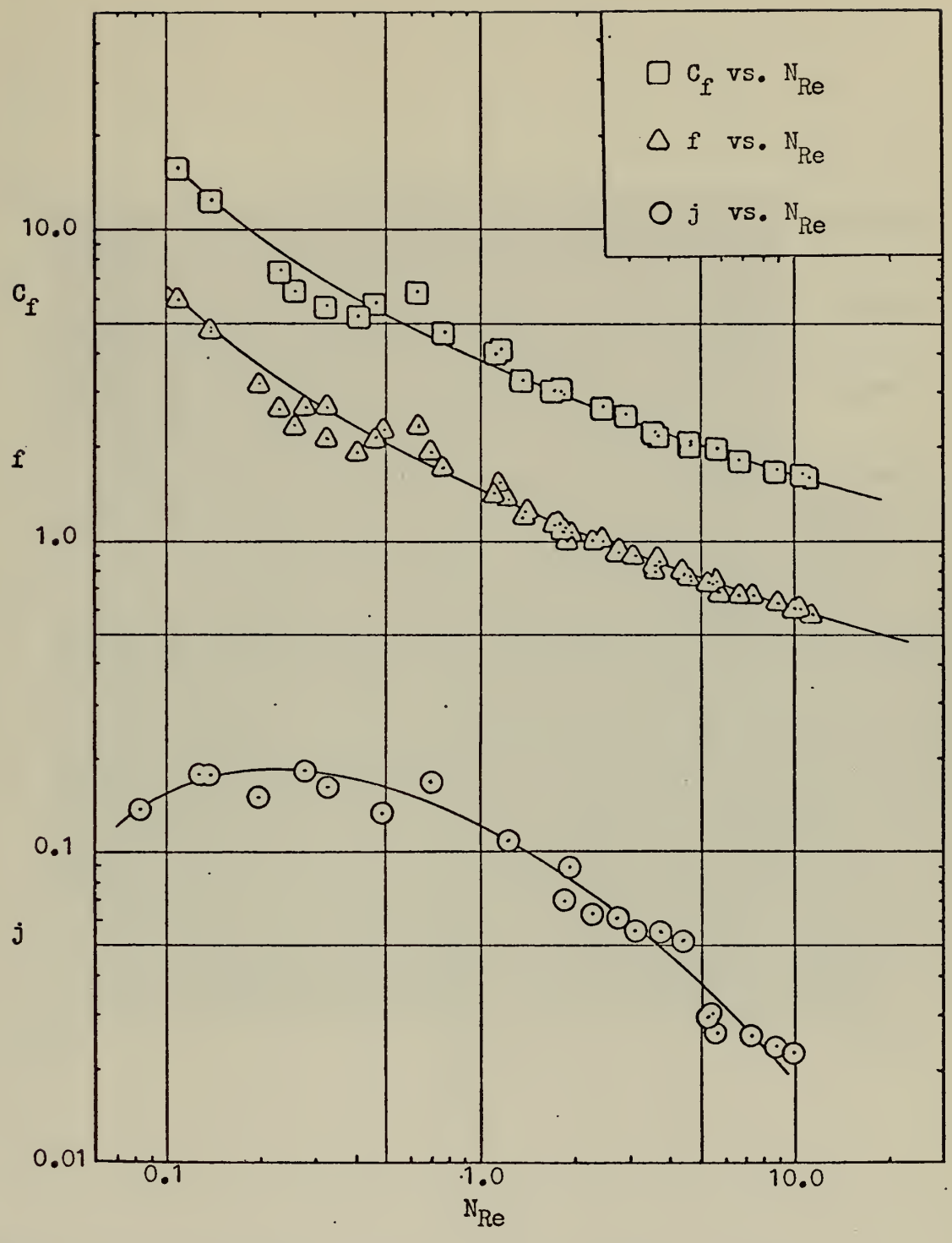

Figure 20. Heat Transfer and Flow Friction Characteristics of Grade 3 Steel Wool

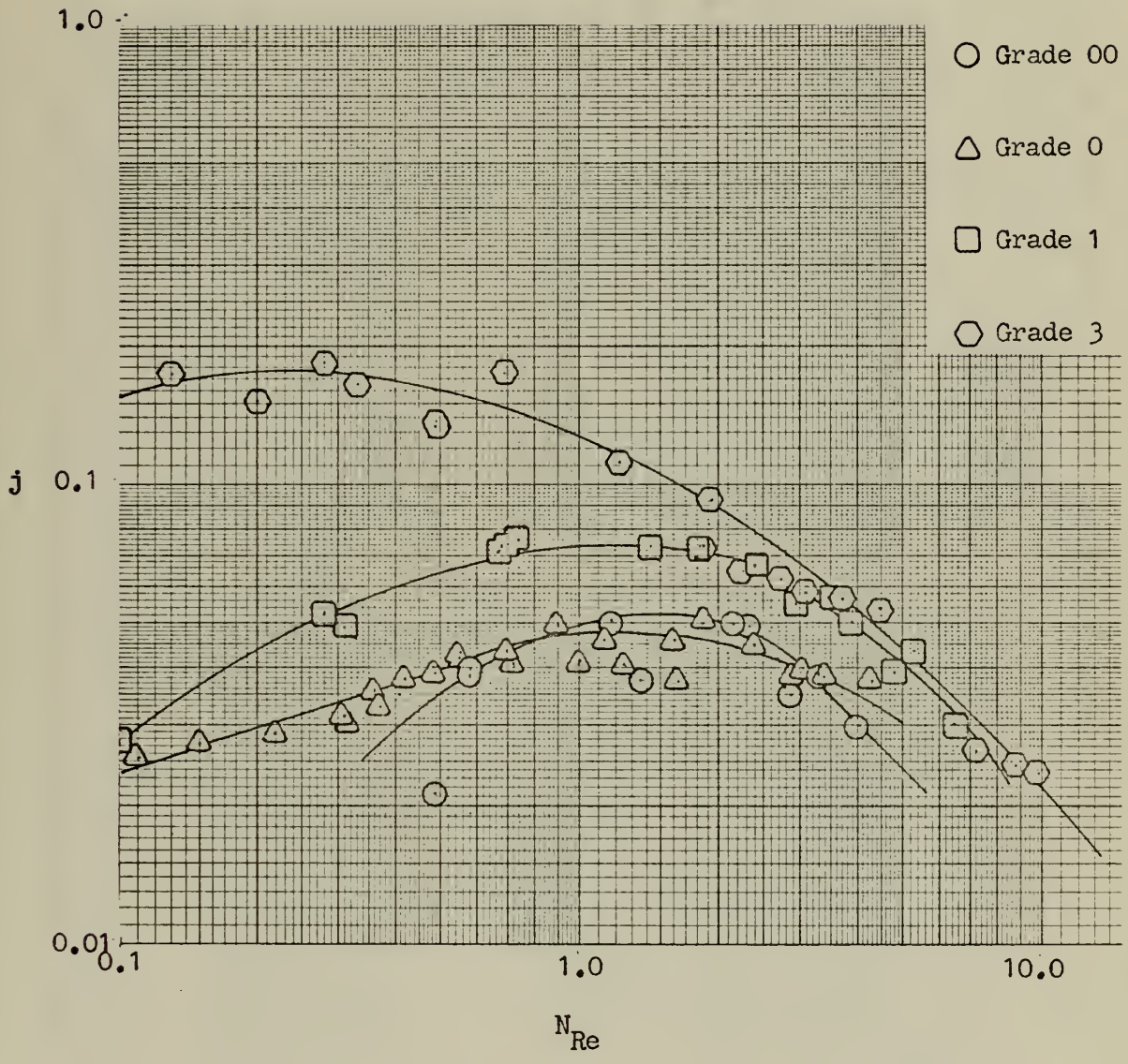

Figure 21. Colburn j-Factor Versus Reynolds Number

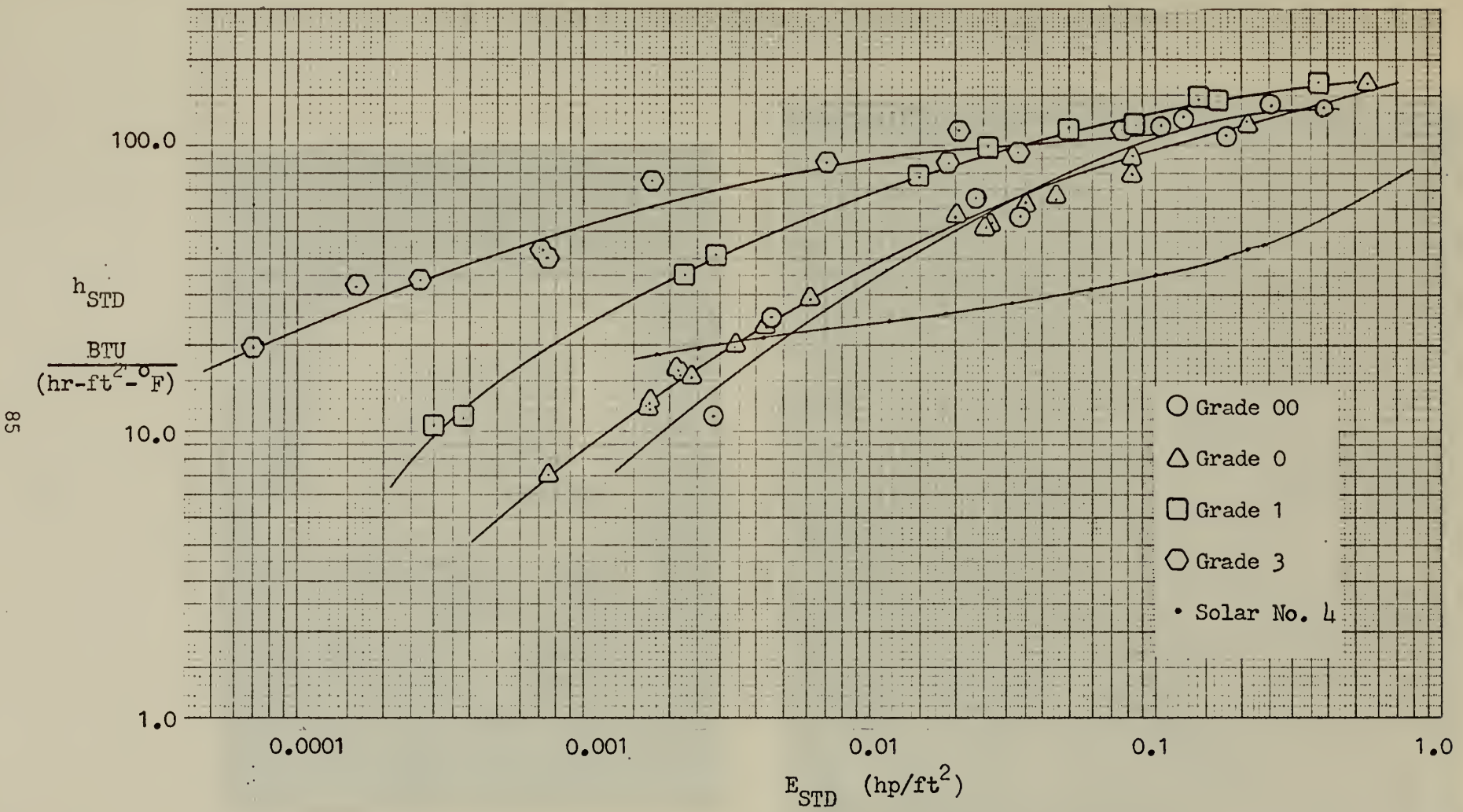

Figure 22. Heat Transfer Power Versus Flow Friction Power Per Unit Area.

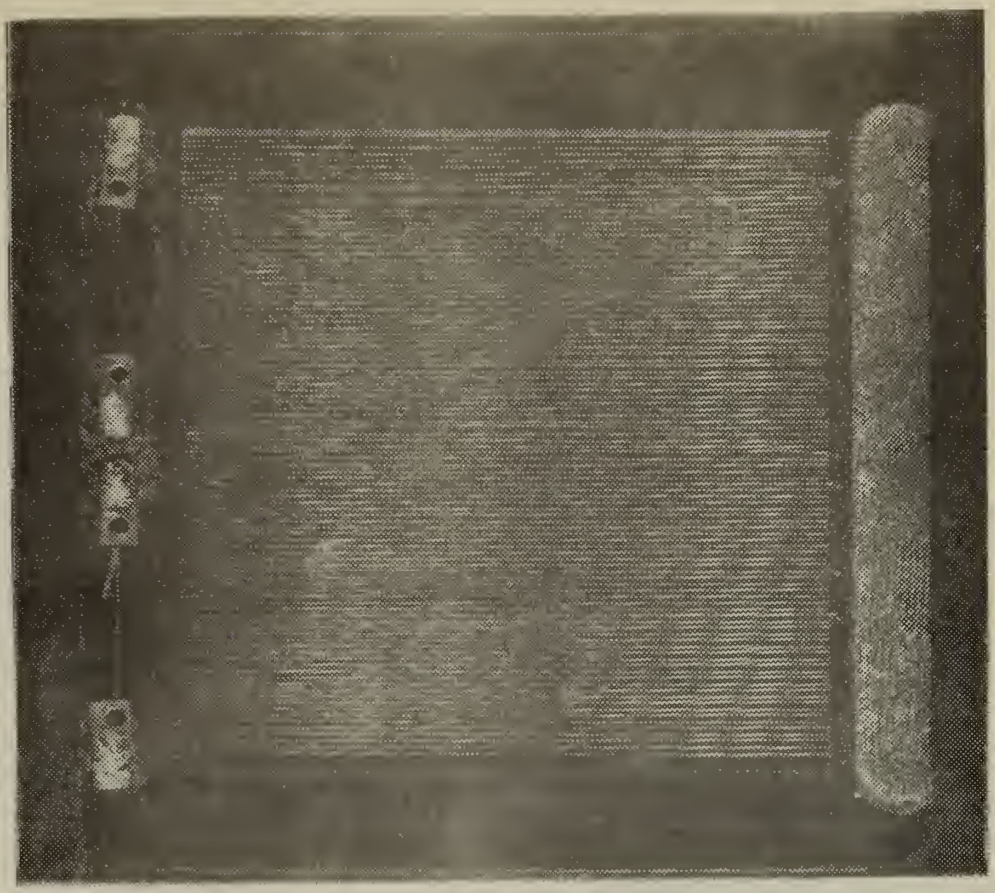

Figure 23. 0.003 in. Wire Heater Frame

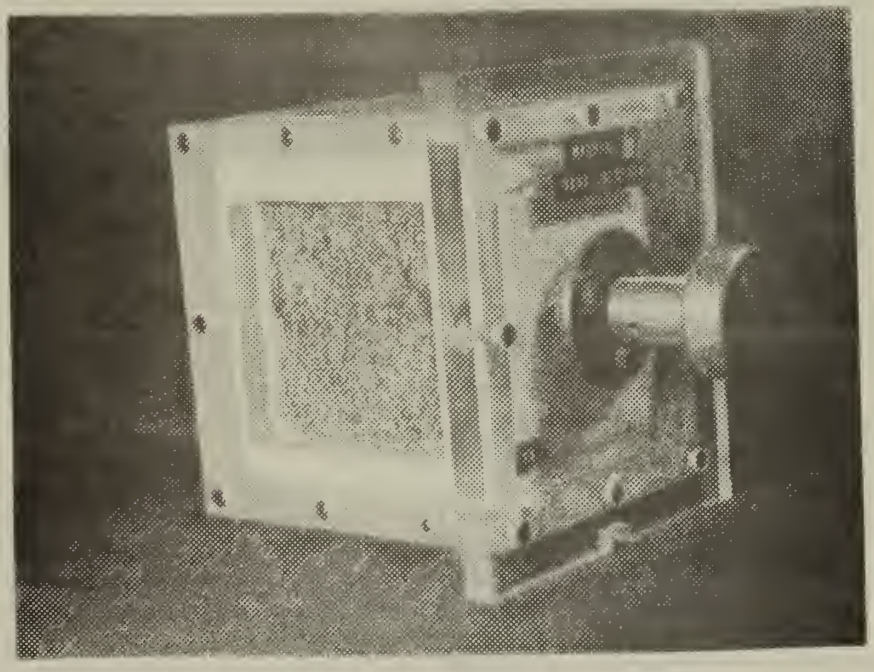

Figure 24. Test Section

Table II N_{tu} as a Function of Maximum Slope and Longitudinal Conduction Parameter

N_{tu} \ λ	Maximum Slope 0	.005	.010	.015	.020	.025	.030	.035	.040	.060	.080	.100	.500	1.0	10	∞
1.0	.368	-	-	-	.374	-	-	-	.377	.380	.382	.384	-	-	-	.400
1.1	.403	-	-	-	.408	-	-	-	.413	.417	.420	.425	-	-	-	.445
1.2	.434	-	-	-	.440	-	-	-	.445	.447	.452	.459	-	-	-	.488
1.3	.461	-	-	-	.467	-	-	-	.472	.475	.480	.487	.497	-	-	.529
1.4	.483	-	-	-	.489	-	-	-	.494	.498	.503	.511	.522	-	-	.568
1.5	.502	-	-	-	.507	-	-	-	.512	.517	.521	.530	.542	-	-	.603
1.6	.517	-	-	-	.522	-	-	-	.527	.530	.536	.544	.560	-	-	.637
1.8	.536	-	-	-	.539	-	-	-	.542	.547	.553	.561	.589	-	-	.697
2.0	.541	-	-	-	.545	-	-	-	.548	.556	.563	.571	.615	.646	.723	.748
2.2	.544	-	-	-	.549	-	-	-	.557	.566	.574	.582	.640	.677	.764	.791
2.4	.549	-	-	-	.557	-	-	-	.567	.577	.585	.592	.662	.703	.798	.827
2.6	.557	-	-	-	.566	-	-	-	.577	.587	.595	.603	.682	.726	.826	.857
2.8	.567	-	-	-	.577	-	-	-	.587	.598	.606	.615	.699	.745	.850	.882
3.0	.577	-	-	-	.587	-	-	-	.598	.608	.617	.626	.714	.761	.869	.903
3.2	.587	-	-	-	.598	-	-	-	.609	.619	.628	.637	.727	.775	.886	.920
3.4	.598	-	-	-	.610	-	-	-	.620	.630	.640	.647	.738	.787	.899	.934
3.6	.609	-	-	-	.621	-	-	-	.631	.641	.650	.658	.749	.798	.911	.946
3.8	.621	-	-	-	.632	-	-	-	.642	.652	.660	.668	.758	.807	.920	.956
4.0	.632	-	-	-	.643	-	-	-	.653	.662	.670	.678	.767	.815	.928	.964
4.5	.660	-	-	-	.670	-	-	-	.678	.687	.694	.701	.784	.831	.941	.978
5.0	.688	-	-	-	.697	-	-	-	.704	.711	.717	.722	.800	.843	.951	.987
5.5	.715	-	-	-	.722	-	-	-	.727	.733	.737	.742	.812	.852	.956	.992
6.0	.741	-	-	-	.746	-	-	-	.750	.753	.757	.760	.822	.859	.960	.995
6.5	.767	-	-	-	.769	-	-	-	.771	.773	.774	.776	.830	.865	.962	-
7.0	.792	-	-	-	.792	-	-	-	.791	.791	.791	.792	.837	.870	.964	1.000
7.5	.816	-	-	-	.812	-	-	-	.810	.808	.806	.805	.844	.874	.965	-
8.0	.840	-	-	-	.832	-	-	-	.827	.824	.821	.817	.849	.877	.966	-
9.0	.885	-	-	-	.872	-	-	-	.861	.853	.847	.840	.858	.882	.967	-
10.0	.929	.922	.916	.911	.906	.901	.897	.893	.890	.880	.869	.860	.864	.886	.968	1.000
11.0	.970	.959	.953	.946	.939	.933	.927	.921	.917	.901	.888	.878	.870	.889	.968	-
12.0	1.010	.998	.988	.979	.970	.962	.955	.948	.942	.922	.906	.893	.873	-	-	-
13.0	1.049	1.034	1.022	1.009	.999	.990	.980	.973	.965	.941	.922	.907	.875	-	-	-
14.0	1.085	1.068	1.053	1.039	1.027	1.016	1.005	.996	.987	.958	.937	.921	.877	-	-	-
15.0	1.121	1.102	1.085	1.068	1.053	1.040	1.028	1.017	1.007	.975	.950	.932	.879	.893	-	-
16.0	1.156	1.133	1.112	1.094	1.077	1.063	1.049	1.037	1.026	.990	.963	.942	.881	-	-	-
18.0	1.223	1.193	1.167	1.144	1.123	1.105	1.088	1.073	1.060	1.016	.984	.960	.885	-	-	-
20.0	1.286	1.249	1.217	1.189	1.164	1.143	1.123	1.105	1.089	1.039	1.003	.975	.887	.894	-	1.000
22.0	1.347	1.302	1.264	1.231	1.202	1.177	1.154	1.134	1.116	1.059	1.018	.987	.889	-	-	-
24.0	1.404	1.352	1.308	1.269	1.237	1.208	1.182	1.160	1.140	1.077	1.032	.997	.891	-	-	-
26.0	1.460	1.399	1.348	1.305	1.268	1.236	1.208	1.183	1.161	1.092	1.043	1.005	.893	-	-	-
28.0	1.515	1.444	1.387	1.339	1.298	1.262	1.231	1.204	1.180	1.106	1.053	1.013	.894	-	-	-
30.0	1.565	1.487	1.423	1.370	1.325	1.286	1.253	1.224	1.198	1.118	1.061	1.019	.895	.895	-	1.000
32.0	1.617	1.528	1.458	1.399	1.351	1.309	1.273	1.241	1.214	-	-	-	-	-	-	-
34.0	1.665	1.568	1.490	1.427	1.374	1.330	1.291	1.258	1.228	-	-	-	-	-	-	-
36.0	1.712	1.605	1.521	1.453	1.397	1.349	1.308	1.273	1.242	-	-	-	-	-	-	-
38.0	1.757	1.641	1.551	1.478	1.418	1.367	1.324	1.287	1.254	-	-	-	-	-	-	-
40.0	1.801	1.676	1.579	1.501	1.437	1.384	1.339	1.300	1.266	-	-	-	-	-	-	1.000
45.0	1.908	1.757	1.643	1.554	1.481	1.422	1.372	1.328	1.292	-	-	-	-	-	-	-
50.0	2.010	1.833	1.702	1.601	1.520	1.455	1.400	1.353	1.313	-	-	-	-	-	-	1.000
55.0	2.107	1.902	1.756	1.644	1.555	1.483	1.425	1.375	1.332	-	-	-	-	-	-	-
60.0	2.199	1.967	1.803	1.680	1.585	1.508	1.445	1.392	1.347	-	-	-	-	-	-	1.000

GRADE CO STEEL WOOL - FRICTION FACTOR DATA

RUN	MDOT	NR FR	FAN F	CF	CFTH	DIFCF
1	12.92	0.08	6.47330	21.92587	26.22597	-4.30010
2	31.19	0.20	3.29417	11.15779	12.01401	-0.85622
3	36.13	0.23	2.89320	9.79967	10.64235	-0.84268
4	79.19	0.51	1.71273	5.80133	5.93749	-0.13616
5	95.55	0.61	1.49829	5.07505	5.26636	-0.19131
6	197.35	1.26	0.93914	3.18138	3.58297	-0.40159
7	229.65	1.47	0.86304	2.92372	3.36308	-0.43936
8	262.59	1.68	0.80477	2.72645	3.19285	-0.46641
9	323.11	2.06	0.66880	2.26607	2.97085	-0.70478
10	387.64	2.47	0.62147	2.10604	2.80944	-0.70339
11	412.33	2.63	0.60511	2.05076	2.76182	-0.71106
12	393.97	2.51	0.64220	2.17635	2.79737	-0.62102
13	476.94	3.04	0.50001	1.69489	2.65802	-0.96313
14	545.47	3.48	0.48459	1.64306	2.57531	-0.93225
15	623.21	3.97	0.46378	1.57305	2.50325	-0.93020

Table III

GRADE O STEEL WOOL - FRICTION FACTOR RUNS

RUN	MDOT	NR FR	FAN F	CF	CFTH	DIFCF
1	36.64	0.21	3.16962	10.52867	11.71398	-1.18531
2	36.55	0.21	3.18507	10.57999	11.73739	-1.15740
3	50.25	0.28	2.60520	8.65387	9.08098	-0.42711
4	50.25	0.28	2.57459	8.55216	9.08094	-0.52877
5	62.04	0.35	2.25236	7.48183	7.73305	-0.25122
6	62.04	0.35	2.24210	7.44775	7.73291	-0.28516
7	66.88	0.38	2.16408	7.18859	7.31540	-0.12681
8	66.41	0.37	2.17709	7.23182	7.35274	-0.12092
9	79.97	0.45	1.81715	6.03620	6.44154	-0.40535
10	90.90	0.51	1.67776	5.57323	5.90757	-0.33435
11	108.87	0.61	1.47654	4.90487	5.26146	-0.35659
12	140.96	0.79	1.25341	4.16376	4.51820	-0.35444
13	139.21	0.78	1.28519	4.26931	4.54991	-0.28060
14	171.52	0.97	1.19471	3.96889	4.06849	-0.09961
15	218.10	1.23	1.03267	3.43075	3.62558	-0.19484
16	244.39	1.38	0.98195	3.26238	3.45068	-0.18829
17	161.00	0.91	1.25312	4.16286	4.20287	-0.04001
18	245.19	1.39	0.97594	3.24241	3.44269	-0.20028
19	294.26	1.66	0.85244	2.83233	3.20294	-0.37061
20	345.50	1.95	0.79664	2.64723	3.02507	-0.37784
21	324.35	1.83	0.75581	2.51144	3.09513	-0.58369
22	414.06	2.33	0.69448	2.30816	2.85859	-0.55043
23	502.38	2.82	0.68794	2.28707	2.70936	-0.42228
24	616.67	3.46	0.65043	2.16335	2.57736	-0.41401
25	457.57	2.57	0.67642	2.24841	2.77816	-0.52976
26	585.91	3.30	0.59726	1.98620	2.60649	-0.62029
27	769.55	4.32	0.53332	1.77524	2.46311	-0.68787
28	676.39	3.79	0.56239	1.87105	2.52706	-0.65601

Table IV

GRADE 1 STEEL WOOL - FRICTION FACTOR DATA

RUN	MDOT	NR FR	FAN F	CF	CFTH	DIFCF
1	10.80	0.10	5.70884	15.97843	21.17030	-5.19187
2	12.60	0.12	5.94058	16.62704	18.42164	-1.79459
3	13.09	0.13	5.83343	16.32715	17.78107	-1.45391
4	15.07	0.15	5.38046	15.05933	15.70058	-0.64125
5	30.26	0.29	3.09263	8.65595	8.82646	-0.17050
6	34.24	0.33	2.89335	8.09819	8.02800	0.07019
7	33.78	0.33	2.92283	8.18072	8.11408	0.06664
8	72.47	0.70	1.71666	4.80481	4.84508	-0.04027
9	70.21	0.68	1.78999	5.01006	4.94356	0.06650
10	84.10	0.81	1.49030	4.17129	4.45738	-0.28610
11	96.02	0.93	1.49104	4.17339	4.15975	0.01364
12	161.22	1.55	1.09987	3.07866	3.28708	-0.20842
13	200.85	1.94	0.99511	2.78555	3.03164	-0.24609
14	266.17	2.58	0.82385	2.30638	2.77595	-0.46956
15	314.91	3.05	0.77040	2.15694	2.65524	-0.49830
16	385.99	3.75	0.71334	1.99751	2.53396	-0.53645
17	389.46	3.78	0.72909	2.04164	2.52927	-0.48763
18	430.19	4.18	0.65172	1.82518	2.47866	-0.65348
19	522.58	5.07	0.57303	1.60526	2.39438	-0.78911
20	525.58	5.10	0.56461	1.58168	2.39202	-0.81033
21	593.66	5.77	0.57760	1.61851	2.34665	-0.72815
22	588.20	5.71	0.57416	1.60883	2.35017	-0.74134
23	708.37	6.89	0.47077	1.31983	2.29045	-0.97062
24	804.55	7.82	0.43115	1.20936	2.25574	-1.04638

Table V

GRADE 3 STEEL WOOL - FRICTION FACTOR DATA

RUN	MDOT	NR FR	FAN F	CF	CFTH	DIFCF
1	954.46	10.57	0.60511	1.65333	2.18923	-0.53590
2	954.34	10.57	0.60542	1.65417	2.18925	-0.53508
3	1005.70	11.15	0.59015	1.61302	2.17945	-0.56642
4	796.12	8.83	0.62457	1.70486	2.22645	-0.52159
5	795.26	8.82	0.62590	1.70849	2.22669	-0.51820
6	601.17	6.67	0.67412	1.83847	2.30004	-0.46157
7	601.29	6.67	0.67390	1.83788	2.29998	-0.46210
8	507.78	5.64	0.73439	2.00216	2.35465	-0.35249
9	508.42	5.65	0.73120	1.99347	2.35417	-0.36071
10	424.40	4.71	0.74522	2.03120	2.42421	-0.39301
11	420.49	4.67	0.76954	2.09746	2.42823	-0.33078
12	330.36	3.67	0.79832	2.17543	2.54521	-0.36978
13	325.40	3.61	0.83353	2.27136	2.55352	-0.28216
14	261.52	2.90	0.94764	2.58202	2.68863	-0.10661
15	261.53	2.90	0.94753	2.58170	2.68861	-0.10691
16	261.13	2.90	0.93404	2.54496	2.68966	-0.14470
17	221.73	2.46	0.99255	2.70422	2.81169	-0.10747
18	221.73	2.46	0.99251	2.70409	2.81168	-0.10759
19	221.72	2.46	0.98500	2.68365	2.81171	-0.12806
20	166.11	1.85	1.08984	2.96907	3.08341	-0.11434
21	166.16	1.85	1.08993	2.96934	3.08244	-0.11311
22	162.92	1.81	1.13378	3.08878	3.10397	-0.01519
23	169.83	1.89	1.10759	3.01746	3.05967	-0.04221
24	169.83	1.89	1.10762	3.01753	3.05968	-0.04215
25	167.88	1.87	1.18670	3.23296	3.07202	0.16094
26	167.41	1.85	1.06656	2.90567	3.07917	-0.17350
27	167.42	1.85	1.05316	2.86917	3.07914	-0.20997
28	154.68	1.71	1.12328	3.06016	3.16907	-0.10891
29	124.85	1.38	1.19706	3.26107	3.44936	-0.18829
30	100.70	1.11	1.46836	4.00009	3.80077	0.19932
31	104.63	1.16	1.53966	4.19431	3.72464	0.46967
32	68.99	0.77	1.73339	4.72198	4.61429	0.10769
33	57.90	0.64	2.34971	6.40092	5.11421	1.28670
34	41.96	0.47	2.13194	5.80765	6.29563	-0.48798
35	36.82	0.41	1.93862	5.28101	6.89474	-1.61373
36	29.72	0.33	2.12317	5.78375	8.07186	-2.28811
37	23.62	0.26	2.35244	6.40830	9.63802	-3.22972
38	20.41	0.23	2.69709	7.34714	10.85471	-3.50757
39	12.61	0.14	4.70579	12.81903	16.35512	-3.53609
40	9.74	0.11	5.89741	16.06513	20.59951	-4.53439

Table VI

GRADE 00 STEEL WOOL – HEAT TRANSFER DATA

FRICTION DATA				HEAT TRANSFER DATA						
RUN	NR	F		COND PARAM	MAX SLOPE	NTU	NR	J	ALFA	MDOT
1	0.08	7.67983		0.0	0.43370	1.20	0.08	0.00270	0.0326	13.02
2	0.10	6.48785		0.0	0.43577	1.21	0.10	0.00272	0.0400	16.02
3	0.19	3.47646		0.0	0.53428	1.76	0.19	0.00396	0.0770	30.79
4	0.22	3.08775		0.0	0.53814	1.86	0.22	0.00420	0.0889	35.57
5	0.49	1.77740		0.0	0.89996	9.34	0.49	0.02102	0.1966	78.62
6	0.59	1.58995		0.0	1.20651	17.50	0.58	0.03939	0.2342	93.68
7	0.59	1.58995		0.0	1.19072	17.02	0.58	0.03832	0.2342	93.68
8	1.20	0.97491		0.0	1.35466	22.26	1.19	0.05010	0.4812	192.44
9	1.40	0.89086		0.0	1.17933	16.68	1.38	0.03754	0.5592	223.92
10	2.22	0.69380		0.0	1.34748	22.02	2.19	0.04952	0.8957	358.26
11	2.39	0.66392		0.0	1.34323	21.87	2.36	0.04921	0.9619	384.74
12	2.91	0.52202		0.0	1.13802	15.48	2.87	0.03484	1.1666	466.61
13	3.35	0.49178		0.0	1.19151	17.04	3.30	0.03835	1.3450	537.93
14	4.12	0.40498		0.0	1.06944	13.56	4.06	0.03051	1.6547	661.81

Table VII

GRADE 0 STEEL WOOL - HEAT TRANSFER DATA

	FRICTION DATA			HEAT TRANSFER DATA					
RUN	NR	F	COND PARAM	MAX SLOPE	NTU	NR	J	ALFA	MDOT
1	0.22	3.35793	0.0	0.80480	7.27	0.22	0.02860	0.1481	40.15
2	0.22	3.35637	0.0	0.80183	7.20	0.22	0.02835	0.1486	40.30
3	0.32	2.51456	0.0	0.82385	7.66	0.32	0.03015	0.2158	58.50
4	0.32	2.57833	0.0	0.83423	7.88	0.31	0.03100	0.2131	57.77
5	0.32	2.47547	0.0	0.83338	7.86	0.31	0.03094	0.2134	57.85
6	0.32	2.53480	0.0	0.83951	7.99	0.31	0.03145	0.2119	57.43
7	0.36	2.24917	0.0	0.88756	9.06	0.36	0.03564	0.2426	65.77
8	0.36	2.30929	0.0	0.89762	9.28	0.35	0.03653	0.2399	65.03
9	0.38	2.13975	0.0	0.85559	8.34	0.37	0.03282	0.2539	68.84
10	0.37	2.25412	0.0	0.87013	8.66	0.37	0.03410	0.2497	67.69
11	0.43	2.07882	0.0	0.90821	9.52	0.42	0.03747	0.2872	77.86
12	0.43	2.10354	0.0	0.90820	9.52	0.42	0.03747	0.2872	77.86
13	0.48	1.94433	0.0	0.92278	9.85	0.47	0.03878	0.3214	87.12
14	0.48	1.95413	0.0	0.92278	9.85	0.47	0.03878	0.3214	87.12
15	0.56	1.69590	0.0	0.95421	10.61	0.55	0.04174	0.3777	102.38
16	0.55	1.74265	0.0	0.96524	10.88	0.55	0.04282	0.3733	101.21
17	0.73	1.43705	0.0	0.94424	10.36	0.72	0.04078	0.4916	133.28
18	0.71	1.49336	0.0	0.96822	10.96	0.70	0.04311	0.4795	129.98
19	0.91	1.28692	0.0	1.02793	12.45	0.90	0.04901	0.6103	165.45
20	1.02	1.21862	0.0	0.95156	10.54	1.01	0.04147	0.6898	187.01
21	1.15	1.11269	0.0	0.98910	11.48	1.14	0.04514	0.7808	211.68
22	1.02	1.16424	0.0	0.94143	10.30	1.00	0.04050	0.6880	186.51
23	1.30	1.00608	0.0	0.93825	10.22	1.28	0.04020	0.8763	237.57
24	1.65	0.90059	0.0	0.99230	11.56	1.62	0.04548	1.1068	300.06
25	1.90	0.85391	0.0	1.03585	12.65	1.87	0.04978	1.2829	347.79
26	1.71	0.80807	0.0	0.90569	9.46	1.68	0.03724	1.1502	311.82
27	2.43	0.70789	0.0	0.98279	11.32	2.40	0.04455	1.6308	442.10
28	2.96	0.67601	0.0	0.91597	9.70	2.92	0.03814	2.0099	544.88
29	3.42	0.60724	0.0	0.91985	9.79	3.37	0.03849	2.3177	628.31
30	3.11	0.58947	0.0	0.93962	10.25	3.06	0.04033	2.1025	569.98
31	4.37	0.52555	0.0	0.90502	9.45	4.31	0.03717	2.9598	802.38
32	0.15	4.38002	0.0	0.79159	6.99	0.15	0.02752	0.0986	26.74
33	0.11	5.59647	0.0	0.76246	6.41	0.11	0.02524	0.0737	19.99
34	0.07	8.56106	0.0	0.72358	5.66	0.07	0.02230	0.0447	12.11
35	0.04	13.74768	0.0	3.18631	2.00	0.04	0.00788	0.0282	7.65

Table VIII

GRADE 1 STEEL WOOL - HEAT TRANSFER DATA

	FRICTION DATA			HEAT TRANSFER DATA					
RUN	NR	F	COND PARAM	MAX SLOPE	NTU	NR	J	ALFA	MDOT
1	0.10	5.66045	0.0	0.67811	4.82	0.10	0.02720	0.0514	10.77
2	0.10	5.66045	0.0	0.68340	4.92	0.10	0.02774	0.0514	10.77
3	0.28	3.27277	0.0	0.89611	9.25	0.28	0.05214	0.1425	29.86
4	0.32	2.93011	0.0	0.86948	8.65	0.31	0.04876	0.1601	33.54
5	0.68	1.75940	0.0	1.03931	12.74	0.67	0.07184	0.3446	72.21
6	0.69	1.72974	0.0	1.04705	12.95	0.68	0.07296	0.3476	72.85
7	0.75	1.70905	0.0	1.06634	13.48	0.74	0.07591	0.3824	80.14
8	1.48	1.18089	0.0	1.04821	12.98	1.46	0.07311	0.7508	157.33
9	1.86	1.02195	0.0	1.05085	13.05	1.83	0.07352	0.9422	197.43
10	2.43	0.86063	0.0	1.00056	11.76	2.40	0.06629	1.2303	257.82
11	3.00	0.78257	0.0	0.92209	9.84	2.95	0.05544	1.5187	318.24
12	3.57	0.77318	0.0	0.92975	10.02	3.52	0.05644	1.8145	380.22
13	3.94	0.68312	0.0	0.88027	8.89	3.88	0.05009	2.0071	420.59
14	4.85	0.58316	0.0	0.78560	6.87	4.78	0.03870	2.4669	516.94
15	5.37	0.60107	0.0	0.82747	7.74	5.29	0.04358	2.7311	572.31
16	6.62	0.45425	0.0	0.70891	5.39	6.53	0.03033	3.3828	708.86

Table IX

GRADE 3 STEEL WOOL - HEAT TRANSFER DATA

	FRICTION DATA			HEAT TRANSFER DATA					
RUN	NR	F	COND PARAM	MAX SLOPE	NTU	NR	J	ALFA	MDOT
1	0.08	19.25006	0.0	0.80704	7.31	0.08	0.13885	0.0326	7.61
2	0.08	15.99779	0.0	0.80593	7.29	0.08	0.13841	0.0327	7.62
3	0.14	4.77877	0.0	0.89889	9.31	0.13	0.17674	0.0533	12.43
4	0.20	3.18014	0.0	0.83870	7.97	0.20	0.15131	0.0800	18.65
5	0.20	3.18731	0.0	0.83965	7.99	0.20	0.15169	0.0799	18.63
6	0.28	2.73948	0.0	0.91104	9.59	0.28	0.18186	0.1109	25.85
7	0.28	2.73941	0.0	0.91103	9.59	0.28	0.18185	0.1109	25.85
8	0.33	2.68309	0.0	0.86554	8.56	0.33	0.16235	0.1321	30.80
9	0.50	2.25342	0.0	0.80282	7.22	0.49	0.13702	0.1965	45.82
10	0.50	2.21496	0.0	0.79592	7.08	0.49	0.13429	0.1982	46.21
11	0.70	1.90665	0.0	0.88761	9.06	0.69	0.17179	0.2777	64.74
12	1.25	1.35282	0.0	0.73280	5.84	1.23	0.11077	0.4963	115.72
13	1.94	1.03763	0.0	0.67913	4.84	1.92	0.09177	0.7728	180.17
14	1.90	1.03415	0.0	0.62296	3.83	1.87	0.07267	0.7587	176.90
15	2.30	1.02732	0.0	0.60060	3.45	2.27	0.06536	0.9163	213.64
16	3.16	0.90589	0.0	0.57978	3.06	3.11	0.05796	1.2556	292.73
17	2.79	0.92206	0.0	0.59134	3.28	2.75	0.06221	1.1082	258.38
18	3.76	0.84908	0.0	0.57530	2.97	3.70	0.05623	1.4927	348.02
19	5.36	0.73042	0.0	0.52164	1.62	5.29	0.03073	2.1330	497.29
20	4.56	0.78667	0.0	0.56843	2.83	4.49	0.05363	1.8069	421.26
21	5.68	0.68614	0.0	0.48644	1.42	5.60	0.02685	2.2630	527.60
22	7.39	0.66139	0.0	0.47727	1.37	7.29	0.02604	2.9493	687.60
23	8.90	0.63848	0.0	0.45558	1.28	8.77	0.02422	3.5535	828.49
24	9.98	0.61371	0.0	0.44567	1.24	9.85	0.02351	4.0026	933.19
25	5.53	0.72561	0.0	0.52291	1.63	5.46	0.03084	2.2110	515.49

Table X

APPENDIX A: DESCRIPTION OF EQUIPMENT

A. AIR SUPPLY AND FLOW MEASUREMENT

A 30 HP, multi-stage Spencer Turbo-Compressor rated at 550 CFM (for intake at atmospheric pressure) provided an induced draft through the test section.

The air flow rate was measured with an ASME standard orifice section. The concentric orifices had throat diameters of 0.308, 0.462, 0.775, 1.232, 1.540, 1.971, and 2.310 inches. These values correspond to throat diameter to pipe diameter ratios (β) of 0.10, 0.15, 0.25162, 0.40, 0.50, 0.64, and 0.75 respectively. Pressure taps were located one pipe diameter upstream and one-half pipe diameter downstream of the orifice plate, as specified by [1].

B. HEATER SYSTEM

The heater system used was essentially that used by Bruno [5], although it was completely rewired. Fourteen separate bakelite frames were each wound with two parallel-connected heater elements. The heater elements were 0.0031 inch nichrome wire, (Fig. 23) which was selected largely due to the comparatively low coefficient of thermal expansion of nichrome. Each heater element has a nominal resistance of 800 ohms. An individual switch controlled both heaters per bakelite frame (i.e., 14 such switches) and these switches were in turn controlled by a master switch which was used to cut off the power to the heaters to simulate the step change in air inlet temperature . Thus the number of heaters (as well as the voltage supplied) could be adjusted to provide the 20°F temperature rise for any flow rate up to approximately 1,000 pounds per hour.

C. HEATER POWER SUPPLY

A General Electric Speed Variator motor-generator, operating on 220 volts AC at 35 amps and producing 250 volts DC at up to 28 amps, provided the electrical power to the heaters. The actual voltage supplied was regulated with the rheostat on the field winding of the MG set and at the test section with a 100 ohm Ohmite wound resistor (for currents less than 4 amperes).

The current and voltage at the source were monitored with a Roller-Smith 150 a. ammeter and a Simpson multimeter, respectively. At the test section the current and voltage were monitored with a Westinghouse 10 a. ammeter and 300 v. voltmeter.

D. MATRIX HOLDER AND TEST SECTION

Both the holder and test section (Fig. 24) were fabricated from plexiglass. The matrix holder is a drawer which slides into the test section. By removing the rear, upstream, and downstream faces of the holder, the test section of steel wool may be inserted with minimum packing effort, thereby causing negligible inhomogeneity in the porosity. The flow channel is 3.1875 inches square and samples up to approximately 3 inches long can be handled. A network of seven .003 inch steel wires was strung across the downstream face of the holder to restrain the steel wool from being sucked down the duct. These wires were not thought to interfere with the friction or heat transfer performance of the sample, and experience indicated that they are probably unnecessary anyhow. A similar network was placed in the upstream face to prevent interference between strands of steel wool and the upstream thermocouples. This network is also thought to be unnecessary. Styrofoam insulation lined the interior of the matrix holder and also served to hold the steel wool in place.

The test section, into which the holder slides, contains the matrix upstream and downstream thermocouples and pressure taps. In previous installations the matrix downstream temperature was measured by thermocouples mounted in the holder, rather than the test section. However, the possibility of shorts or breakage from pertruding strands of steel wool dictated the movement of the thermocouples downstream by approximately 0.5 inch. No significant error in the maximum slope technique is thought to have been introduced by this movement of the most important sensor.

E. INLET CONE AND FLOW STRAIGHTENER

This section was designed and tested by Piersall [23], and was found to provide a uniform velocity profile for the air entering the matrix.

Additionally an alteration was made in the radiation shielding of the reference thermocouples, located at exit from the inlet cone, which may have improved the uniformity of the velocity profile. Originally all the reference thermocouples were contained in one 3/8 inch aluminum tube mounted across the center of the channel. In this reconstruction these thermocouples were placed in five 1/8 inch nickel-plated tubes, evenly spaced across the channel. This is thought to delocalize the intensity of the disturbance caused by the presence of the thermocouples in the stream.

F. PRESSURE MEASURING SYSTEM

One pressure tap was located in both the upstream and downstream face of the test section (i.e., on either side of the matrix). As previously mentioned, two taps were also located at the orifice section.

Each pressure tap was connected by Poly-flo flexible tubing to a high pressure or low pressure manifold and protected by a Hoke quick-closing valve. The high and low pressure manifolds were connected to the high and low pressure sides of the following instruments:

2 Merriam Instrument Company, 50 in. manometers
1 Ellison Draft Gage Company, 0-2 in. inclined manometer
1 Ellison Draft Gage Company, 0-4 in. inclined manometer.

These manometers were also protected with quick-closing valves. Thus, with the proper valve lineup, each of the four pressures measured per data run was simultaneously measured on four manometers until the mass flow rate and orifice plate combination required that the more limited manometers be isolated.

Atmospheric pressure was measured by a PRINCO mercury barometer.

G. TEMPERATURE MEASURING SYSTEM

Temperature sensors were located at the exit from the inlet cone (t_1), entrance to the test section (t_2), exit from the test section (t_3), and 15.5 inches upstream from the orifice section (t_o).

Temperature t_1 was measured by two different sets of five 30 gage iron-constantan thermocouples connected in series. Each thermocouple was wrapped in teflon tape to prevent shorting. As previously mentioned, the reconstructed apparatus has different housing for these thermocouples than that designed by Traister [29]. The ten thermocouples were housed two to each of five nickel-plated brass tubes. The two thermocouples in each tube were from the two different sets of t_1 sensors. The tubes were cut-away to the front while closed to the downstream side, where they faced the heaters. This system is thought to provide superior sensitivity and radiation shielding to the old system, where all ten thermocouples were housed in one aluminum tube.

Temperature t_2 was measured by a set of five .001 inch diameter iron-constantan thermocouples in series. The output of this thermopile was referenced against one of the t_1 thermopiles so that the net output to the recorder was (t_2-t_1).

Temperature t_3 was measured exactly as t_2, so the output to the recorder was (t_3-t_1).

The two outputs (t_2-t_1) and (t_3-t_1) were amplified by Hewlett-Packard 8803A DC amplifiers and recorded on a Hewlett-Packard 7702B two-channel recorder.

The orifice temperature, t_o, was measured by a 30 gage cooper-constantan thermocouple sheathed in stainless steel. It was referenced to an ice junction and the output read on a Leeds and Northrup Millivolt Potentiometer.

H. NOISE CONTROL SYSTEM

A substantial amount of noise in the (t_3-t_1) and (t_2-t_1) signals was frequently encountered. To filter this out, Mallory 2.0 microfarad capacitors were placed between the negative side of the signal and ground. The time constant of the circuit with the addition of these capacitors was less than the minimum time constant of the heater-thermocouple system reported by Bruno [5].

Additionally a Sprague 1000 micro-farad capacitor was placed in the power supply circuit to filter any noise from the motor-generator. This had no effect on the transient response of the apparatus, since the master switch isolated the power supply from the heaters.

APPENDIX B: DATA REDUCTION RELATIONSHIPS

A. GEOMETRICAL RELATIONSHIPS

Once an average cross-section for a fiber is assumed, the heat transfer area of the medium is determined. In this study the average cross-section was assumed to be an equilateral triangle with side length w, where w is the median mean width of the fiber specified for the particular grade steel wool by [7]. Therefore:

Cross-sectional area = $A_{fiber} = w^2(\sqrt{3}/4)$

Perimeter of cross-section = 3w

Hydraulic diameter of fiber = $4\left(\frac{A_{fiber}}{Perimeter}\right) = w/\sqrt{3}$ (B-1)

Volume of steel in sample = $V_{steel} = (A_{fiber})$(Total length of fibers)

Heat transfer area = A = (Perimeter)(Total length of fibers)

$= (3w)(V_{steel}/A_{fiber}) = 4\sqrt{3}\,V_{steel}/w$

But the volume of steel is equal to the weight of the sample divided by the density of steel. Therefore:

$$V_{steel} = W_s/\rho_s$$

$$A = 4\sqrt{3}\,W_s/(\rho_s w) \quad \text{(B-2)}$$

Porosity = $\varphi = 1 - V_{steel}/V_{bulk} = 1 - W_s/(\rho_s A_{fr} L)$ (B-3)

Specific surface = $\beta = A/V_{bulk} = 4\sqrt{3}\,W_s/(w\rho_s A_{fr} L)$ (B-4)

Free flow area = $A_c = \varphi A_{fr}$ (except for crossed rod matrices) (B-5)

Equations (B-1, B-2, B-3, & B-5) are substituted into equations (1) through (6) as appropriate to determine the geometrical characteristics for use in the various models.

B. MASS FLOW RATE

The mass flow rate was calculated from the ASME Power Test Code [1] with Murdock's [21] interpolation scheme.

$$\dot{m} = 359\left[\frac{C}{\sqrt{1-\bar{\beta}^4}}\right] d_o^2 F_a Y \sqrt{\Delta P_o \gamma} \qquad \text{(B-6)}$$

where

C = orifice coefficient of discharge

$\bar{\beta}$ = ratio of orifice diameter to pipe diameter

d_o = orifice diameter in inches

F_a = orifice plate thermal expansion factor

Y = fluid thermal expansion factor

γ = specific weight of fluid flowing = P/RT if a perfect gas

P = absolute static pressure at orifice (lbf/ft^2)

R = specific gas constant for air = 53.35 ft-lbf/lbm-°F

T = absolute temperature at orifice (°R)

ΔP_o = pressure drop across orifice in inches of water

Substitution of the identities for K and in (B-6) yields:

$$\dot{m} = 359 \frac{C}{\sqrt{1-\bar{\beta}^4}} d_o^2 F_a Y \sqrt{\Delta P_o \left(\frac{P}{RT}\right)} \qquad \text{(B-7)}$$

From Fig. 40A of [1] one finds:

$$Y = 1 - (0.41 + 0.35\bar{\beta}^4)\frac{x}{k}$$

where

$$k = c_p/c_v = 1.4 \text{ (for air)}$$

$$x = \Delta P_o/P \qquad \text{(any consistent units).}$$

Also from [1], Fig. 38:

$F_a = 1$

$P = (P_{atm} - P_o/13.6)(70.75)\text{lbf/ft}^2$

P_{atm} = local atmospheric pressure in inches of Hg

P_o = static pressure upstream of orifice plate in inches H_2O

When all these identities are substituted into (B-7) with the units adjusted to give $\dot{m}$ in (lbm/hr), the equation becomes:

$$\dot{m} = \frac{589.81C}{\sqrt{1-\bar{\beta}^4}}\left[\frac{d_o^2(1-(0.41 + 0.35\bar{\beta}^4)}{99.02}\right]\left[\frac{\Delta P_o}{(P_{atm} - P_o/13.6)}\right]\left[\frac{\Delta P_o(P_{atm} - P_o/13.6)}{t_o + 459.7}\right]^{1/2}$$

The orifice coefficient of discharge is found from Murdock's tables and interpolation scheme.

C. MAXIMUM SLOPE

The following sketch of the general time-temperature history downstream of the core will illustrate the relationships involved.

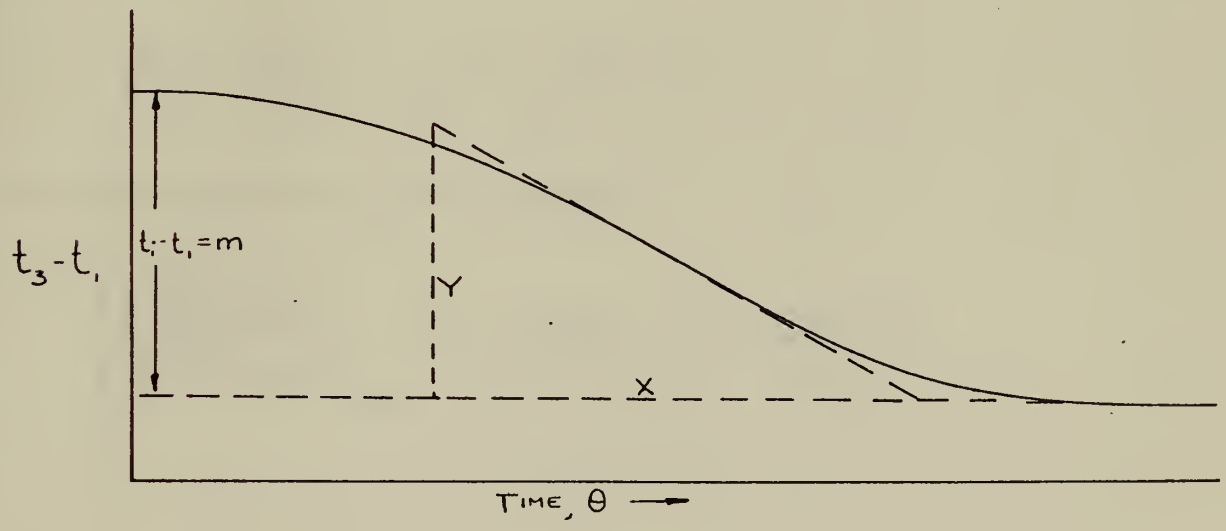

The maximum slope of the general time-temperature history is a function of N_{tu} and λ.

$$\left[\frac{d\left(\frac{t_3-t_i}{t_1-t_i}\right)}{d\left(\tau/N_{tu}\right)}\right]_{max} = \Phi\left(N_{tu}, \lambda\right)$$

The non-dimensional variables are:

τ = generalized time variable $\cong hA\theta/(W_s c_s)$

$N_{tu} = hA/\dot{m}c_p$

$\tau/N_{tu} = \left[\dot{m}c_p/(W_s c_s)\right]\theta$

Therefore

$$d\left(\tau/N_{tu}\right) = \frac{\dot{m}c_p}{W_s c_s} d\theta \qquad \text{(B-9)}$$

Furthermore

$$\frac{t_3 - t_i}{t_1 - t_i} = \frac{t_3 - t_1}{t_1 - t_i} + 1$$

and its derivative is

$$d\left(\frac{t_3 - t_i}{t_1 - t_i}\right) = \frac{1}{(t_1 - t_i)} d(t_3 - t_1) \qquad \text{(B-10)}$$

Combination of (B-9) and (B-10) yields:

$$\left[\frac{d\left(\frac{t_3 - t_i}{t_1 - t_i}\right)}{d\left(\tau/N_{tu}\right)}\right]_{max} = \frac{W_s c_s}{\dot{m}c_p (t_1 - t_i)} \frac{d(t_3 - t_1)}{d\theta} \qquad \text{(B-11)}$$

In terms of the recorder output the various quantities in (B-11) are:

$$\left[\frac{d}{d\theta}(t_3 - t_1)\right]_{MAX} = Y/X$$

X/(Chart speed) = $X/CS = d\theta$

$d(t_3 - t_1) = Y$

$(t_1 - t_i) = m$

Equation (B-11) becomes in these terms:

$$\left[\frac{d\left(\frac{t_3 - t_i}{t_1 - t_i}\right)}{d\left(T/N_{tu}\right)}\right]_{MAX} = \left(\frac{W_s c_s}{\dot{m} c_p}\right)\left(\frac{Y}{mX}\right) CS \qquad \text{(B-12)}$$

This value of the maximum slope and the known value of λ (in this study, $\lambda = 0$) are used to enter Table II or Fig. 1 to determine the corresponding value of N_{tu}.

D. COLBURN J FACTOR

The Colburn j factor is defined as

$$j = N_{St} N_{Pr}^{2/3} = \frac{h}{G c_p} N_{Pr}^{2/3} \qquad \text{(B-13)}$$

In this case the mass flux, G, is based on A_c rather than A_{fr}, although at 98% porosity there is not much difference. Substitution of $G = \dot{m}/A_c$ and multiplication of (B-13) by A/A yields:

$$j = \frac{hA}{\dot{m} c_p} \cdot \frac{A_c}{A} \cdot N_{Pr}^{2/3}$$

But $N_{tu} = (hA/\dot{m}c_p)$ and therefore:

$$j = N_{tu}\left(\frac{A_c}{A}\right) N_{Pr}^{2/3}$$

E. HEAT TRANSFER POWER AND FRICTION POWER

The heat transfer power per unit area per degree temperature difference is:

$$h = \frac{c_p \mu}{N_{Pr}^{2/3}} \left(\frac{1}{l}\right) N_{Re} j \qquad \text{(B-14)}$$

(where l is the characteristic length used in N_{Re}).

At standard conditions of 500°F and one atmosphere [13]

c_p = 0.2477 BTU/lbm-°F

μ = 0.0678 lbm/hr-ft

ρ = 0.0413 lbm/ft^3

N_{Pr} = 0.671

Substitution of these values into (B-14) leads to:

$$h_{STD} = 0.02195 \left(\frac{1}{l}\right) N_{Re} j \quad \frac{BTU}{hr\text{-}ft^2\text{-}°F} \qquad \text{(B-15)}$$

The flow friction power per unit of area is [13]

$$E = f\left[\frac{1}{2g_c}\left(\frac{1}{l}\right)^3 \left(\frac{\mu^3}{\rho_m^2}\right) N_{Re}^3\right] \qquad \text{(B-16)}$$

Evaluation of (B-16) at standard conditions yields:

$$E_{STD} = 1.11 \times 10^{-7}\left[\left(\frac{1}{l}\right)^3 f\left(\frac{N_{Re}}{10^3}\right)^3\right] \; hp/ft^2 \qquad \text{(B-17)}$$

F. OTHER RELATIONSHIPS

The relationships pertaining to the Reynolds number and the two friction factors have been completely derived in the section on theoretical background.

BIBLIOGRAPHY

1. American Society of Mechanical Engineers, Power Test Code Supplements, Instruments and Apparatus, PTC-19.5; 4, Flow Measurements, Chap. 4, New York: ASME 1959.

2. Ball, Stuart F., "Experimental Determination of Heat Transfer and Flow Friction Characteristics for Several Plate Fin Type Compact Heat Exchanger Surfaces," Master's Degree Thesis, Naval Postgraduate School, Monterey, California, 1966.

3. Beavers, G. S. and Sparrow, E. M., "Non-Darcy Flow Through Fibrous Porous Media," Journal of Applied Mechanics, pp. 711-714, December 1969.

4. Brady, George S., Materials Handbook, Ninth Edition, pp. 724, 725, 737, McGraw-Hill Book Co., Inc., New York, 1963.

5. Bruno, Marco J., "Experimental Techniques to Determine N_{tu} of Compact Heat Exchanger Surfaces," Master's Degree Thesis, Naval Postgraduate School, Monterey, California, 1968.

6. Colburn, Allan P., "A Method of Correlating Forced Convection Heat Transfer Data and a Comparison with Fluid Friction," American Institute of Chemical Engineers Transactions, v. 29, pp. 174-209, 1933.

7. Federal Specification, FF-S-740a, Steel Wool, 8 October 1965.

8. Gebhart, Benjamin, Heat Transfer, Second Edition, McGraw-Hill Book Co., Inc., New York, 1971.

9. Green, Leon and Duwez, Pol, "Fluid Flow Through Porous Metals," Journal of Applied Mechanics, v. 18, pp. 39-44, March 1951.

10. Hilsenrath, J. et al, Tables of Thermodynamic and Transport Properties of Air, Argon, Carbon Monoxide, Hydrogen, Nitrogen, Oxygen, and Steam, Permagon Press, New York, 1960.

11. Howard, C. P., "The Single Blow Problem Including the Effects of Longitudinal Conduction," ASME Paper No. 64-GTP-11, 1964.

12. Hubbert, M. K., Field Equations of the Flow of Liquids Through Porous Solids, paper presented at Sixth International Congress for Applied Mechanics, Paris, France, 22-29 September 1946.

13. Kays, W. M. and London, A. L., Compact Heat Exchangers, Second Edition, McGraw-Hill Book Co., Inc., New York, 1964.

14. Kline, S. J. and McClintock, F. A., "Describing Uncertainties in Single-Sample Experiments," Mechanical Engineering, pp. 3-8, January, 1953.

15. Kohlmayr, G. F., "Exact Maximum Slopes for Transient Matrix Heat Transfer Testing," Pratt and Whitney Aircraft, Report PWA-2641.

16. Kohlmayr, G. F., "An Indirect Curve Matching Method for Transient Matrix Heat Transfer Testing in the Low N_{tu} Range," Pratt and Whitney Aircraft, Report PWA-3158.

17. Kohlmayr, G. F., "Extension of the Maximum Slope Method to Arbitrary Upstream Fluid Temperature Changes," Pratt and Whitney Aircraft, Report PWA-3228.

18. Kreith, Frank, Principles of Heat Transfer, Second Edition, International Textbook Co., Scranton, Pennsylvania, 1965.

19. Locke, G. L., "Heat Transfer and Flow Friction Characteristics of Porous Solids," TR No. 10, Department of Mechanical Engineering, Stanford University, Stanford, California, 1 June 1950.

20. London, A. L., "Compact Heat Exchangers, Part II," Mechanical Engineering, pp. 31-34, June 1964.

21. Murdock, J. W., "Tables for Interpolation and Extrapolation of ASME Coefficients for Square-Edged Concentric Orifices," ASME Paper No. 64-WA/FM-6.

22. Muskat, M., The Flow of Homogeneous Fluids Through Porous Media, J. W. Edwards, Inc., Ann Arbor, Michigan, 1937.

23. Piersall, C. H., "Experimental Evaluation of Several High Performance Surfaces for Compact Heat Exchangers," Master's Degree Thesis, Naval Postgraduate School, Monterey, California, 1965.

24. Pucci, P. F., Ball, S. F., and Traister, R. E., "Heat Transfer and Flow Friction Characteristics of Several Plate-Fin Type Compact Heat Exchanger Surfaces," Naval Postgraduate School, Report NPS-59PC7081A, 31 August 1967.

25. Pucci, P. F., Howard, C. P., and Piersall, C. H., "The Single-Blow Transient Testing Technique for Compact Heat Exchanger Surfaces," ASME Paper No. 66-GT-93, 1966.

26. Scheidegger, A. E., "Flow Through Porous Media," Applied Mechanics Surveys, pp. 893-900, Spartan Books, Washington, D. C., 1966.

27. Scheidegger, A. E., The Physics of Flow Through Porous Media, The Macmillian Company, New York, N. Y., 1960.

28. Schlichting, H., Boundary Layer Theory, Sixth Edition, McGraw-Hill Book Company, New York, N. Y., 1968.

29. Traister, R. E., "Experimental Evaluation of Heat Transfer and Flow Friction Characteristics of Several Compact Heat Exchanger Surfaces Utilizing the Single Blow and Cyclic Methods," Master's Degree Thesis, Naval Postgraduate School, Monterey, California, 1967.

30. Trost, H. J., Jr., "The Use of the Analog Computer With the Single Blow Transient Testing Technique for Compact Heat Exchanger Surfaces," Master's Degree Thesis, Naval Postgraduate School, Monterey, California, 1967.

31. Wheeler, A. J., "Single-Blow Transient Testing of Matrix-Type Heat Exchanger Surfaces at Low Values of N_{tu}," TR. No. 68, Department of Mechanical Engineering, Stanford University, Stanford, California, May 1968.

INITIAL DISTRIBUTION LIST

		No. Copies
1.	Defense Documentation Center Cameron Station Alexandria, Virginia 22314	2
2.	Library, Code 0212 Naval Postgraduate School Monterey, California 93940	2
3.	Department of Mechanical Engineering, Code 59 Naval Postgraduate School Monterey, California 93940	2
4.	Professor P. F. Pucci, Code 59Pc Department of Mechanical Engineering Naval Postgraduate School Monterey, California 93940	5
5.	Ens. Richard H. Funke, USN USS CHARLES F. ADAMS (DDG-2) FPO New York, New York 09501	2

Security Classification

DOCUMENT CONTROL DATA - R & D

(Security classification of title, body of abstract and indexing annotation must be entered when the overall report is classified)

1. ORIGINATING ACTIVITY (Corporate author)	2a. REPORT SECURITY CLASSIFICATION
Naval Postgraduate School Monterey, California 93940	Unclassified
	2b. GROUP

3. REPORT TITLE

Heat Transfer and Flow Friction Characteristics of Fibrous Metals

4. DESCRIPTIVE NOTES (Type of report and, inclusive dates)

Master's Thesis, June 1972

5. AUTHOR(S) (First name, middle initial, last name)

Richard H. Funke

6. REPORT DATE	7a. TOTAL NO. OF PAGES	7b. NO. OF REFS
June 1972	111	31

8a. CONTRACT OR GRANT NO.	9a. ORIGINATOR'S REPORT NUMBER(S)
b. PROJECT NO.	
c.	9b. OTHER REPORT NO(S) (Any other numbers that may be assigned this report)
d.	

10. DISTRIBUTION STATEMENT

Approved for public release; distribution unlimited.

11. SUPPLEMENTARY NOTES	12. SPONSORING MILITARY ACTIVITY
	Naval Postgraduate School Monterey, California 93940

13. ABSTRACT

The single-blow transient testing facility of the Naval Postgraduate School was reconstructed. With this apparatus the flow friction and heat transfer characteristics of four grades of steel wool, considered to be representative of fibrous metals, were determined. The flow friction characteristics were determined on the basis of the isothermal pressure drop across the medium, while the heat transfer results were determined by means of the single-blow transient testing technique.

The heat transfer results are presented as the Colburn j-factor. The flow friction results are presented in two forms: as the Fanning friction factor, f; and as the correlating friction factor, C_f. All results are presented as a function of Reynolds number based on the product of the experimentally determined permeability and tortuosity parameter of each sample.

DD FORM 1 NOV 65 1473 (PAGE 1)

S/N 0101-807-6811

Security Classification

A-31408

KEY WORDS	LINK A		LINK B		LINK C	
	ROLE	WT	ROLE	WT	ROLE	WT
Regenerator						
Recuperator						
Heat exchanger						
Steel wool						
Fibrous metal						

Thesis 136737
F937 Funke
c.1 Heat transfer and flow friction characteristics of fibrous metals.